Doctoral Dissertation

Screening of Near-infrared Chemical Probes Library for *In vivo* Blood Vessel Imaging and Analysis of its Target Protein on the Endothelial Cells

MUHAMMAD ASRI ABDUL SISAK

June 2022

Graduate School of Engineering
Osaka University

Contents

General Introduction

Blood vessels are present in almost all the organs, reflecting their importance for oxygen and nutrient delivery to the cells (**Figure 1**). Blood vessels are made up of vascular endothelial cells that line the inner surface and play an important role in the delivery of essential nutrients, growth factors, and oxygen to all tissues, as well as transporting blood throughout the body. It is therefore crucial to be able to visualize blood vessels so that their many related diseases and conditions such as atherosclerosis, aneurysm, thrombosis, and ischemia can be diagnosed and studied. Current methods or techniques for blood vessels imaging are by using magnetic resonance imaging (MRI), x-ray/computerized tomography (CT) scan, and positron emission tomography (PET) (**Figure 2**). For the past few decades, live imaging has transformed biomedical research by enabling visualization and analysis of dynamic cellular processes as they occur in their native systems. Fluorescence-based imaging is one of the most popular techniques in live imaging owing to its sensitivity, selectivity, and technical ease.[1] However, the discovery of novel *in vivo* fluorescent probes can be challenging. Usually, a prespecified target protein (e.g., one that is differentially expressed across cell types) is screened against a library of ligands (antibody, peptide, or small molecule). In subsequent steps, ligands that emerge from a screening are often conjugated to a nanoparticle, such as a quantum dot or

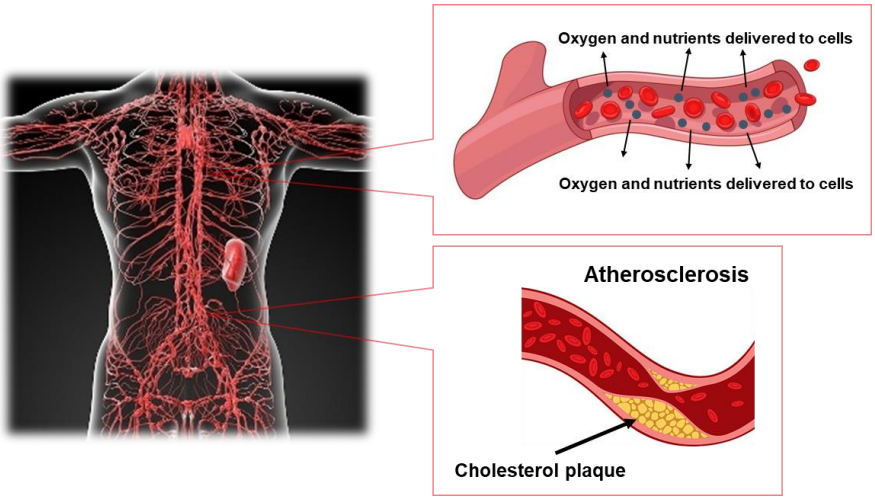

Figure 1. Schematic illustration of function and key role of blood vessel in the human body as well as an example of blood vessels related disease: atherosclerosis.

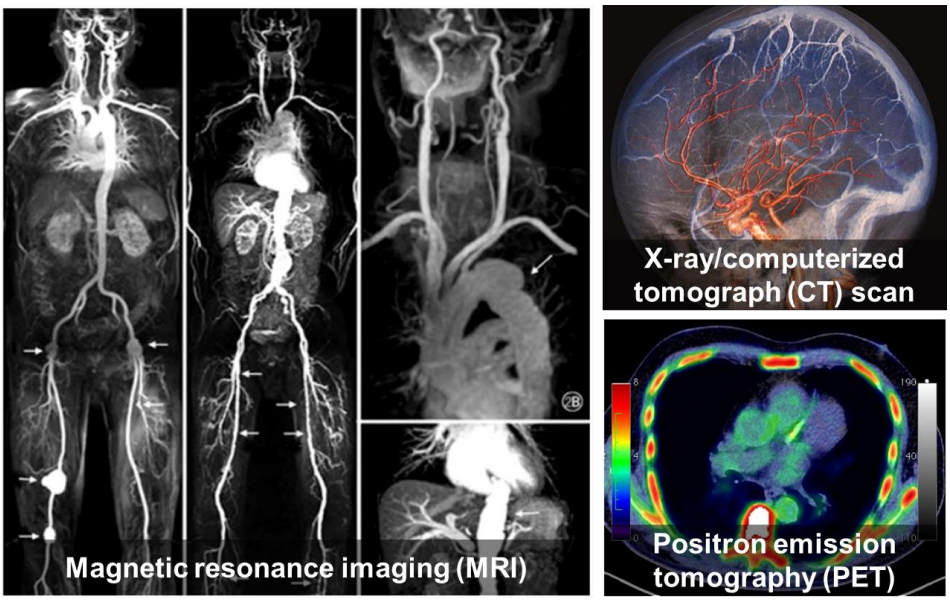

Figure 2. Current techniques available for blood vessel imaging using Magnetic resonance imaging (MRI), X-ray/computerized tomography (CT) scan, and Positron emission tomography (PET).

magneto-fluorescent nanoparticle, to confer imaging capabilities and favorable pharmacokinetics.[2–6] While this target-based approach has generated many *in vivo* fluorescent probes, it can only be applied when there is a priori knowledge of a suitable candidate targeting ligand (**Figure 3**).

An alternative approach for the discovery of new fluorescent probes is to systematically screen a library of fluorescent probes on cultured cells *in vitro* with different phenotypes.[7–10] This approach does not rely upon prespecified imaging targets, and by analogy to forward genetic screens, can lead to the discovery of imaging probes that act through novel mechanisms and reveal new biological processes (**Figure 4**).

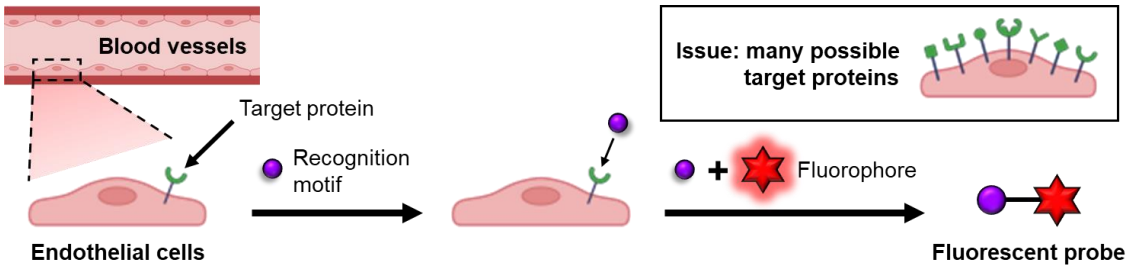

Figure 3. Schematic illustration of a conventional method to design a fluorescent probe through hypothesis driven approach.

Although cell-based assays are effective for preliminary screening to gather information on cytotoxicity,[11] 2D cell culture assays sometimes provide misleading and nonpredictive data for *in vivo* translation responses due to their unnatural microenvironment.[12] This means that cells cannot maintain their original organ functions and morphologies in conventional 2D cell culture systems.

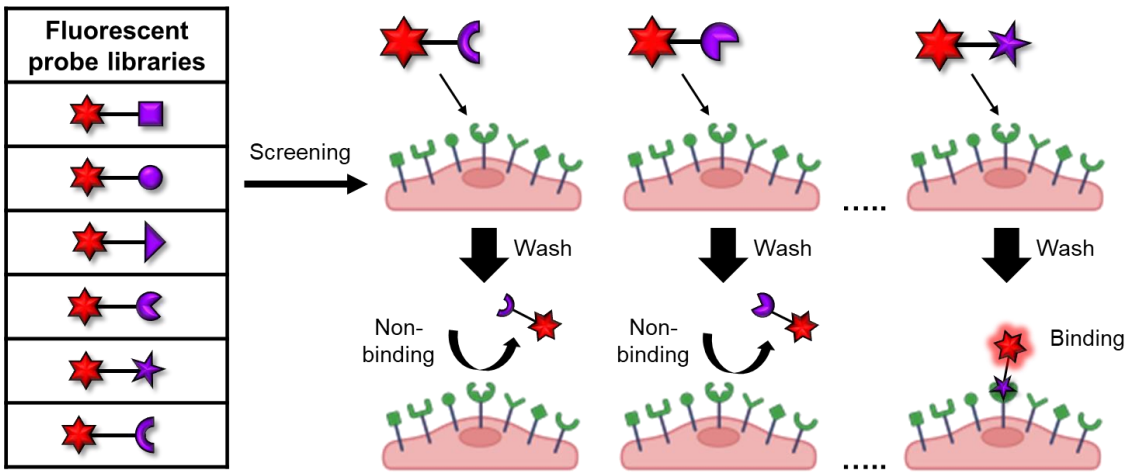

Figure 4. Schematic illustration of alternative method to screen the fluorescent probes which having diversity structures in a library format. This method named as diversity-oriented fluorescence library approach (DOFLA).

We therefore sought to develop a more generalizable and reliable approach to the discovery of *in vivo* fluorescent probes in order to enable integrative studies of chemistry in real tissues. Thus, the development of a technique for constructing a three-dimensional (3D) tissue having a structure and function similar to a living body *in vivo* is highly sought after. As shown in **Figure 5**, numerous studies on fabrication techniques of blood capillary models have been reported, such as bio-printing, organ-on-chip or microfluidic device, electrospinning techniques, cells sheet as well as scaffold structure.[13-21] However, some problems remain such as the inability to control of the geometry of the three-dimensional arrangement or the biocompatibility: even in 3D bioprinted scaffolds it is still difficult to precisely tune their endothelialization after adding the cells and some synthetic vascular grafts for clinical application were found associated with thrombosis, aneurysm, and intimal hyperplasia occurrence due to their lack of compliance (possibility to strain/expanse or contract).[22] Electrospinning method has another limitation which is

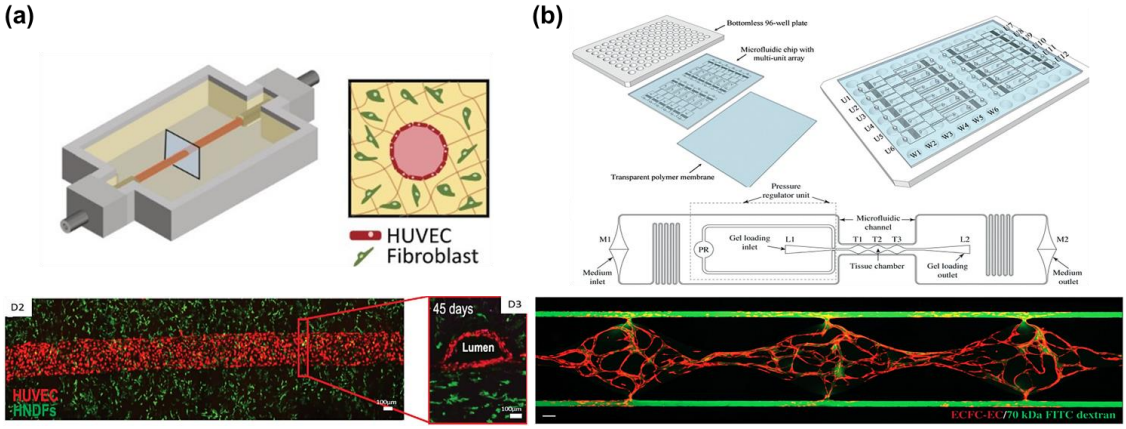

Figure 5. Fabrication of *in vitro* 3D-blood capillary models. (**a**) 3D-bioprinting[20] and (**b**) microchip/microfluidic[21] methods that have been used in previous studies to fabricate 3D-blood capillary models.

the low cell invasion of the scaffolds, generally due to a too small pore size, and cell sheet is challenged by the difficulty to keep the tissue integrity and its low mechanical strength of the stacked cell sheet tissue.[14] All these limit their use as a tissue model for high-throughput assay. For instance, organ-on-chip technique which is strictly designed for *in vitro* applications is not suitable for the high-throughput system due to its complicated handling requirements and their biological issues due to the sources of the cells which are limited and of high cost (e.g. primary cells or induced pluripotent stem cell, iPSc).[11] Hydrogel also shows the ability to fabricate the 3D-tissue models owing to their biocompatibility and mechanical properties.[14,23,24] Recently photo-crosslinkable hydrogels in particular were developed, collagen-poly (ethylene glycol) diacrylate (PEGDA) hydrogel for instance providing cell-adhesive and tunable mechanical strength characteristics, suitable for vascular engineering applications.[23] Therefore, there is still a need for an *in vitro*, human tissue model that is simple, accessible, reproducible, and quick to produce which could fulfill the demand for the microarray analysis. The ability to fabricate functional human tissue would be beneficial for numerous applications not only for fluorescent probes screening but also for drug screening,[26] disease modeling,[27] or tissue and organ repair[28] applications. Over the past three decades, various functions of organs and tissues, such as the lung, liver, kidney, and gut, have been fabricated as *in vitro* models.[11] Previous report on the reconstruction of 3D-blood capillary models are subjected to certain limitations such as high time consumption and complicated handling

that make them unsuitable for high throughput assay.[14,28–31] Thus, a handy 3D platform of organized blood capillary models could provide more reliable data for the various required applications (as an example of screening fluorescent probe) instead of the conventional monolayer-cultured cells (**Figure 6**).

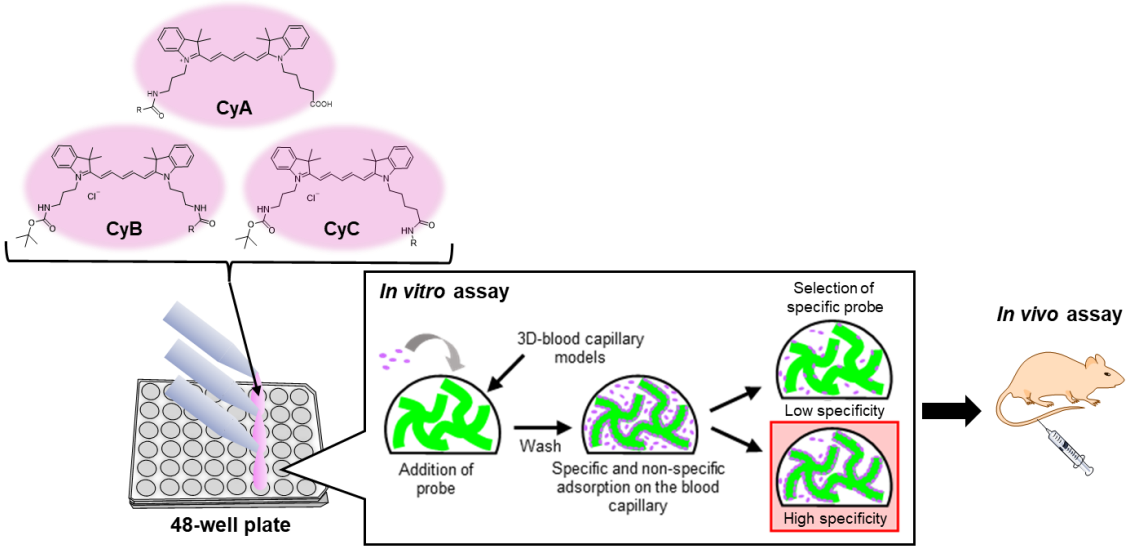

Figure 6. Schematic illustration shows *in vitro* assay process of the selection of the organic probe with the highest specific adsorption property on the surface of blood capillaries. The best probe was then further use for *in vivo* assay.

Outline of this thesis

This thesis includes the following four chapters.

Chapter 1

Fabrication of 3D-blood Capillary Models (3D-BCM) for Microarray Analysis of Near-Infrared (NIR) Chemical Probes Library

In this chapter, 3D-blood capillary models were constructed by using physiological collagen microfibers (CMF), which provide the extracellular matrix in the complex tissue. Micro-droplets of fibrin gels containing CMF, endothelial cells, and fibroblasts were cultured for five days in 48-wells plate to provide a medium-throughput system for screening applications. Blood capillaries networks were formed by optimizing the concentration of CMF used and the number of cells. Finally, this screening method was a powerful assay for the application on the selection of not only a specific chemical probe for blood capillary live-imaging, but also a drug, aptamer, and peptide with potential blood vessel targeting property.

Chapter 2

Screening of Near-Infrared Chemical Probes for *In vivo* Blood Vessels Imaging via 3D-blood Capillary Models

In chapter 2, we report the discovery of a blood vessel organic probe at near-infrared (NIR) wavelength range (BV-NIR) through an engineered blood capillary-based screening system, which is a more physiological model than a conventional cell culture condition. This selected Cy5 based probe showed the highest specific adsorption property out of 240 candidates on the endothelium and was equivalent to an anti-CD31 antibody in terms of intensity. The BV-NIR probe indicating strong and stable *in vitro*, *ex vivo*, and *in vivo* imaging of the endothelium even after histological immunostaining processes, shows potential as a convenient tool for live imaging as well as for co-visualization with a specific antibody.

Chapter 3

Mechanism Assay of Interaction between Blood Vessels-Near Infrared Probe and Cell Surface Marker Proteins of Endothelial Cells

In chapter 3, the discovery of a new near-infrared probe (CyA-B2) by screening chemical probe library in our previous report which showed the most specific binding on the blood capillaries of the 3D-tissue models gives us interest to study more about the binding site of this probe to the surface of endothelial cells main component cell of blood capillaries. By studying the competition assays of CyA-B2 using several potential surface markers of endothelial cells found through the chemical database (ChEMBL) and manually selected CD133 gave the lowest IC_{50} (half maximal inhibitory concentration) value. Hence, CD133 protein which is expressed on the endothelial cell membrane was postulated to be the binding site due to the suppression of CyA-B2 on the blood capillaries by the competition assays. Since, CD133 is also expressed on many types of cancer cells, it would be useful to use CyA-B2 as a bioprobe to monitor or diagnostic tumor growth.

Chapter 4

Near-Infrared Chemical Probes on the 3D-lymphatic Capillary Models (3D-LCM) and its Possible Target Protein

Finally, in chapter 4 the *in vitro* model screening method that was developed in chapter 1 inspired us to use it on other types of vascular tissue (lymphatic models, etc.). The 3D-lymphatic capillary models (3D-LCM) that was also prepared for high-throughput systems was then used to screen the chemical probe libraries.

References

[1] L. G. Freidus, P. Pradeep, P. Kumar, Y. E. Choonara, V. Pillay, *Drug Discovery Today* **2018**, *23*, 115.

[2] M. E. Åkerman, W. C. W. Chan, P. Laakkonen, S. N. Bhatia, E. Ruoslahti, *Proc. Natl. Acad. Sci. U. S. A.* **2002**, *99*, 12617.

[3] N. Nitin, L. E. W. LaConte, O. Zurkiya, X. Hu, G. Bao, *J. Biol. Inorg. Chem.* **2004**, *9*, 706.

[4] E. A. Schellenberger, F. Reynolds, R. Weissleder, L. Josephson, *ChemBioChem* **2004**, *5*, 275.

[5] X. Michalet, F. F. Pinaud, L. A. Bentolila, J. M. Tsay, J. Doose, J. J. Li, G. Sundaresan, A. M. Wu, S. S. Gambhir, S. Weiss, *Science (80-.).* **2005**, *307*, 538.

[6] X. H. Peng, X. Qian, H. Mao, A. Y. Wang, Z. G. Chen, S. Nie, D. M. Shin, *Int. J. Nanomedicine* **2008**, *3*, 311.

[7] J. A. Joyce, P. Laakkonen, M. Bernasconi, G. Bergers, E. Ruoslahti, D. Hanahan, *Cancer Cell* **2003**, *4*, 393.

[8] G. R. Rosania, J. W. Lee, L. Ding, H. S. Yoon, Y. T. Chang, *J. Am. Chem. Soc.* **2003**, *125*, 1130.

[9] R. Weissleder, K. Kelly, E. Y. Sun, T. Shtatland, L. Josephson, *Nat. Biotechnol.* **2005**, *23*, 1418.

[10] B. K. Wagner, H. A. Carrinski, Y. H. Ahn, K. K. Yun, T. J. Gilbert, D. A. Fomina, S. L. Schreiber, Y. T. Chang, P. A. Clemons, *J. Am. Chem. Soc.* **2008**, *130*, 4208.

[11] H. Kimura, Y. Sakai, T. Fujii, *Drug Metab. Pharmacokinet.* **2018**, *33*, 43.

[12] K. Bhadriraju, C. S. Chen, *Drug Discov. Today* **2002**, *7*, 612.

[13] M. D. Sarker, S. Naghieh, N. K. Sharma, X. Chen, *Journal of Pharmaceutical Analysis* **2018**, *8*, 277.

[14] M. A. Abdul Sisak, F. Louis, M. Matsusaki, *Polymer Journal* **2020**, *52*, 871.

[15] C. Tomasina, T. Bodet, C. Mota, L. Moroni, S. Camarero-Espinosa, *Materials* **2019**, *12*, DOI 10.3390/ma12172701.

[16] L. Ouyang, J. P. K. Armstrong, Q. Chen, Y. Lin, M. M. Stevens, *Advanced Functional Materials* **2020**, *30*, DOI 10.1002/adfm.201908349.

[17] A. Brown, H. He, E. Trumper, J. Valdez, P. Hammond, L. G. Griffith, *Biomaterials* **2020**, *243*, 119921.

[18] R. Ichiro Tanaka, K. Sakaguchi, S. Umezu, *Artificial Life and Robotics* **2020**, *25*, 199.

[19] B. A. Juliar, J. A. Beamish, M. E. Busch, D. S. Cleveland, L. Nimmagadda, A. J. Putnam, *Biomaterials* **2020**, *230*, DOI 10.1016/j.biomaterials.2019.119634.

[20] D. B. Kolesky, K. A. Homan, M. A. Skylar-Scott, J. A. Lewis, *Proc. Natl. Acad. Sci. U.S.A.* **2016**, *113*, 3179.

[21] D. T. T. Phan, X. Wang, B. M. Craver, A. Sobrino, D. Zhao, J. C. Chen, L. Y. N. Lee, S.C. George, A. P. Lee, C. C. W. Hughes, *Lab Chip* **2017**, *17*, 511.

[22] A. Hasan, A. Memic, N. Annabi, M. Hossain, A. Paul, M. R. Dokmeci, F. Dehghani, A. Khademhosseini, *Acta Biomaterialia* **2014**, *10*, 11.

[23] J. Ru Choi, K. Wey Yong, J. Yu Choi, A. C Cowie, *BioTechnique* **2019**, *66*, 40.

[24] Y. Zhu, Q. Zhang, X. Shi, D. Han, *Advanced Materials* **2019**, *31*, 1.

[25] M. Clotworthy, *Expert Opin. Drug Discov.* **2012**, *7*, 543.

[26] B. S. Freedman, C. R. Brooks, A. Q. Lam, H. Fu, R. Morizane, V. Agrawal, A. F. Saad, M. K. Li, M. R. Hughes, R. Vander Werff, D. T. Peters, J. Lu, A. Baccei, A. M. Siedlecki, M. T. Valerius, K. Musunuru, K. M. Mcnagny, T. I. Steinman, J. Zhou, P. H. Lerou, J. V Bonventre, *Nat. Commun.* **2015**, *6*, 1.

[27] R. Langer, J. P. Vacanti, *Science (80-.).* **1993**, *260*, 920.

[28] H. Sekine, T. Shimizu, K. Sakaguchi, I. Dobashi, M. Wada, M. Yamato, E. Kobayashi, M. Umezu, T. Okano, *Nat. Commun.* **2013**, *4*, 1399.

[29] J. S. Jeon, S. Bersini, M. Gilardi, G. Dubini, J. L. Charest, M. Moretti, R. D. Kamm, *Proc. Natl. Acad. Sci. U. S. A.* **2015**, *112*, 214.

[30] N. Jusoh, S. Oh, S. Kim, J. Kim, N. L. Jeon, *Lab Chip* **2015**, *15*, 3984.

[31] Y. Nashimoto, T. Hayashi, I. Kunita, A. Nakamasu, Y. S. Torisawa, M. Nakayama, H. Takigawa-Imamura, H. Kotera, K. Nishiyama, T. Miura, R. Yokokawa, *Integr. Biol. (United Kingdom)* **2017**, *9*, 506.

Chapter 1

Fabrication of 3D-blood Capillary Models (3D-BCM) for Microarray Analysis of Near-Infrared (NIR) Chemical Probes Library

1.1. Introduction

The regular method of screening compounds in the field of drug discovery begins with the 2D cell culture-based assays, followed by animal model assays, before reaching the clinical trials.[1] However, in these methods, many of the drugs fail during clinical trials, which might be due to a lack of clinical efficacy and/or an unacceptable toxicity.[2] Even though the 2D cell-based assays are effective for preliminary screening at least to have information on cytotoxicity, they sometimes provide misleading and non-predictive data for *in vivo* responses due to their unnatural microenvironments.[3] Therefore, the creation of a technique for constructing a three-dimensional (3D) tissue having a structure and function similar to a living body *in vitro* is strongly demanded and could also provide more reliable data for various applications.

To fulfill the demand in the medical field, research on constructing a tissue having such 3D structure *in vitro* has been actively conducted to form a model as similar as possible to the living body.[4] Numerous studies on fabrication techniques of blood capillary models have been reported, such as bio-printing, organ-on-chip or microfluidic device, electrospinning techniques, cells sheet as well as scaffold structure.[5-11] However, all these methods have limitation to be used as a high-throughput assay. For instance, organ-on-chip technique which is strictly designed for *in vitro* applications is not suitable for the high-throughput system due to its complicated handling requirements and their biological issues due to the sources of the cells which are limited and of high cost (e.g. primary cells or induced pluripotent stem cell, iPSc).[12] However, there is still a need for an *in vitro*, human tissue model that is simple, accessible, reproducible, and quick to produce which could fulfill the demand for the microarray analysis.

Generally, tissues are composed of cells and extracellular matrix (ECM). The ECM is a complex 3D matrix that guides cell adhesion, proliferation, differentiation, morphology, and gene expression.[13] While several synthetic components were already used for recreating engineered vasculature, natural components are generally found more suitable, especially in form of hydrogel, being similar in nature to ECM. Hydrogel also shows the ability to fabricate the 3D-tissue models owing to their biocompatibility and mechanical properties.[6,14,15] Fibrin is one of the examples of natural biomaterial used in tissue engineering which derives from the native ECM.[16,17] Fibrin is also one of the natural polymers that had been used in vascular tissue models for various applications such as implantation [18] and tissue engineering.[19-21] The main advantages of using natural materials to support cells in tissue models are that these molecules are naturally recognized by cells and are more probable to stimulate physiological responses in cells such as cells migration, proliferation, and remodeling of the matrix.

In our previous study, we have fabricated a spheroid called tissue balls using collagen microfibers (Figure S1a). However, due to the thickness (>500 µm) and the high turbidity of the tissue balls, it has a limited observation ability. Nonetheless, the fact to use collagen microfibers dispersion instead of classic collagen gels made by dilution allows to reach a final high concentration which is more similar to *in vivo*. This fibers form allows also to provide a physiologic environment for the cells, allowing forces and energy transmissions, as well as biological signals regulating cells functional responses, especially for vasculature formation through integrin-induced adhesion of endothelial cells.[22] Therefore, the solution for these issues leads to a thinner and more transparent tissue in order to overcome the thickness and turbidity issues, respectively. Here, we fabricated the 3D-blood capillary models using collagen microfibers (CMF) [22-25] where fibrin acts as a tissue scaffold. A micro-droplet of tissue consisting of a coculture of HUVEC and fibroblast in an optimized amount of CMF with a constant concentration of fibrinogen and thrombin was seeded on each of the wells to be cultured in a 48-well plate and to serve as a microarray analysis for screening of chemical probes as an example of application.

1.2. Experiment

1.2.1. Materials

Collagen I sponge was kindly donated by Nippon Ham Foods Ltd. Osaka, Japan. Normal human dermal fibroblast (NHDF, CC-2509), human umbilical vein endothelial cells (HUVECs, C2517A), and Endothelial Cell Growth Medium-2 (EGM-2, CC-4147) were purchased from Lonza (Basel, Switzerland). GFP expressed human umbilical vein endothelial cells (GFP-HUVECs) was purchased from Angio-Proteomie (Massachusetts, USA). Trypsin was purchased from Gibco BRL, Life Technologies (Rockville, MD, USA). Dulbecco modified Eagles's medium (DMEM High-Glucose, 08458) and 4% paraformaldehyde (PFA, 09154-85) were purchased from Nacalai tesque (Kyoto, Japan). Anti-CD31 antibody was purchased from Dako (M0823, Hamburg, Germany). Thrombin (T4648), fibrinogen (F8630), phosphate-buffered saline (PBS, D5652), Triton-X 100 (T8787), and bovine serum albumin (BSA, A3294) were purchased from Sigma-Aldrich (St. Louis, MO, USA). Alexa 647 (anti-mouse, A21235) was purchased from Invitrogen (Waltham, MA, USA). Hoechst 33342 (H3570) was purchased from Thermo Fisher Scientific (Waltham, MA, USA). SDS-Tris-Glycine (DCB-423468), Tris SDS (DCB-423437), Page Blue 83 Stain Reagent (CBB-R250, DCB-423406), and protein marker (SIMASIMA Prestained Broad Range Protein, DCB- SS2000-3) were purchased from Cosmo Bio Co. Ltd.

1.2.2. Preparation and Characterization of Collagen Microfibers (CMFs)

For the preparation of collagen microfibers (CMFs), we used the method described in our previous study.[25] Briefly, collagen I sponge was crosslinked in a vacuum dryer (HD-15H, iLW, Osaka, Japan) and then incubated at 200 °C for 24 h. Subsequently, crosslinked collagen I (10 mg/mL in Milli-Q water) was homogenized (Violamo VH-10 homogenizer, AS ONE, Osaka, Japan. S10N-10G with 10 mm diameter and 115 mm length probe) for 6 min and subsequently sonicated (VC50, Sonics and Materials, Newtown, CT, USA) for 20 s/cycle (100 cycles) with cooling in an ice bath for 10 s, resulting in smaller size fragments of collagen. The dispersion was filtered by a 42 μm nylon mesh (PA-42, AS ONE, Osaka, Japan) and then freeze-dried (Freeze dryer FDU-2200, Eyela Co., Tokyo, Japan) for three days. The obtained CMF was kept in a

desiccator at room temperature until use. The average length of CMF was measured from the phase contrast microscopy image while using ImageJ software (version 1.53a, National Institute of Health, Bethesda, MD, USA).

The characterization of CMF was previously reported.[22] Briefly, there are two types of CMF which are after homogenization (CMF-200) and sonication (CMF-50) treatment, respectively. The characterizations of CMF-200 were analyzed by circular dichroism (CD) spectrum and sodium dodecyl sulfate-polyacrylamide gel electrophoresis (SDS-PAGE) to check the triple helix structure and molecular weight, respectively. It was not possible to check the CMF-50 using the same methods due to the insolubility of cross-linked fiber in the organic solvent. However, we believe that the characteristics of the collagen were still maintained even after sonication treatment.

Circular dichroism (CD): CD spectra were obtained using a CD spectrometer (JASCO model PTC-348WI, J-1500, Tokyo, Japan). The samples (0.05 mg/mL) were prepared in acetic acid (50 mM) in a quartz cell. Spectra were recorded from 200 to 250 nm with 0.5 nm increments at a scanning rate of 100 nm/min. Raw CD signal was normalized by the concentration and by the number of residues.

SDS-PAGE: Samples (0.5 wt. %) were diluted in running buffer for SDS-Tris-Glycine. Samples were then mixed with β-ME sample treatment for Tris SDS for sterilization. Next, samples were heated at 90 °C for 5 min and then 5 µL of protein marker (SIMASIMA Prestained Broad Range Protein) and 10 µL of sample were loaded onto a polyacrylamide gel in the running buffer. Electrophoresis was carried out at 20 mA per gel for 56 min. After that, samples in the gel were staining with Page Blue 83 Stain Reagent (CBB-R250) for 1 h and subsequently destaining the samples in a solution containing water (87.5%), methanol (5%), and acetic acid (7.5%). The molecular weight of each band of collagen were visualized on a Bio-Rad ChemiDoc^{TM} MP Imaging System.

1.2.3. Fabrication of the 3D-Blood Capillary Models (3D-BCM) in 48-Well Plate

For the preparation of 3D-blood capillary models, we used the method as described in our previous study.[22] Briefly, normal human dermal fibroblast (NHDF) and human umbilical vein endothelial cells (HUVECs) were trypsinized (5 min, 37 °C) and

then centrifuged at 1000 rpm for 5 min at room temperature for collecting the cells by removing the supernatant. 5 U/mL of thrombin was mixed with cells (NHDF and HUVEC) in Dulbecco modified Eagles's medium (DMEM High-Glucose) and regarded as solution 1. Then, solution 2 comprising 15 mg/mL of CMF-50 mixed with 5 mg/mL of fibrinogen in DMEM (FBS free). Thus, the 10 µL of fibrin gels containing 0.15 mg of CMF-50, 1.5 x 10^4 of NHDF, and 7.5 x 10^3 of HUVECs (or green fluorescent protein labeled HUVEC/GFP-HUVEC for studying vascular network formation in live imaging analysis) were seeded in each well of a 48-well plate. After that, the tissue drops were incubated at 37 °C for 30 min to allow the gelation process upon the reaction of fibrinogen and thrombin. The steps were repeated for different concentrations of CMF (0, 5, 10, 20 and 25 mg/mL) and different volumes of seeded drops [5 µL (2.5 µL solution 1 + 2.5 µL solution 2) and 30 µL (15 µL solution 1 + 15 µL solution 2)]. Number of cells for different volumes of seeded drops was also changed [5 µL (7.5 x 10^3 of NHDF and 3.75 x 10^3 of HUVECs) and 30 µL (4.5 x 10^4 of NHDF and 2.25 x 10^4 of HUVECs)]. Finally, the tissues were cultured for 5 days at 37 °C, 5 % CO_2, with mixed cell culture medium which is DMEM and Endothelial Cell Growth Medium-2 (EGM-2) at ratio 1:1. The mix culture medium was changed every 2 days.

1.2.4. Immunofluorescence Staining and Histological Analysis

After 5 days of culture, the tissues were fixed with 4% paraformaldehyde (PFA) for 20 min at room temperature (RT). Then, the tissues were evaluated in order to know the capillary network formation using immunofluorescence staining of the endothelial cell surface marker: CD31. First, the cells in the tissue were rinsed 3× in phosphate-buffered saline (PBS) and permeabilized with 0.2 % Triton-X 100 in PBS for 20 min at RT. Next, 1 % of bovine serum albumin (BSA) in PBS was added into the tissue for 60 min to block the unspecific staining of the antibody. After washing 3× with PBS, tissues were incubated with the CD31 primary antibodies (1:100, diluted in 1% BSA in PBS) overnight at 4 °C. Later, tissues were washed 3× with PBS and then the secondary antibody, Alexa 647 (anti-mouse, 1:200 in PBS with 1 % BSA), mixed with Hoechst 33342 for nuclei staining (1:1000 in PBS with 1 % BSA), was added and incubated for 1 h at RT. The images were obtained using a confocal laser scanning microscopy (CLSM,

CQ1 from Yokogawa Corporation). For histology analysis, the fixed 3D tissues were washed 3× with PBS and sent to the Applied Medical Research company (Osaka, Japan) for paraffin embedding and immunohistochemistry. Sectioned 3D tissues were stained with hematoxylin eosin (HE) or CD31 staining. Images were obtained using a FL EVOS Auto microscope (Thermo Fisher Scientific) for measuring the tissue thickness and observing the lumen of the capillaries.

1.2.5. Analysis of Blood Capillaries Formation

To quantify blood capillary formation, the mean fluorescence intensity of the total area (2D image) of the blood capillaries was measured by ImageJ software. The fluorescence intensity was given by the fluorescence image of the anti-CD31 antibody (specific marker for endothelial cells) bounded with its secondary antibody (Alexa 647). In addition, total branching points (indicates the connecting point of the blood capillaries) were analyzed by Imaris software (ver. 9.2.1, Oxford Instruments), using the "Filament Algorithm" function.

Statistical analysis: All data are presented as mean ± standard deviation (s.d.), from three independent experiments unless otherwise specified. Statistical comparisons between groups were analyzed using two-tailed Student's *t*-tests. A *p*-value *<0.01 and **<0.001 was considered to be statistically significant. *N.S.* indicates no significant difference. Statistical analysis for Figure 1.9d and Figure 1.10b were performed using EzAnova software (version 0.98) with Tukey multiple comparison test (one-way ANOVA). A *p*-value *<0.05, **<0.01 and ***<0.001 was considered to be statistically significant. *N.S.* indicates no significant difference.

1.3. Results and discussion

1.3.1. Preparation of Collagen Microfibers (CMFs) and its Characterization

The CMF was named as CMF-200 and CMF-50, as the average length was obtained at around 197 ± 35.6 μm and 47 ± 12.8 μm for the CMF before and after the sonication step, respectively (**Figure 1.1a**). In **Figure 1.1b**, the results of CD spectral analysis showed a positive peak at around 215 to 225 nm, similar to collagen I (native),

confirming that the CMF was not denatured and that the triple helical structure of the collagen molecule was still maintained even after the homogenization process.[25,26] In parallel, the molecular weight of CMF by SDS-PAGE revealed the typical pattern for type I collagen chains, with bands at 210 kDa (β), 130 kDa (α1), and 120 kDa (α2) molecular weights. Thus, it was confirmed that the characteristics of CMF to the collagen were not altered following the homogenization process.

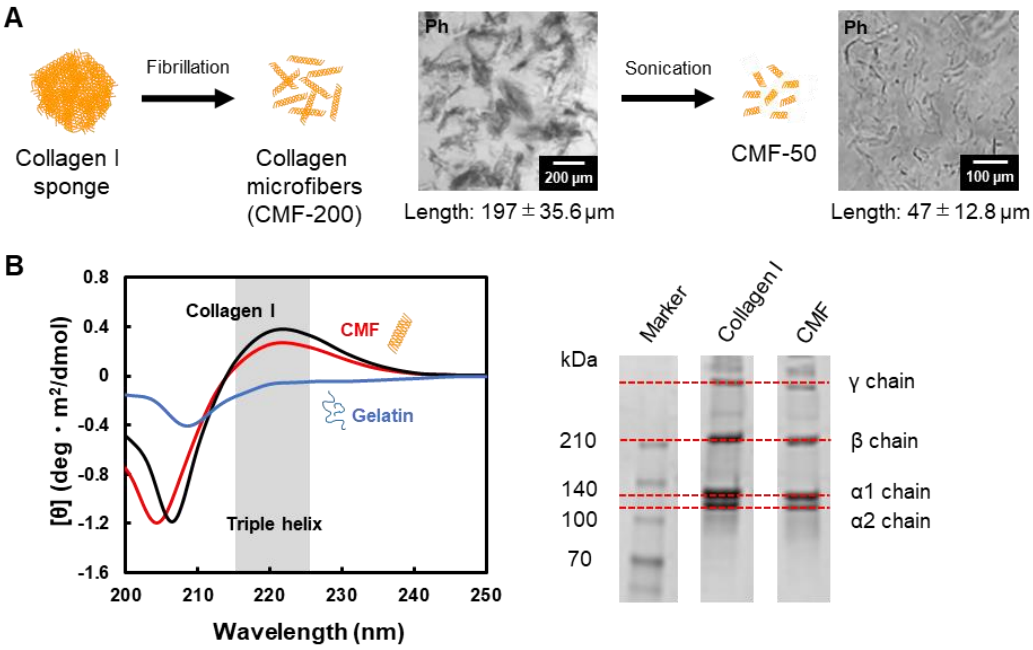

Figure 1.1. (**a**) Preparation of collagen microfibers 200 and 50 (CMF 200 and CMF 50, respectively) and their phase contrast (Ph) images to indicate the lengths. (**b**) Circular Dichroism (CD) spectrum of CMF to demonstrate that its helical structure was maintained after homogenization treatment (left). The SDS-PAGE measurement (right) to show the retained molecular weight of CMF after homogenization treatment. CMF was compared with collagen type I and gelatin for CD measurement and collagen I for SDS-PAGE.

1.3.2. The Effect of CMF-50 and CMF-200 on the Vasculature Formation

In the previous study, the 3D-blood capillary models were fabricated by coculture between NHDF and HUVEC and seeding together with CMF in a 96-well non-adherent plate (modified method from [23,24]). Then, the mixtures were centrifuged to undergo the sedimentation process of the cells and the CMF. After one day of culture in the 96-well

it resulted in a sphere shape (called as tissue ball) as shown in **Figure 1.2**. However, as we observed the blood capillary networks of the tissue balls (2 mm of ball diameter) by CLSM, the images of blood capillaries (as demonstrated in **Figure 1.2**) were not possible to fully observe, especially in the centre of the tissue which might be due to the limitation of the CLSM, unable to scan a thickness of more than 500 µm. Besides that, high turbidity of the tissue balls also limits the penetration of laser through the tissue. Only tissue clarifying can increase the lens working distance, but it is not compatible with live imaging.[27] Thus, the solution was to produce a thinner and more transparent tissue.

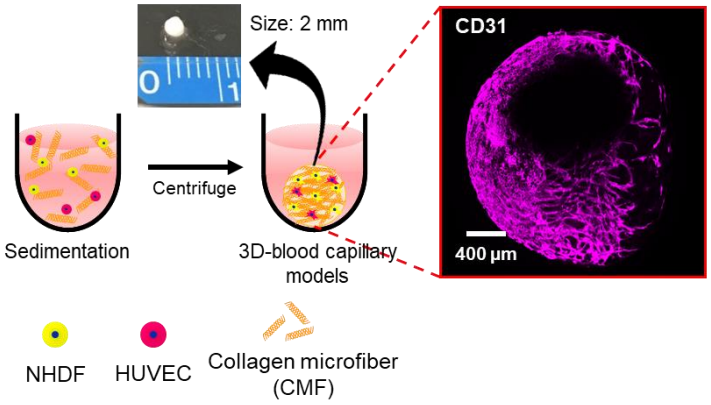

Figure 1.2. Preparation of 3D-blood capillary models using 'sedimentary culture' methods. The confocal image showed the dark area in the centre of tissue balls.

Then, from the previous preparation of CMF, a comparison was performed between the CMF-200 and CMF-50 for the formation of vascular networks in the 3D-models, embedded in a fibrin gel (**Figure 1.3a**). CLSM images of tissues using CMF-50 showed the formation of vascular networks whereas the CMF-200 could not induce good vasculature network probably due to the observed aggregation of the CMF in the tissues which disturbs the cell-cell interaction. No aggregation of CMF was shown for CMF-50 which was found homogenously distributed throughout the tissues, subsequently allowing a more homogenous formation of vasculature. Therefore, the CMF-50 tissue had significantly higher CD31 fluorescence volume (3.1-fold higher) as well as the number of branch points (5.9-fold higher) compared to the CMF-200 as illustrated by the graph in **Figure 1.3b**.

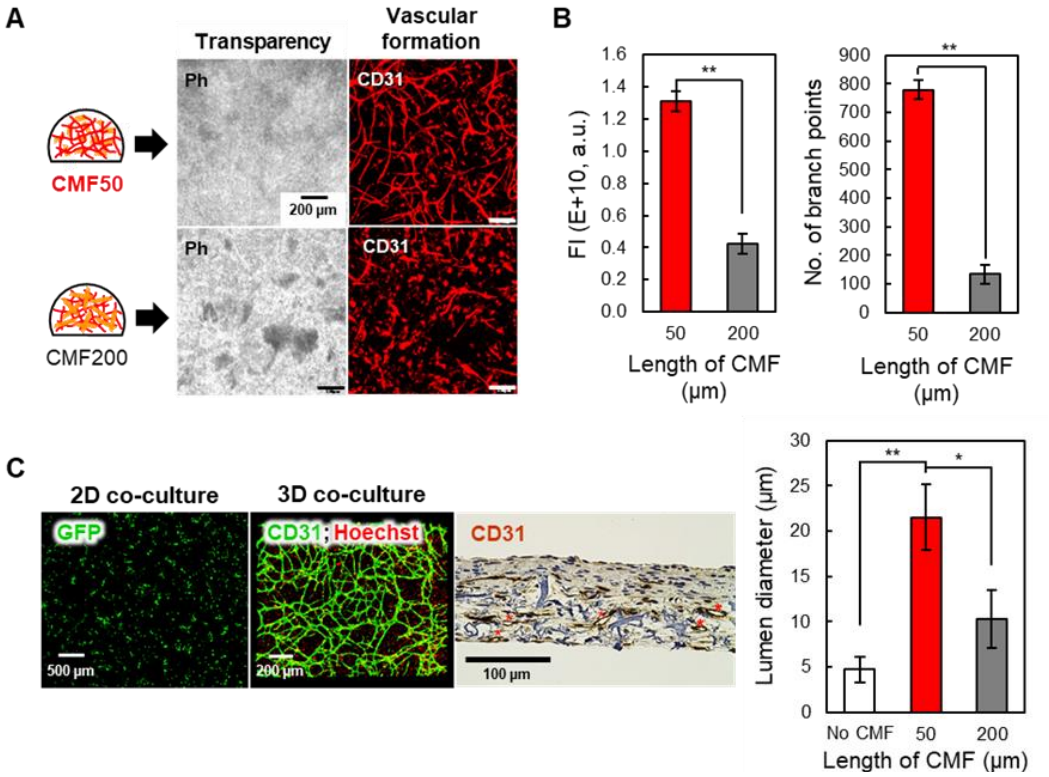

Figure 1.3. (**a**) The effect of CMF-50 and CMF-200 on the vascular formation. The phase contrast images were used to indicate the transparency of the 3D-tissue and anti CD31 antibody was used to demonstrates the formation of vascular networks in the 3D-tissue models. (**b**) Quantification graphs of fluorescence area and total intensity of branch points for comparison between the 3D tissues made from CMF-50 and CMF-200. These data were quantified using IMARIS software. Data presented as mean ± s.d., (n=3), $*p < 0.05$, $**p < 0.01$. (**c**) The difference between 2D and 3D co-culture of HUVEC and NHDF for the formation of blood capillaries network (shown by GFP and CD31 and the histology image show the vascular lumen (red asterisk) on the 3D-tissue models with CMF-50. The graph shows the lumen diameter of 3D-blood blood capillary models when using CMF 0, CMF-50 and CMF-200. The lumen diameter was measured by histology data. Data presented as mean ± s.d., (n=3), $*p < 0.05$, $**p < 0.01$.

In addition, the formation of blood capillary networks in the 3D co-culture was compared to the 2D monolayer co-culture as illustrated in **Figure 1.3c**. The capillary networks were absent in 2D co-culture (visualized from GFP labeled endothelial cells) while in the 3D co-culture the vasculature structure was successfully formed. This was further confirmed by histological staining on 3D co-culture system that showed vascular lumens (red asterisk in **Figure 1.3c**). This was basically due to the presence of CMF that

interacts with the integrins of the endothelial cells to induce open lumen vascularization as well as acting as a microscaffold to maintain the 3D tissue structure.[22] While CMF-200 allowed an increase in the size of the lumens observed (10 ± 3 µm, mean inner diameter), compared to tissues without any CMF, CMF-50 was found with a lumen diameter greater than 20 µm (21 ± 4 µm), due to the larger spaces between the fibers [22], suitable for endothelial cell migration, capillary maturation, and for opening up the vascular lumen structure.

1.3.3. Fabrication of 3D-blood Capillary Models (3D-BCM)

In this study, a 3D blood capillary model was fabricated using fibrin gel which could be the key to provide a thinner and less turbidity tissue for live imaging in order to address the issues from the previous tissue balls models. The CMF was also further sonicated after the homogenization process to get smaller fragments (CMF-50), which allow to overcome the issue of aggregation occurring with the bigger size CMF-200, resulting in the less formation of blood capillaries. Therefore, CMF-50 was further used for the fabrication of 3D-blood capillary models.

The next step was to optimize the seeding process. As mentioned in the methods part, two solutions containing different compounds need to be mixed to activate the gelation process. The different possible sequences of order for the mixing of the two solutions were thus compared by dropping first the solution 1 (cells and thrombin) and then the solution 2 (CMF and fibrinogen) and the opposite way. As shown in **Figure 1.4a**, the tissues with the order of solution 1 on solution 2 gave a homogenously capillary network compared to the heterogeneous network on the tissues with the order of solution

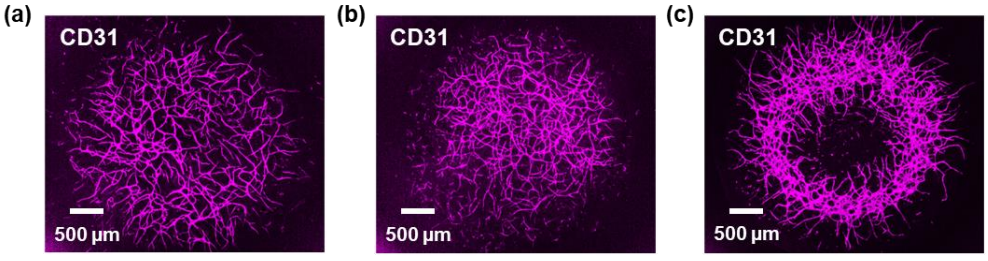

Figure 1.4. The sequence of the drop between solution 1 (thrombin with cells) and solution 2 (fibrinogen with CMF 50). (**a**) Solution 1 → Solution 2, (**b**) Solution 2 → Solution 1, and (**c**) Solution 1→ Solution 2 with mixing.

2 on solution 1 (**Figure 1.4b**). In addition, the importance of the mixing step after dropping the two solutions for the tissues was checked, resulting in an empty capillary network area in the middle of the tissues, probably due to a heterogeneous aggregation of the CMF in the centre of the drop tissues (**Figure 1.4c**).

Hence, we chose the sequence with the order of solution 1 to solution 2, without mixing, for the further experiments. The validity of this method for microarray analysis was characterized by its culture inside a 48-well plate to serve as medium-high throughput microarray analysis. The quantification of each sample for the mean fluorescence intensity of their CD31 endothelial marker and its total branching points using ImageJ and Imaris softwares, respectively. The 3D-blood capillary models were successfully cultured and observe by CLSM (**Figure 1.5**) in a reproducible way. For the mean fluorescence intensity (**Figure 1.6a**), the results showed that all the 48 samples of a 48-wells plate had a similar fluorescence intensity (36.0 ± 1.8). Their total branching points (**Figure 1.6b**), which indicate complexity of the network formation, were successful found in the range of 1020 to 1620 (1292.2 ± 174.9) as measured by Imaris software.

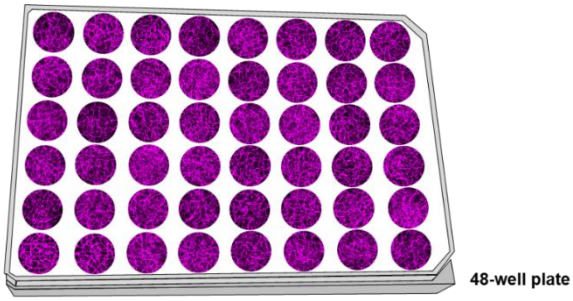

Figure 1.5. Representative CD31 immunostaining (endothelial marker) of the 48 different 3D-blood capillary models constructed in the medium-throughput 48-well plate illustration.

1.3.4. The Effect of Different Amounts of CMF in the 3D-BCM

Before obtaining the reproducibility of the Figure 1.5 model, we also investigated the effect of amounts of CMF in the 3D-blood capillary models and optimized it. Different amounts of CMF (0, 0.05, 0.1, 0.15, 0.2 and 0.25 mg per drop tissue) were used and cultured in the same condition as described in the methods. After being cultured for 5 days, the 3D-tissue models were fixed and immunostained by the anti-CD31 antibody

(specific marker for endothelial cells) whose fluorescence was monitored and observed by CLSM as shown in **Figure 1.7a**. From the quantification data of the mean fluorescence intensity (**Figure 1.7b**), all conditions excepted the 0.15 mg of CMF showed a significantly lower CD31 staining, compared to the condition without CMF. This phenomenon also happened for total branching points data (**Figure 1.7c**). Although the tissue model without CMF seemed to form similar blood capillary network than the 0.15 mg CMF one, the thickness of the tissue was later found much thinner compared to the 0.15 mg CMF tissue model (**Figure 1.7d, left**), as measured on the histology data. These results showed that the CMF could act as a filler to provide a thicker tissue. Therefore, this higher thickness provided by the CMF induced significantly higher opened lumen structures of the blood capillaries as shown in the tissue section of the histology data (red

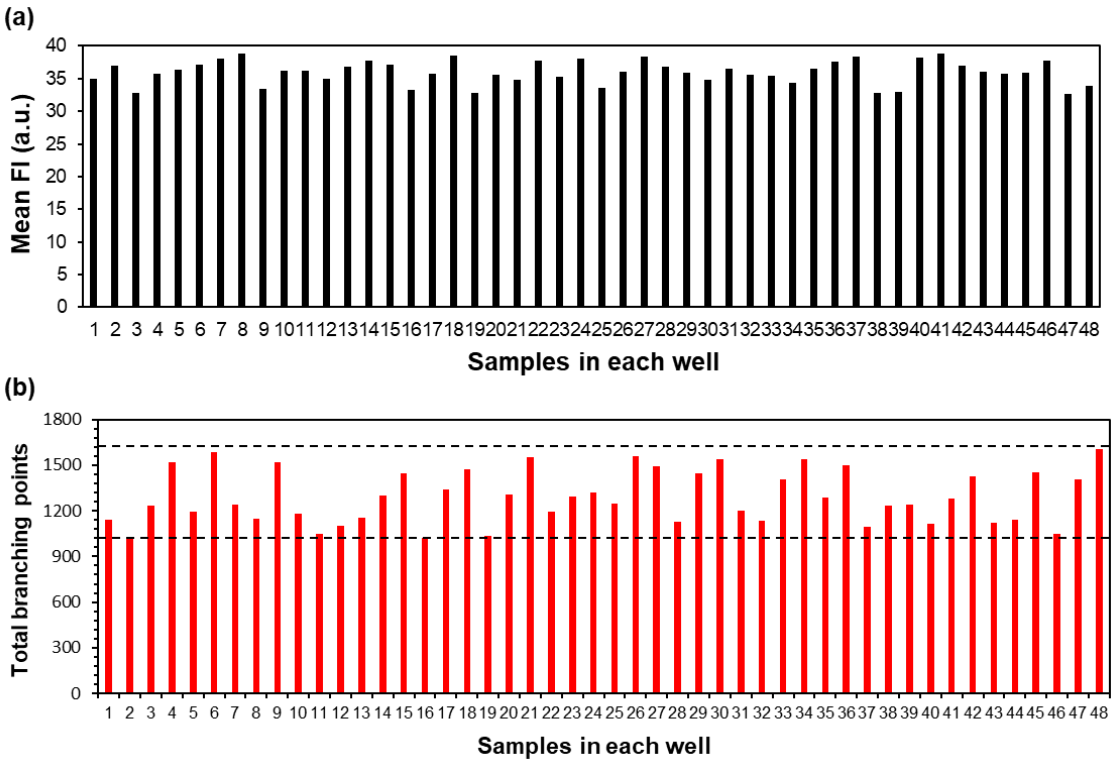

Figure 1.6. Assessment of the reproducibility of the three-dimensional (3D) model of blood capillary to be used as a microarray assay. (**a**) Mean fluorescence intensity of each sample in a 48-well plate. (**b**) Total branching points from each of the 3D-blood capillary models (48 samples). Dotted lines indicate the range of the branching points of all samples in the plate (1020–1620) to validate the quality of each sample.

asterisk) in **Figure 1.7d, right** (2.31 ± 0.22 μm and 20.93 ± 0.55 μm of inner diameters for 0 and 0.15 mg CMF, respectively).[22]

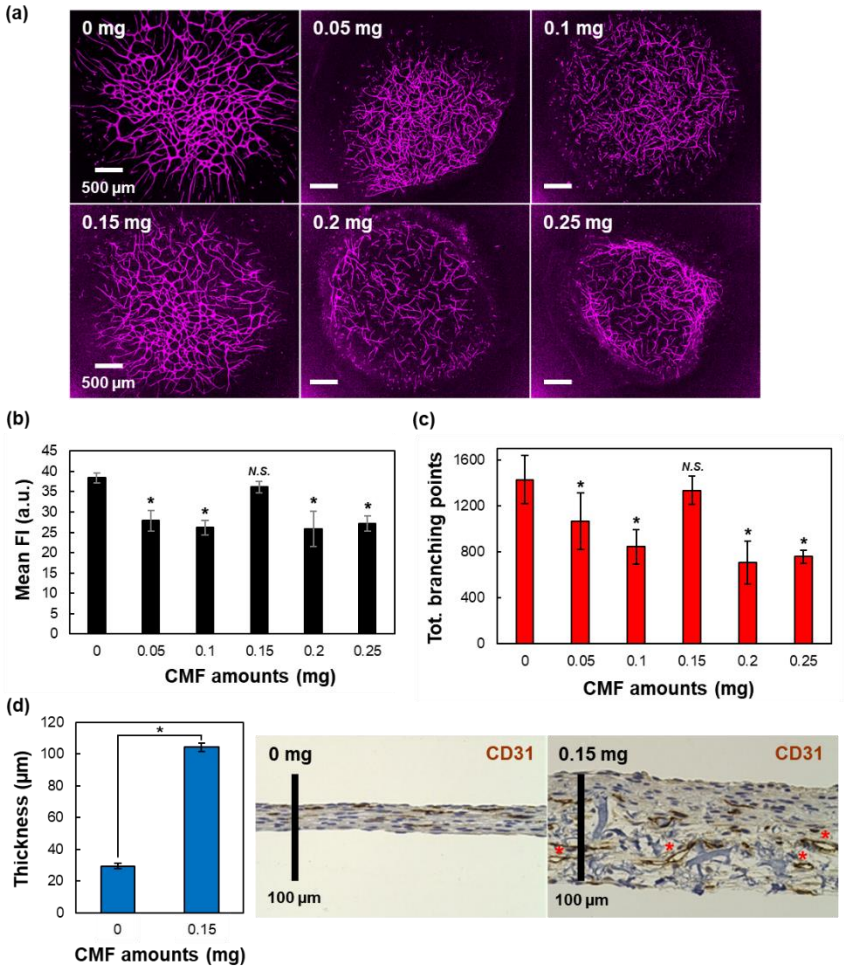

Figure 1.7. The effects of using different amounts of collagen microfibers (CMFs) in fibrin gels. (**a**) Confocal images of 3D-blood capillary models with different amounts of CMF (0, 0.05, 0.10, 0.15, 0.20, and 0.25 mg). The blood capillaries were immunostained by anti-CD31 antibody and fluorescence using Alexa Fluor 647. (**b**) Quantification data for mean fluorescence intensities and their (**c**) total branching points for each sample in different CMF amounts. (**d**) Histology data showing the open lumen (red asterisk) and the graph of thickness between 3D tissue of blood capillary using 0 mg and 0.15 mg of CMF, respectively. Data are presented as mean ± s.d. (*) indicates that data are significantly different ($p < 0.01$). *N.S.* indicates no significant difference.

1.3.5. The Role of NHDF for the Vasculature Formation

NHDF is the fibroblast cells that generally support the vascular formation. For the next optimization step, we also investigated the necessity of NHDF in coculture with

HUVEC in our tissues. The tissue was observed by CLSM and the images of the blood capillaries network were acquired as shown in **Figure 1.8a**. From the images, the importance of NHDF for the vascular formation was clearly highlighted, the tissues without NHDF presenting almost only individual endothelial cells not connected in a vasculature network. The analysis of the mean CD31 fluorescence intensity of the tissue with and without NHDF confirmed that the tissues with NHDF had higher vascular structures than the tissues without (**Figure 1.8b**). This result was supported by the total branching points analysis that also significantly showed a higher branching or networking for the tissues with NHDF compared to tissues without (**Figure 1.8c**). From this experiment, we could confirm the already reported important role of the NHDF as supporting cells for vascular formation.[28,29]

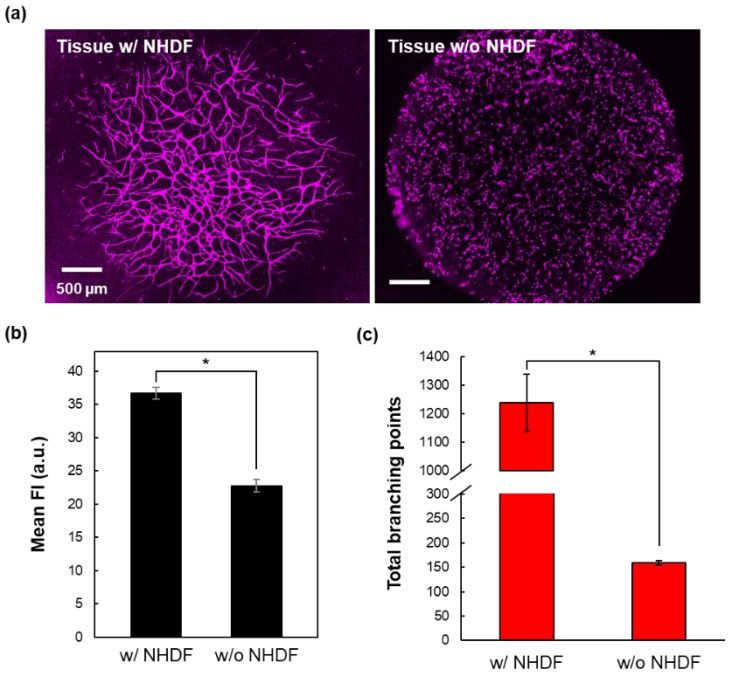

Figure 1.8. Normal human dermal fibroblast (NHDF) role for vasculature formation in CMF-fibrin gels. (**a**) Representative confocal images of 3D-blood capillary models with (left) and without NHDF (right). The blood capillaries were immunostained by anti-CD31 antibody. Comparison between with and without NHDF in the 3D-blood capillary models by mean fluorescence intensity (**b**) and total branching points (**c**). Data are presented as mean ± s.d. (*) indicates that data are significantly different ($p < 0.01$).

1.3.6. Importance of the Cell Culture Medium Volume during the Culture

The ability to culture the 3D-blood capillary model was further investigated in particular for its use in microarray analysis. In this study, we used 48- and 96-wells plates to serve as medium and high-throughput assays, respectively. The 3D-tissues which were cultured in 48- and 96-wells plates were of the same volume (10 µL drop), but the available well volumes allowed to add more culture medium in the 48-well plate. After 5 days of culture, the tissues were observed by CLSM as shown in **Figure 1.9a** leading to 96-wells plate tissues showing a lower vascular formation network compared to the tissues in the 48-wells plate. This might be due to the insufficient culture medium volume in the 96-wells plate (300 µL of culture medium), compared to the 48-wells plate (1.2 mL of culture medium), even when the culture medium in the 96-wells was changed every day. The quantification data confirmed that the mean fluorescence intensity and total branching points of tissues in the 48-wells plate were significantly higher than that in the 96-wells plate tissues (**Figure 1.9b**).

1.3.7. Comparison of Different Volumes of Seeded Drops of 3D-BCM

As in the previous experiments, the 10 µL volume of drops was arbitrary chosen for the investigations, we then decided to optimize the volume of the drops by lowering (5 µL) and increasing (30 µL) the final drop volume. In this study, the conditions were kept constant except for cells number. After 5 days of tissues culture, the 5 µL conditions was found with partially formed capillaries network, mainly in the centre of the drops, compared to the 10 and the 30 µL tissues (**Figure 1.9c**). This was proven by the mean CD31 fluorescence intensity and the total branching points data where the 5 µL tissues were significantly lower than the tissues with a volume of 10 µL (except mean CD31 fluorescence intensity) and 30 µL (**Figure 1.9d**). Although 30 µL tissues could also successfully form networks, the final diameter of the tissues was much larger compared to 10 µL tissues. This larger tissue leaded to uneasy image acquisitions by confocal microscopy when using the high magnification of objective lens (4×), requiring several images to reconstruct the full tissue image. This fact makes the 30 µL drops model inconvenient and particularly unsuitable for the quantification analysis of the high-throughput screening process.

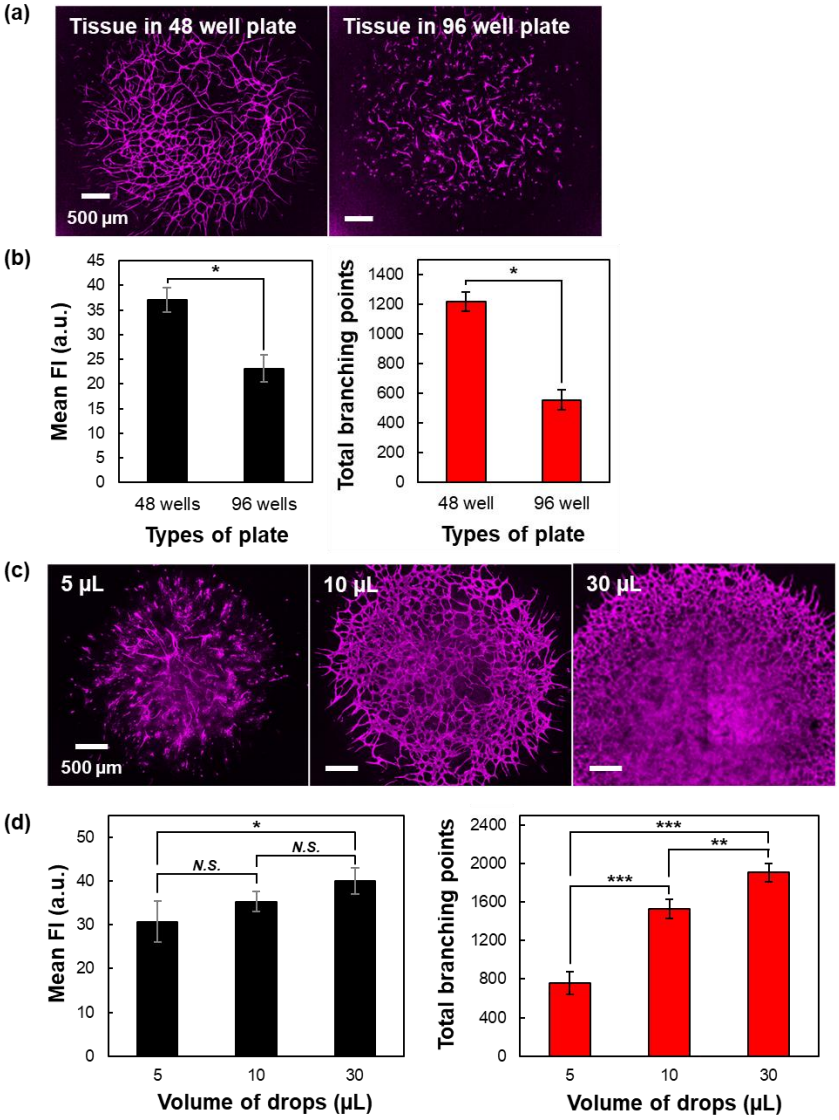

Figure 1.9. Comparison of cell culture medium and drops volumes for the optimized microarray assay culture of the 3D-blood capillary model. (**a**) Confocal CD31 images of 3D-blood capillary model in 48-well (left) and 96-well (right) plates and (**b**) their graph of mean fluorescence intensity and total branching points measured by ImageJ and Imaris software, respectively. (*) indicates that data are significantly different ($p < 0.01$). (**c**) Confocal images of the different volume of seeded drops (5, 10 and 10 µL) cultured in the 48-well plate and (**d**) their quantification data of mean fluorescence intensity (MFI) and total branching points for each volume of drops. Data presented as mean ± s.d. (*, **, ***) indicate that data are significantly different (*$p < 0.05$, **$p < 0.01$ and ***$p < 0.001$) calculated by ANOVA analysis. *N.S.* indicates no significant difference.

1.3.8. Time-related Formation of Vascular Networks

Another step was to monitor the time effect on the vascular network formation during the 5 days of culture. In this experiment, we used green fluorescent protein labeled the EC (GFP-HUVEC) cells in order to enable visualization of daily formation of vascular networks in live without cell fixation. The confocal images shown in **Figure 1.10a** highlight the vascular network which started to form from day 3. This phenomenon was supported by quantitative data where the mean fluorescence intensity as wells as total branching points were increasing day by day (**Figure 1.10b**). As the time for culturing the tissues was relatively short, this will be an advantage point for preparing the 3D tissues which could be used as microarray analysis, and thus be a powerful tool for screening assay.

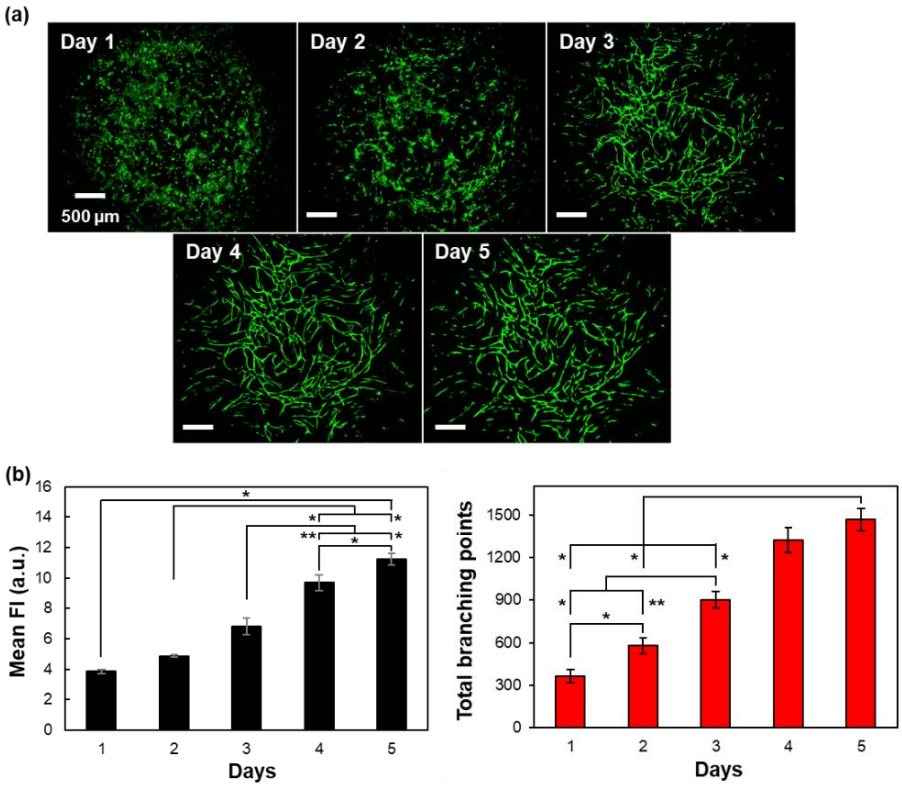

Figure 1.10. Time-related formation of vascular networks. (**a**) Confocal images of 3D-blood capillary models to show the formation of vascular networks during culture (day 1–5), using green fluorescent protein labeled the EC (GFP-HUVEC) to live-image the formation of vascular networks without fixing the tissue. (**b**) Quantification data for mean fluorescence intensity (MFI) and total branching points during culture time. Data presented as mean ± s.d. (n = 2). (*, **) indicates that data are significantly different (*p < 0.05 and **p < 0.01) calculated by ANOVA analysis.

1.4. Conclusion

The micro-droplet of 3D-blood capillary models using collagen microfiber-based fibrin gels were successfully fabricated and cultured in a 48-wells plate to serve as a medium or relatively high-throughput assay. The blood capillary tissues were validated, and their reproducibility was proven by the quantification of their mean CD31 fluorescence intensity and their total branching points measured based on their confocal images. This method can be a powerful microarray assay for screening application, providing useful data due to their more physiologically relevance as compared to 2D assay. In addition to the imaging probes screening example shown here, another possible application of this model could be for drug discovery and screening of anti-angiogenic agents, blood vasculature being critical for tumor and metastasis progression in cancer patients.

1.5. References

[1] R. Edmondson, J. J. Broglie, A. F. Adcock, L. Yang, *ASSAY and Drug Development Technologies* **2014**, *12*, 207.

[2] I. Kola, *Clinical Pharmacology & therapeutics* **2008**, *83*, 227.

[3] K. Bhadriraju, C. S. Chen, *Drug Discovery Today* **2002**, *7*, 612.

[4] L. E. Niklason, R. S. Langer, *Transpl Immunol* **1997**, *5*, 303.

[5] M. D. Sarker, S. Naghieh, N. K. Sharma, X. Chen, *Journal of Pharmaceutical Analysis* **2018**, *8*, 277.

[6] M. A. Abdul Sisak, F. Louis, M. Matsusaki, *Polymer Journal* **2020**, *52*, 871.

[7] C. Tomasina, T. Bodet, C. Mota, L. Moroni, S. Camarero-Espinosa, *Materials* **2019**, *12*, DOI 10.3390/ma12172701.

[8] L. Ouyang, J. P. K. Armstrong, Q. Chen, Y. Lin, M. M. Stevens, *Advanced Functional Materials* **2020**, *30*, DOI 10.1002/adfm.201908349.

[9] A. Brown, H. He, E. Trumper, J. Valdez, P. Hammond, L. G. Griffith, *Biomaterials* **2020**, *243*, 119921.

[10] R. ichiro Tanaka, K. Sakaguchi, S. Umezu, *Artificial Life and Robotics* **2020**, *25*, 199.

[11] B. A. Juliar, J. A. Beamish, M. E. Busch, D. S. Cleveland, L. Nimmagadda, A. J. Putnam, *Biomaterials* **2020**, *230*, DOI 10.1016/j.biomaterials.2019.119634.

[12] H. Kimura, Y. Sakai, T. Fujii, *Drug Metabolism and Pharmacokinetics* **2018**, *33*, 43.

[13] M. W. Tibbitt, K. S. Anseth, *Biotechnology and Bioengineering* **2009**, *103*, 655.

[14] J. Ru Choi, K. Wey Yong, J. Yu Choi, A. C Cowie, *BioTechnique* **2019**, *66*, 40.

[15] Y. Zhu, Q. Zhang, X. Shi, D. Han, *Advanced Materials* **2019**, *31*, 1.

[16] J. L. Drury, D. J. Mooney, *Biomaterials* **2003**, *24*, 4337.

[17] R. I. Litvinov, J. W. Weisel, *Matrix Biology* **2017**, *60–61*, 110.

[18] D. D. Swartz, J. A. Russell, S. T. Andreadis, *American Journal of Physiology - Heart and Circulatory Physiology* **2005**, *288*, 1451.

[19] L. Yao, J. Liu, S. T. Andreadis, *Pharmaceutical Research* **2008**, *25*, 1212.

[20] D. Eyrich, F. Brandl, B. Appel, H. Wiese, G. Maier, M. Wenzel, R. Staudenmaier, A. Goepferich, T. Blunk, *Biomaterials* **2007**, *28*, 55.

[21] L. Yao, D. D. Swartz, S. F. Gugino, J. A. Russell, S. T. Andreadis, *Tissue Engineering* **2005**, *11*, 991.

[22] H. Liu, S. Kitano, S. Irie, R. Levato, M. Matsusaki, *Advanced Biosystems* **2020**, *4*, 2000038.

[23] D. Su, C. L. Teoh, S.-J. Park, J.-J. Kim, A. Samanta, R. Bi, U. S. Dinish, M. Olivo, M. Piantino, F. Louis, M. Matsusaki, S. S. Kim, M. A. Bae, Y.-T. Chang, *Chem* **2018**, *4*, 1128.

[24] F. Louis, S. Kitano, J. F. Mano, M. Matsusaki, *Acta Biomaterialia* **2019**, *84*, 194.

[25] Y. Naka, S. Kitano, S. Irie, M. Matsusaki, *Materials Today Bio* **2020**, *6*, 100054.

[26] M. L. Tiffany, S. Krimm, *Biopolymers* **1969**, *8*, 347.

[27] D. S. Richardson, J. W. Lichtman, *Cell* **2015**, *162*, 246.

[28] C. Kniebs, F. Kreimendahl, M. Köpf, H. Fischer, S. Jockenhoevel, A. L. Thiebes, *Organogenesis* **2019**, *00*, 1.

[29] K. Chwalek, M. v. Tsurkan, U. Freudenberg, C. Werner, *Scientific Reports* **2014**, *4*, 4.

Chapter 2

Screening of Near-Infrared Chemical Probes for *In vivo* Blood Vessels Imaging via 3D-blood Capillary Models

2.1 Introduction

Blood vessels are made up of vascular endothelial cells that line the inner surface and play an important role in the delivery of essential nutrients, growth factors, and oxygen to all tissues, as well as transporting blood throughout the body. It is therefore crucial to be able to perform live imaging on blood vessels so that their many related diseases and conditions such as atherosclerosis, aneurysm, thrombosis, and ischemia can be studied. Live imaging has transformed biomedical research by enabling visualization and analysis of dynamic cellular processes as they occur in their native systems.

Easy and high-resolution methods of imaging blood vessels *in vivo* or *in situ* are currently limited. There have been reports describing staining of endothelial cells by small molecule modified nanoparticles.[1–5] However, the screening approach was from an *in vitro* profiling where cells may markedly lose their responsiveness and function because of the 2D environment.[6] Therefore, the development of a technique for constructing a 3D tissue having a structure and function similar to a living body *in vitro* is highly sought after. Previously, 3D-blood capillary models were also reconstructed but these methods are subjected to certain limitations such as high time consumption and complicated handling that make them unsuitable for high throughput assay.[7–11] Thus, a relative easy and simple 3D platform of organized blood capillary models could provide more reliable data for the various required applications instead of the conventional monolayer-cultured cells.

Herein, in this chapter we demonstrate an approach by a screening of imaging probes with enhanced binding to vascular endothelial cells. We used an *in vitro* 3D-

human blood capillary model fabricated in 48-microwell plates using collagen microfibers (CMFs) to provide the extracellular matrix in the complex tissue. This method demonstrates a tissue fabrication technique that is rapid, simple, accessible, and reproducible, which could thereby fulfill the demand for throughput model systems.[12] Endothelial cells in this blood capillary model showed a significantly higher expression of specific endothelial membrane proteins such as hematopoietic progenitor cell antigen (CD34), vascular endothelial growth factor receptor 1 (VEGFR1), and intercellular adhesion molecule 1 (ICAM1) than those in 2D culture (**Figure 2.1**). Inspired by the outstanding features of cyanine in earlier reports [13–15] we synthesized a cyanine near infrared (NIR) 240 library, with 80 candidates in each of the CyA, CyB, and CyC groups, using the diversity-oriented fluorescence library (DOFL) approach by introducing structural diversity to a key structure of cyanine to obtain the selectivity to the endothelial cells. The fluorescent NIR probes emit at 670 nm due to their core structure of cyanine which is capable of penetrating biological entities, particularly skin and blood, more deeply and effectively than visible light. The DOFL has already demonstrated its versatility in sensor development, even without the knowledge of the mechanisms for designing a probe rationally.[16,17]

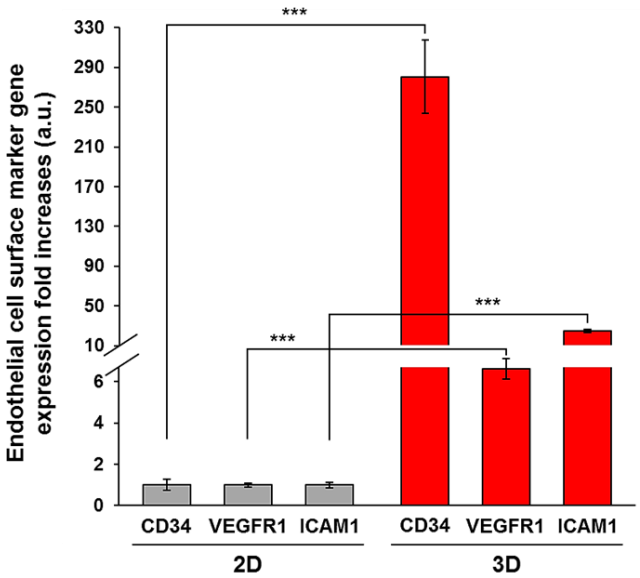

Figure 2.1. Gene expression of hematopoietic progenitor cell antigen (CD34), vascular endothelial growth factor receptor 1 (VEGFR1), and intercellular adhesion molecule 1

(ICAM1) specific to endothelial cells in different conditions (2D in grey and 3D in red). Data presented as mean ± s.d., (n=3), ***p < 0.001.

2.2 Experiment

2.2.1. Materials

Anti-CD31 antibody (polyclonal rabbit, ab28364) was purchased from Abcam (Cambridge, United Kingdom). PureLink RNA Mini Kit was purchased from Invitrogen (Waltham, USA). iSCRIPT cDNA synthesis kit was purchased from Bio-Rad (Hercules, USA). Taqman Fast Advanced Mix, Taqman gene expression assays (FAM): house-keeping gene (PPIA, assay ID: Hs04194521_s1), hematopoietic progenitor cell antigen (CD34, assay ID: Hs02576480_m1), intercellular adhesion molecule 1 (ICAM1, assay ID: Hs00959180_g1), and vascular endothelial growth factor receptor 1 (VEGFR1/FLT1, assay ID: Hs01052961_m1) were purchased from Thermo Fisher Scientific (Waltham, USA). TrueVIEW Autofluorescence Quenching Kit was purchased from Vector Laboratories (Burlingame, CA, USA). Dimethyl sulfoxide (DMSO, APH0315) was purchased from Wako Chemicals (Osaka, Japan).

2.2.2. Screening Process & Quantification Analysis of Chemical Probes

Screening of chemical probes: 240 chemical probes with different substituent on the cyanine core structure that emits in near infrared region ($\lambda_{ex}/\lambda_{em}$: 640/670 nm) were used to find the live-blood vessels imaging (the structures of each substituent were shown in Figure S1). The dried probes were dissolved in DMSO in order to have 10 mM of stock solution. For the experiment, the probes were further diluted in cell culture medium (DMEM) at 1 µM with 0.1 % DMSO. After 20 min of probes incubation on the 3D-blood capillary models (tissues) at 37 °C in the incubator, the tissues were washed with PBS to remove the unbound probes. Live imaging of probes adsorption was then acquired by CLSM (CQ1) at 37 °C. Maximum intensity projection of the full sample (which total thickness 104.2 ± 2.9 µm), 40 % excitation power for each fluorescence channel, 300 ms exposure time, keeping same brightness and contrast for all samples to enable the comparison. The exported images were finally used to analyze the colocalization of the probes to the blood capillaries using Imaris software.

Quantification analysis of the probes colocalization: For the quantification of colocalization of the probe, the adsorption of the probe on the tissue was quantified using Imaris software to give the total fluorescence of probe adsorption on the whole tissue (denoted as P) and the specific fluorescence of probe adsorption on the blood capillaries (denoted as P'). Then, the colocalization (in percentage) was calculated by simply dividing the specific fluorescence intensity (FI) of the bound probes (P') over the total FI of bound probes (P). The specific fluorescence of probe adsorption (P') were quantified by overlapping the fluorescence intensity with the GFP signal (which labels the HUVEC). To ensure the reproducibility of the analysis method between the 240 chemical probes, the same intensity thresholds were always applied for the area determination (P, P', and GFP) on the Imaris software.

2.2.3. Optimization of Concentration and Incubation Time of Chemical Probe

The concentration of CyA-B2 (hit compound) was optimized by using various concentration (0.1, 1.0, 3.0, 5.0 and 10.0 μM) as well as their incubation time (0, 1, 5, 10, 15 and 20 min) for staining on the tissues. All tissues were incubated at 37 °C and washed by PBS prior to live imaging observation by CLSM. The quantification of the specific probes binding (P') values and colocalization (%) were measured by Imaris software for both conditions, concentration and incubation time. Each conditions were carried out in triplicates.

2.2.4. Dynamic Light Scattering (DLS) Measurement of CyA Probes

The size distribution of the CyA probes library were measured by dynamic light scattering (DLS, Malvern Zetasizer, Nano ZS Instruments, UK) using cell culture medium (DMEM, pH 7.4) as a buffer solution and the final concentration of the probes was 1 μM. The measurement was done 3 times for each sample, and particle size (volume), polydispersity index (PDI), and zeta potential were measured.

2.2.5. Investigation of Possible Interactions of the CyA-B2 toward Blood Capillary

For the hydrophobic interaction, the adsorption effect of the probe towards the blood capillaries was examined by incubating the CyA-B2 onto the tissues at different temperatures (4, 10, 20, and 37 °C). For the electrostatic interaction, the adsorption effect of the CyA-B2 towards the blood capillary was examined by addition of NaCl in the culture medium (DMEM containing already 110 mM of NaCl) at different concentrations (1, 10, 50, and 100 mM). Finally, the hydrogen bonding, the adsorption effect of the CyA-B2 towards the blood capillaries was examined by using urea as an inhibitor added into the culture medium at different concentrations (0, 0.01, 0.1, 0.5 and 1.0 M). For the three conditions, the tissues were incubated with 1 µM of CyA-B2 at 37 °C for 20 min and washed with PBS prior to obtain the live image by CLSM. The images were then analyzed by Imaris software to quantify the P' intensities values.

2.2.6. *Ex Vivo* and *In Vivo* Mouse Imaging Using CyA-B2

Ex vivo mouse's aorta imaging using CyA-B2: The animal study was approved by the Osaka University Committee (approval number: 29-3-0) and carried out following the guidelines provided by Osaka University. The 18-25 weeks-old male of C57BL/6 mice were sacrificed and the aorta was isolated after removing the fat tissues around. The aorta was injected with 200 µL of 1 µM CyA-B2 (0.1 % DMSO in PBS, same concentration as *in vitro* models). The aorta was then incubated at 37 °C for 60 min. After that, the aorta was cut longitudinally to expand and expose the endothelium layer. The live image of endothelium layer was obtained by CLSM (FV3000, Olympus, Japan). Then, the aorta was fixed by 4 % PFA and immunostained by anti-CD31 antibody (polyclonal rabbit) to observe the colocalization.

In vivo mouse imaging using CyA-B2: For animal experiments, 200 µL of 400 µM CyA-B2 (20 µM of final concentration with 0.1 % DMSO in PBS) was injected intravenously (i.v.) using a 30G needle into BALB/c male nude mouse (BALB/c slc-nu/nu, Japan SLC, Shizuoka, Japan) and later (after 30 min post injection of CyA-B2) 50 µL of FITC-dextran (2000kDa) was injected as well. FITC-dextran was used as a reference for the intravascular space of the blood vessels. Same procedure was used using Cy5 (20 µM of final concentration in PBS) as a negative control probe. The *in vivo* near-infrared fluorescence images were taken on the *in vivo* imaging system (Maestro EX,

PerkinElmer, MA, USA, CyA-B2 & Cy5 = $\lambda_{ex}/\lambda_{em}$: 640/670 nm, FITC-dextran = $\lambda_{ex}/\lambda_{em}$: 495/519 nm) at selected time points. Anesthesia was maintained with 1.5 % isoflurane (1:3 O_2 / room air gas mixture) using a facemask and body temperature of the mice was kept constant at 37 °C across whole imaging process. After *in vivo* fluorescence imaging for 60 min, mice were euthanized by isoflurane overdose and its tissues and organs were dissected. The mice's organs and tissues (liver, kidneys, aorta, heart, spleen, head, and ears) were observed again by the *in vivo* imaging system and CLSM (FV3000) to see the probe accumulation. All experimental procedures involving animals were performed in accordance with the Animal Ethics Committee of the National Institutes for Quantum and Radiologic Science and Technology (14-1006-10) and Advanced Technology Facilities in Chiba-city, Japan (31 Environmental Preservation ordinance, #21, updated on March 27th, 2020).

2.2.7. Gene Expression

Gene expression was analyzed using real-time quantitative polymerase chain reaction (RT-qPCR). After 5 days of culture in 2D (n=3, containing 8.25×10^5 NHDF and 4.15×10^4 HUVEC per well at the seeding in 12 well plate) and 3D (n=3), all samples were washed in PBS and total RNA extraction was carried out using the PureLink RNA Mini Kit with the DNAse step following the manufacturer's instructions. Samples' RNA content was analyzed with the Nanodrop^{TM} spectrometer (N1000, Thermo Fisher Scientific, Waltham, USA). For RT-qPCR, the RNA samples were submitted to reverse transcription into cDNA using iSCRIPT cDNA synthesis kit. 2 µL of these cDNA samples were amplified using Taqman probes and reagents (Taqman Fast Advanced Mix, Taqman gene expression assays (FAM): house-keeping gene (PPIA), hematopoietic progenitor cell antigen (CD34), intercellular adhesion molecule 1 (ICAM1), and vascular endothelial growth factor receptor 1 (VEGFR1/FLT1). The cDNA synthesis and RT-qPCR reactions were conducted using the StepOnePlus Real-Time PCR System (Thermo Fisher Scientific, Waltham, USA). After preliminary trials, PPIA was chosen as the house keeping gene. Results were moreover standardized by CD31 expression to highlight the gene expression of the endothelial cells.

2.2.8. Immune Response of Mouse toward CyA-B2 and Visualization of CyA-B2 on Paraffin Section

Mice injected with CyA-B2 or PBS (containing 0.1% DMSO) were sacrificed after 1 h and their tissues (aorta, ear, liver, and kidney) were fixed with 4 % PFA and subsequently sent to the Applied Medical Research company (Osaka, Japan) for paraffin embedding and immunohistochemistry. Sectioned tissues were stained with CD3 and F4/80 antibodies. The images were obtained using a FL EVOS Auto microscope (Thermo Fisher Scientific, Waltham, MA, USA) for measuring the area (%) of CD3 and F4/80 using ImageJ software. The sectioned tissues were also deparaffinized and treated, following the provider's protocol with TrueVIEW Autofluorescence Quenching Kit to remove autofluorescence of blood, collagen, and elastin. Then, the CyA-B2 was observed on the tissue sections by a CLSM Fluoview FV3000 (Olympus, Tokyo, Japan).

2.2.9. WST-8 Assay

Cytotoxicity of the CyA-B2 (0.1 % DMSO) was evaluated via WST-8 assay using NHDF and HUVEC. Cells were seeded into a 96-well cell culture plate at a density of ~10000 cells (total of NHDF and HUVEC) per well and cultured for 24 h. DMSO (0.1 %) with and without CyA-B2 (1 µM) was added and the cultures were maintained at 37 °C with 5 % CO_2 for 20 and 60 min. Then, after washing with PBS, 100 µL of WST-8 solution was added to each well, and incubation was continued for 60 min. 80 µL of supernatant from each sample was transferred into a new well of a 96 well-plate and the absorbance at 450 nm was measured in triplicate by a microplate reader (Model 680, Bio-Rad Laboratories, Inc, Japan).

2.2.10. CyA-B2 Staining on the Human Fat Tissue

Living adipose tissue (from human abdominal adipose tissues, isolated at the Kyoto Prefectural University of Medicine Hospital, Ethics Committee approval number: ERB-C-1317-1) were directly stained with the CyA-B2 (1 µM) and incubated for 20 min at 37 °C with 5 % CO_2. The live imaging of the fat tissue with CyA-B2 probes was observed by a CLSM Fluoview FV3000 (Olympus, Tokyo, Japan).

Statistical analysis: Statistical analysis was performed using a two-tailed Student's *t*-test. The results presented are means ± s.d. of three independent experiments. A *p*-value less than 0.05 was considered to be statistically significant. *N.S.* denotes no significant difference.

2.3 Results and discussion

2.3.1 Screening Results of Chemical Probe Libraries

Using the blood capillaries model with CMF-50 tissues, 240 different fluorescent probes were compared in a parallel throughput screening process allowing the simultaneous assessment of 48 probes, concerning their possible specificity against endothelial cells on living tissues. For this assessment, the specific fluorescence intensity (FI) of the probe adsorption on the blood capillaries was analyzed by keeping only the probe fluorescence which overlaps the GFP signal (denoted as P') and the total FI of bound probes (denoted as P) were quantified. **Figure 2.2** shows examples of live imaging of two chemical probes, one with the highest P' and one with the lowest P' (decoded as CyA-B2 and CyA-D8, respectively) adsorbed on the blood capillaries and counterstained by the GFP fluorescence. The CyA-B2 probe was used for comparing the live staining in both 2D and 3D environments. The results showed P' of 1.25 E+08 and 2.17 E+09 for 2D and 3D, respectively, while P gave intensities of 4.09 E+08 and 5.73 E+09, allowing the calculation of 30 % and 38 % of colocalization, respectively, by the division of P' over the sum of specific and non-specific adsorption intensities (P value). When comparing to CyA-D8 in 3D, the values for P' and P were 3.79 E+07 and 1.82 E+08, respectively, which gave 21 % of colocalization. Although both probes showed a moderate difference in specificity, the comparison of the P' values showed that CyA-B2 was 57-fold higher than CyA-D8. For an initial fast screening of the 240 different probes, it was thus decided to rely on the P' values for comparison of the probes. To demonstrate that the P' value is a sufficient relevance to compare the probes together, we validated this method by using anti-CD31 antibody as a positive control although the immunostaining was not live imaging. GFP, CD31, and merged images showed that the P' value (the P value of CD31 was not obtained because of the frequent washings during immunostaining) was 2.35 E+09, while the GFP value was 2.46 E+09, which gave 96 %

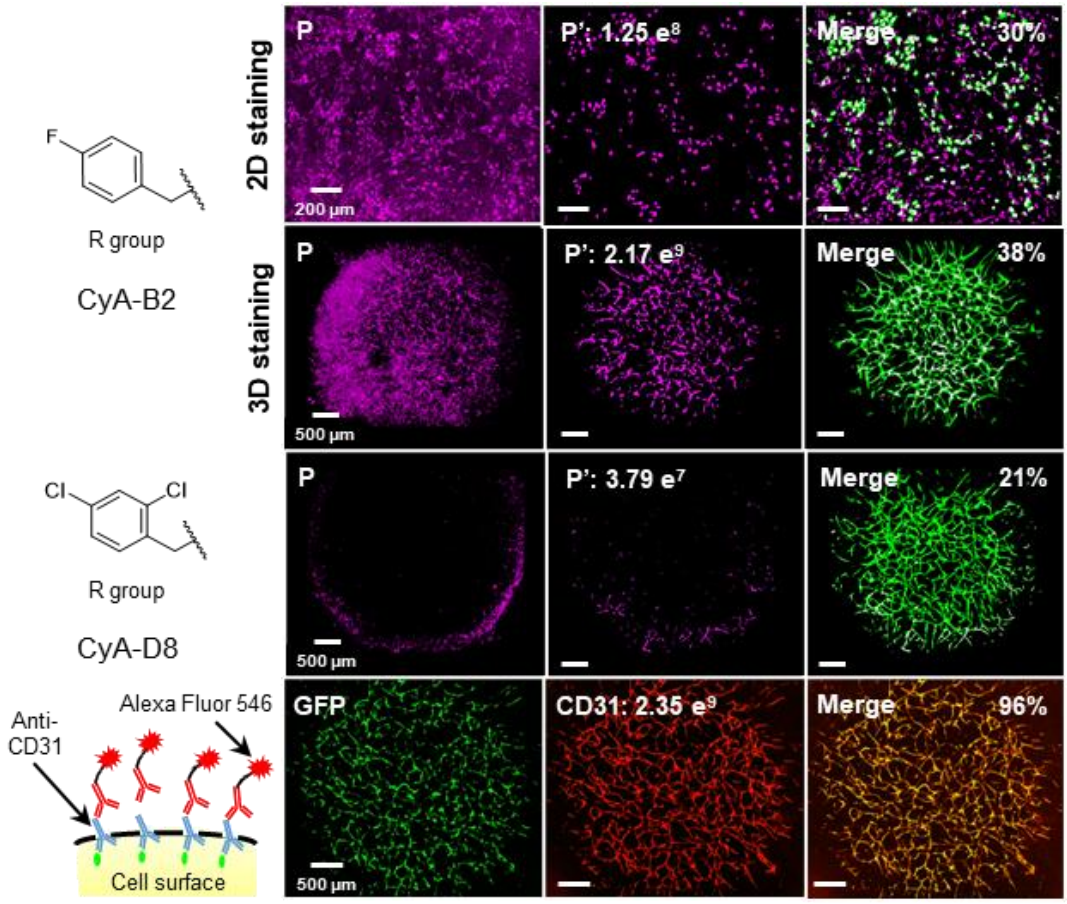

Figure 2.2. Live staining images of the CyA-B2 (magenta) by confocal laser scanning microscopy (CLSM) on green-fluorescence protein expressing human umbilical vein endothelial cells (GFP-HUVEC) and normal human dermal fibroblast (NHDF) in the 2D co-culture and 3D-blood capillary models. The images show the total probe adsorption on the tissue (P), P', and the merge of P' on GFP signal (green) for CyA-B2 (highest P') and CyA-D8 (low P'). Anti-CD31 antibody (red) was used as a positive control. The colocalization values of the probes overlapping the GFP signals were shown to be 30, 38, 21, and 98% for CyA-B2 in 2D, CyA-B2 in 3D, CyA-D8, and anti-CD31-antibody, respectively.

of colocalization for this positive control. Notably, when we again compared the P' values of CyA-B2 (2.17 E+09) and CD31 (2.35 E+09), they were in the same scale range of fluorescence intensity, although CD31 staining needed fixation and frequent washings which induced an increase in the P' value.

The summary of CyA probes with their P' values and colocalization, as well as for the other CyB and CyC probes (data not shown as they all showed low P' values) are

shown in **Figure 2.3**. The 8 probes highlighted with the red color were the ones giving an FI of P' values higher than the threshold, above 1.0 E+09 (red dash line). Representing only 3 % of the total number of the probes tested, this chosen threshold value might indicate sufficient adsorption on the blood capillaries. Notably, the selected 8 probes only came from the CyA library, suggesting the importance of the backbone structure. The blue bar indicates the positive control of CD31 antibody.

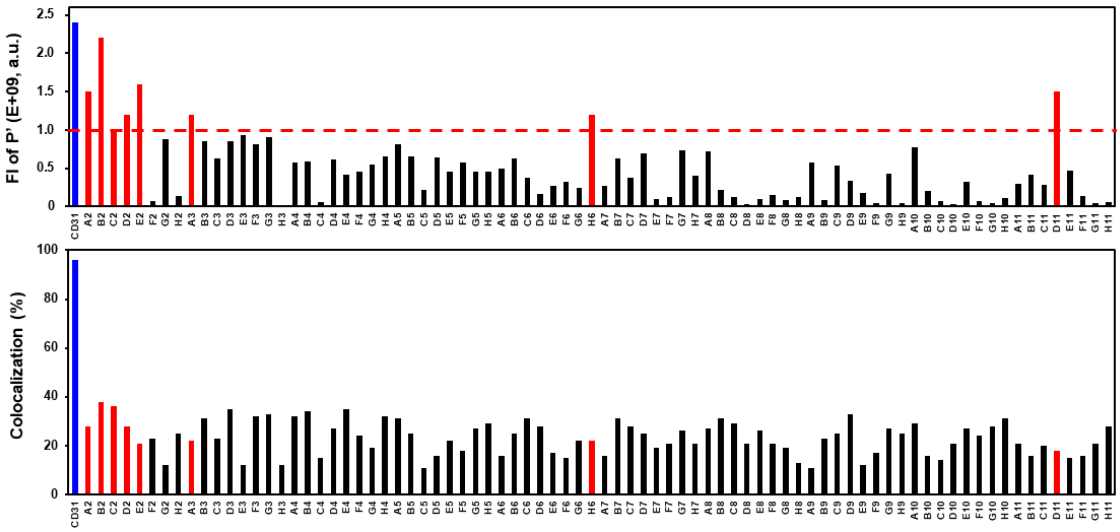

Figure 2.3. The specific adsorption (P') intensity (top) and colocalization (bottom) for the CyA probes library. The dashed line in the P' intensity graph is the threshold from which the probes show high specific adsorption property.

Time dependent adsorption phenomena of CyA-B2 are shown in **Figure 2.4a**. The adsorption process of the probes was rapid and nearly reached saturation after 8 minutes of incubation though slight increases were observed at both 16 and 20 minutes. In the merged image, it was confirmed that the probes were colocalized with the GFP labelled blood capillaries. However, some probes were also adsorbed non-specifically on other areas of the 3D-blood capillary models including NHDF surfaces, affecting as a background noise to decrease the P' value. In **Figure 2.4b**, CyA-B2 was observed in the cytosol analyzed by its colocalization with cell tracker green (CTG) by CLSM, suggesting the uptake by HUVEC. These data clearly indicated that we successfully identified a possible probe for live imaging of endothelial cells by throughput screening from 240 candidates using 3D-blood capillary models. To understand the mechanism of specific

adsorption of CyA-B2 on the surface of the endothelial cells, detailed analyses were performed as follows.

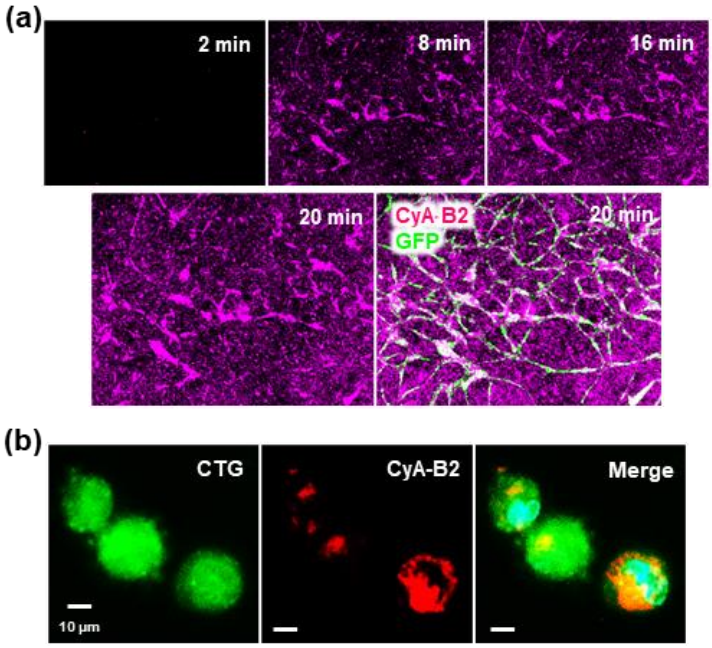

Figure 2.4. (**a**) Time-lapse CLSM live images of the 3D-blood capillary using CyA-B2 at particular times (2, 8, 16, and 20 minutes) during incubation. (**b**) CLSM live images of cell tracker green stained HUVEC in 2D culture using CyA-B2 (red). CTG: Cell tracker green.

2.3.2 Possible Factors for Higher Adsorption of Probe on the Blood Capillaries

Since most of the fluorescent probes having different substituent groups on the benzene ring moiety, we investigated the substituent effect on the fluorescent probes which influences their emission performance [18] or photostability in aqueous media [19] which then might affect their structure stability in aqueous media as the electron density changes. The selected 8 high P' probes (P' > 1.0 E+09) and some low P' probes with similar substitution groups were plotted in the graph according to their types of electron donating and withdrawing group (EDG and EWG) together with a heat map representing the P' values of all the CyA probes (**Figure 2.5**). The EDG and EWG were arranged from low to high activating and deactivating groups, respectively, with the ortho, meta and/or para directing substituents. Both the strongest EDG (C5) and EWG (B9) showed the lowest values in both P' and colocalization, while the middle of EDG (D2 and C2) and

EWG (B2 and H6) indicated relatively higher values. The *p*-fluoro substitution (B2 and H6) seems to be important for the enhancement of both parameters, but we were unable to find a stronger correlation.

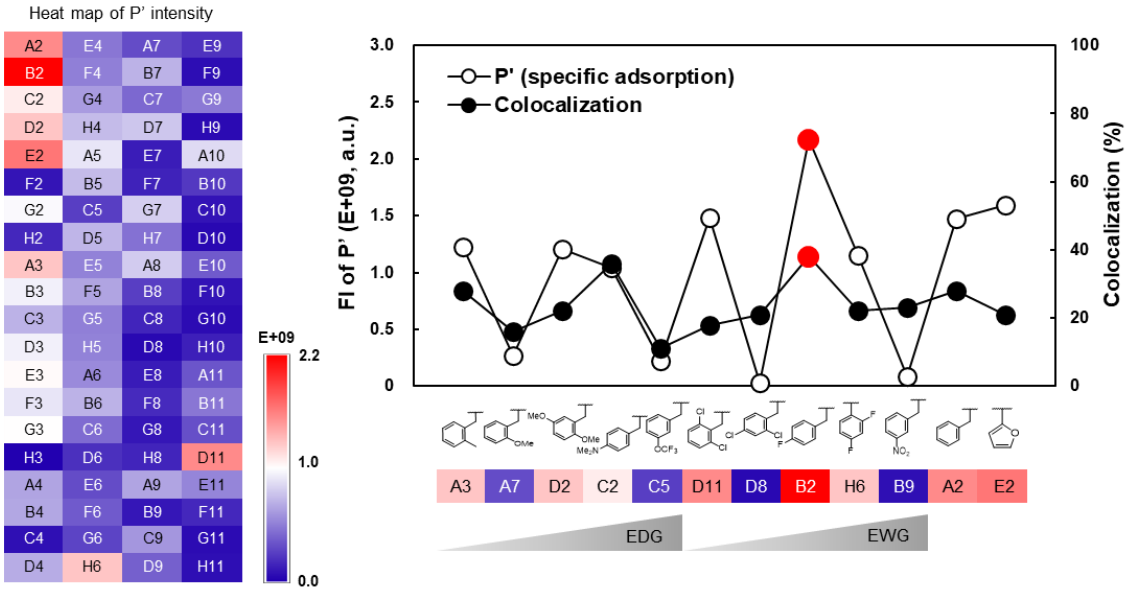

Figure 2.5. The correlation between substitution effect and specific adsorption. Heat map of P' intensity of the CyA probes library (left) and correlation of P' intensity, colocalization and substitution effect of R-groups (right). EDG is electron donating group and EWG is electron withdrawing group.

To identify the other contributory factors in the selected 8 probes with higher P' values we focused on the size distribution of the probes in culture media because their dispersion condition can strongly affect adsorption on endothelial cells (**Figure 2.6**). Interestingly, the size distribution of the top 4 P' probes showed a very narrow peak at 1 to 4 nm, whereas the bottom 4 P' probes showed a broad peak from 3 to 30 nm, suggesting a monodispersity at a single molecule of the top 4 probes and aggregation of the bottom 4 probes. Molecular modeling of CyA-B2 by ChemDraw (Chem3D ver. 16.0) software indicated 1.61 nm of molecular size which was almost the same as the size distribution data. **Figure 2.6b** shows average size and polydispersity index (PDI) values of higher and lower P' probes and the size and PDI values of the lower P' probes indicate 6-fold and 3-fold higher values, respectively. The high dispersion of the high P' probes would make these probes easier to diffuse and to be adsorbed on the blood capillaries, thus giving them a higher FI value as well as higher colocalization (%).

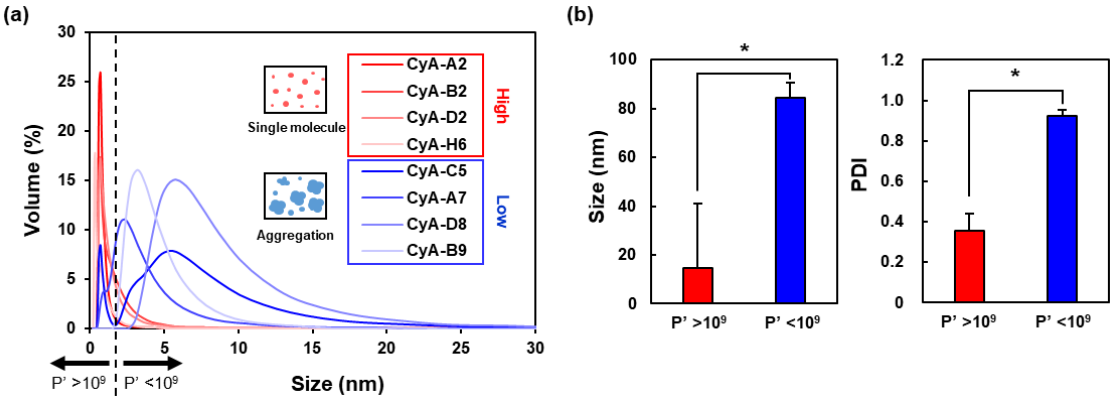

Figure 2.6. (**a**) The size distribution of selected probes with high (> 1.0 E+09) and low (< 1.0 E+09) P' intensities in culture media measured by dynamic light scattering. The insert illustration shows the probes distribution. (**b**) The average size and polydispersity index (PDI) of the selected probes. Data presented as mean ± s.d., (n=4), *p < 0.001.

2.3.3 Possible Interactions of Probe Adsorption to the Blood Capillaries

To clarify the mechanism of the specific adsorption of CyA-B2 onto the surface of endothelial cells, concentration and incubation time effects on P' value and colocalization were evaluated (**Figure 2.7a, b**). The P' values were found to increase as the concentrations of CyA-B2 increased, whereas the colocalization values showed opposite results, suggesting the increase of unspecific adsorption of the probes on 3D-models. However, both the P' value and colocalization gradually increased with increasing incubation time and finally reached saturation after 15 minutes of incubation.

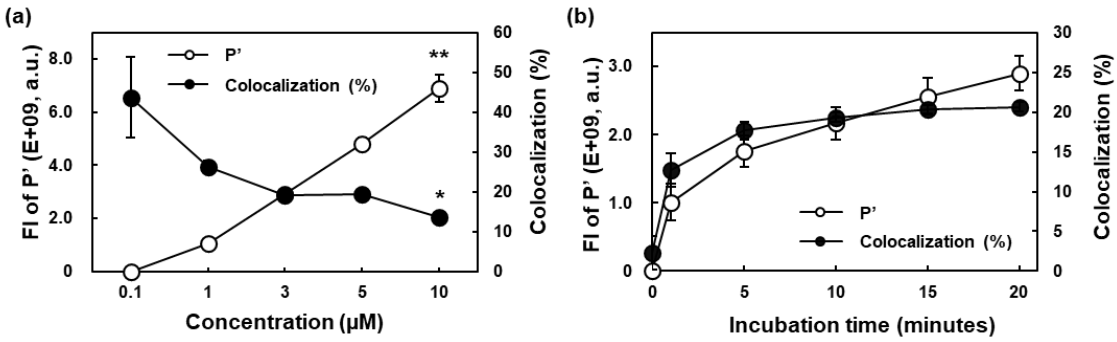

Figure 2.7. The P' intensity and colocalization of CyA-B2 probe against concentration (**a**) and incubation time (**b**), respectively. Data presented as mean ± s.d., (n=3), *p < 0.05, **p < 0.01.

Thus, we decided on 20 minutes of incubation of the probes with the 3D-blood capillary models.

For more detailed understanding of the interactions between the probes and the vascular endothelial cells, P' values were evaluated by changing the concentration of urea and sodium chloride in culture media because they are generally used for suppression experiments of hydrogen bonding and electrostatic interactions, respectively.[20] The P' value did not change significantly even at the highest concentrations of urea (**Figure 2.8a**) and sodium chloride (**Figure 2.8b**), suggesting that neither hydrogen bonding nor electrostatic interactions would be the main interaction although CyA-B2 contains an amide bond for hydrogen bonding and a carboxylate ion for electrostatic interaction. However, when the incubation temperature decreased from 37 °C, the P' value gradually decreased and finally reached half value at 4 °C (**Figure 2.8c**), suggesting the possibility of hydrophobic interaction between the probes and blood capillary surfaces. Since the character of the cyanine framework is actually hydrophobic because its solubility in water is low, this seems to be a reasonable assumption.

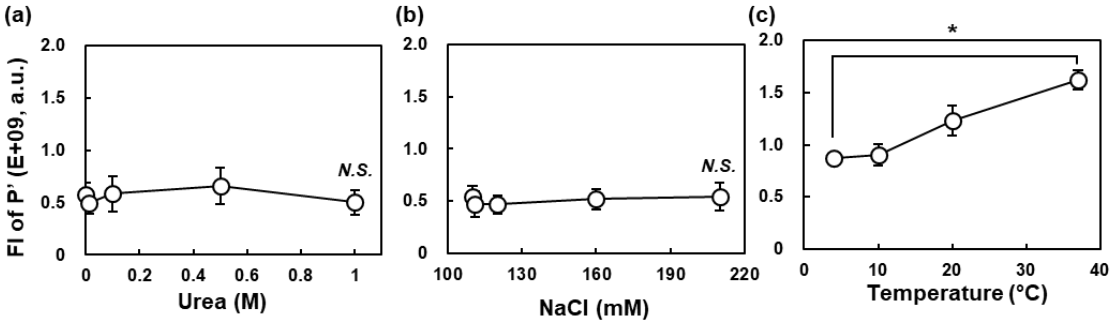

Figure 2.8. The inhibition experiments by the addition of (**a**) urea and (**b**) NaCl and (**c**) temperature increase. Data presented as mean ± s.d., (*n*=3), *N.S.*, not significant; *$p < 0.001$.

2.3.4 *Ex vivo* Imaging of Mouse Aorta using CyA-B2 probe

As the final application of the probe is *in vivo* endothelium imaging, the *ex vivo* binding of the probe on mouse aorta was firstly analyzed to obtain the basic information of how the probes are adsorbed onto actual endothelium surfaces. The probe was injected into the isolated aorta which was subsequently incubated at 37 °C for an hour before CLSM observation. The aorta was then washed, fixed and immunostained by anti-CD31

antibody to observe the colocalization of the probe with CD31 (**Figure 2.9a**). The CLSM images clearly indicated homogenous and good staining on the endothelium surfaces by CyA-B2 molecules and suggested its colocalization with CD31. Moreover, the probes also showed high colocalization in the z-axis with CD31 observed by a reconstructed CLSM 3D- image (**Figure 2.9b**). Interestingly, CD31 was observed in a slightly deeper area of the endothelium although CyA-B2 was found only on the surface of it. These *ex vivo* imaging data clearly suggested the potential of the CyA-B2 molecule for *in vivo* live imaging.

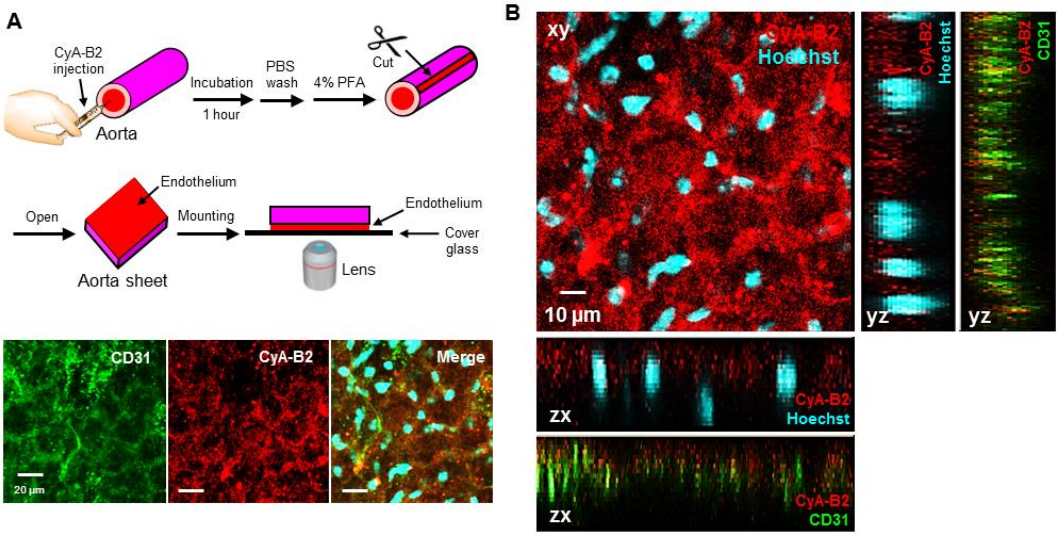

Figure 2.9. (**a**) Illustration of the process of aorta staining with CyA-B2 to visualize endothelium layer and subsequent observation by CLSM (top). CLSM images (bottom) of the endothelium stained with anti-CD31 antibody (green), CyA-B2 (red) and Hoechst (cyan) after fixation. The inner diameter and length of the aorta are 2 mm and 30 mm, respectively. (**b**) Reconstructed CLSM 3D-images of the aorta sheet after staining with anti-CD31 antibody (green), CyA-B2 (red) and Hoechst (cyan).

2.3.5 *In vivo* Imaging of Mouse Blood Vessels using CyA-B2 probe

Following the *ex vivo* analysis, *in vivo* live imaging of endothelium on blood vessels was further explored. A nude mouse received an intravenous (i.v.) injection of CyA-B2 and Cy5 (core framework structure of CyA-B2) as a control, and both fluorescence signals were monitored using the *in vivo* imaging system (Maestro, PerkinElmer, MA, USA) (Figure S2). After an hour of imaging, the mice were sacrificed

and the tissues and organs were dissected. The possible probe-related immune response induction was also assessed on the organ's sections by immunohistochemistry (liver, kidney, ear, and aorta) showing no significant differences in the staining of the mouse $CD3^+$ T-lymphocytes and the mouse $F4/80^+$ macrophages compared to the control vehicle only (PBS with 0.1 % DMSO) (Figure S3). The mouse aorta showed an intense and accumulated CyA-B2 staining due to its inner endothelium (**Figure 2.10a**). Thus, we further observed the mice organs using CLSM for visualization of the endothelium layer in the aorta. **Figure 2.10b** shows the CLSM images of Cy5 (left) and CyA-B2 (center). The randomly unspecific adsorption of Cy5 on the endothelium surface was observed while CyA-B2 clearly showed a structure similar to the cobblestone shape of endothelial cell. Notably, the endothelial cell shape was completely observed even after the fixation process with paraformaldehyde (PFA) (**Figure 2.10b**, right image), suggesting strong and stable adsorption on the surface of the endothelium layer of aorta. The fluorescence area was quantified to compare Cy5 and CyA-B2 (**Figure 2.10c**, left) and unfixed and fixed CyA-B2 (**Figure 2.10c**, right). A significant decrease of Cy5 was observed compared to CyA-B2 due to the specific adsorption property of CyA-B2 onto endothelium. Furthermore, the fluorescence intensity of CyA-B2 was completely maintained (or seemed to be slightly higher) after PFA fixation because of the decrease of background noise by the several washing and fixation steps. To the best of our knowledge, there are

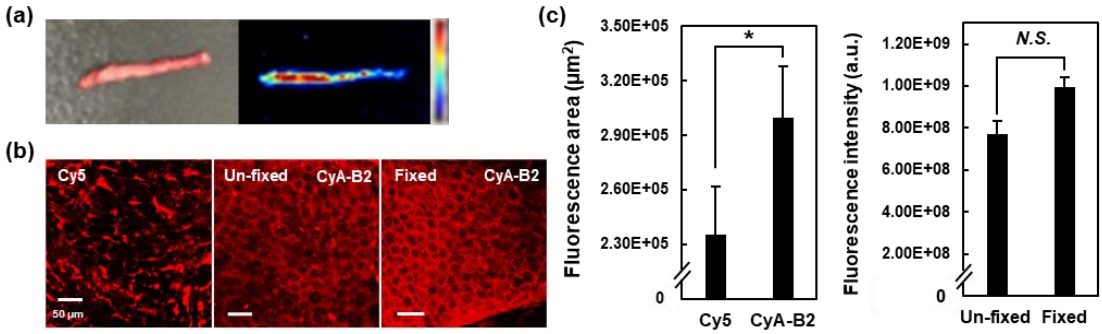

Figure 2.10. (**a**) Picture and *in vivo* fluorescence imaging of the isolated aorta after i.v. injection of CyA-B2 for 60 minutes. The color scale represents high and low intensities for red and blue, respectively. (**b**) CLSM images of the endothelium surface of the isolated aorta stained with Cy5 and CyA-B2 with or without PFA fixation. The Cy5 was used as a negative control. (**c**) The fluorescence area of the CLSM images quantified by Imaris. Data presented as mean ± s.d., (n=3), *p < 0.05, *N.S.*, not significant.

no reports of organic chemical probes with such a strong and stable adsorption property on the endothelium surface together with high cytocompatibility.

In addition to the aorta, we also observed CyA-B2 on the mouse ear, known to contain many blood vessels and easy to observe due to the thinness of the tissues, as shown in **Figure 2.11a**. The confocal images show the CyA-B2 in un-fixed and fixed ear. The probes could visualize well the morphology of blood vessels, and the fixed sample showed clearer visualization probably due to the reduction of background noise by the several washing and PFA fixation steps, as for the aorta. Moreover, good colocalization of the probes with anti-CD31 antibody was found in the merged image. The fluorescence intensity of the P' value and the colocalization of the CyA-B2 in the mouse ear (fixed) was quantified by Imaris software and plotted in the graph shown in **Figure 2.11b**, and then compared to the findings of the *in vitro* studies. While the colocalization was found to be higher *in vivo*, the P' value of CyA-B2 for *in vivo* was lower than *in vitro* which was due to the different staining condition of CyA-B2 in both environments. CyA-B2 was administered to the mouse's blood vessels through i.v. injection in the *in vivo* staining and perfused together with the blood flow. In comparison, in *in vitro* staining, CyA-B2 was directly stained onto the surface of the *in vitro* models without any dynamic effect

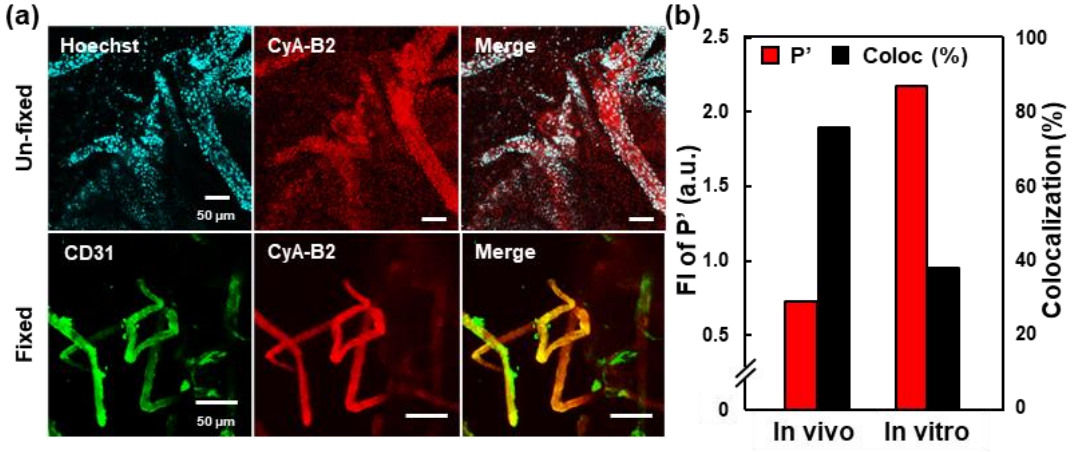

Figure 2.11. (**a**) CLSM images of the mouse ear after i.v. injection of CyA-B2 for 60 min before (un-fixed) and after fixation (fixed). Un-fixed samples were co-stained with Hoechst to visualize nuclei. In the case of the fixed sample, the blood capillaries were immunostained with anti-CD31 antibody to see the colocalization of the CyA-B2. (**b**) The P' intensity of CyA-B2 on the surface of the blood capillaries and the colocalization between CyA-B2 and CD31 of the *in vivo* mouse ear in (a). The data are compared to the *in vitro* results of CyA-B2 on the 3D-blood capillary models.

(blood flow). It suggests that the *in vitro* condition easily induced nonspecific adsorption in areas other than the blood capillary, indicating lower colocalization than in the *in vivo* situation. However, due to the static condition of the *in vitro* model, the remaining amount of the probe on endothelial cells was higher than in the *in vivo* dynamic condition, inducing a lower P' value in the *in vivo* condition than in the *in vitro* condition.

The specific binding of the CyA-B2 probe was also assessed on paraffin-embedded tissues sections of the aorta, ear, liver, and kidney after observation by CLSM (**Figure 2.12a**). The images show that the CyA-B2 remained on the endothelial cells (aorta) and blood vessels (ear, liver, and kidney) on the histology tissue sections even after the deparaffinization process. Finally, to differ from murine animal model, the ability of the CyA-B2 for *in vivo* imaging was also confirmed in human fat tissue, which is also known to contain many capillaries and blood vessels (**Figure 2.12b**) and the results showed a high adsorption of the CyA-B2 probe on the capillaries and blood vessels surrounding the adipocytes. Hence, this novel endothelium probe demonstrates high potential for live imaging for application in both mouse and human blood vessels. It will be useful for potential diagnostic tests or treatments related to blood vessels.

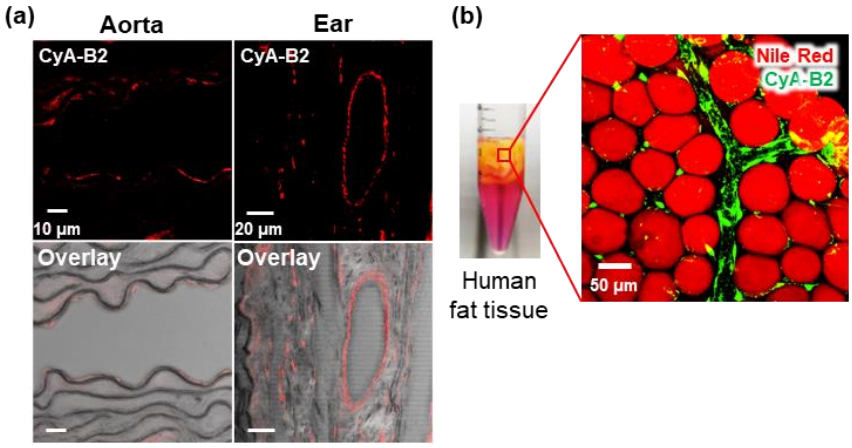

Figure 2.12. (**a**) Paraffin-embedded mouse tissue sections of aorta and ear also showed the staining of CyA-B2 on the endothelial cells and blood vessels, respectively. (**b**) CyA-B2 staining directly to the human fat tissue. Adipocytes were stained by Nile Red while blood capillaries were stained by CyA-B2 (green).

2.4 Conclusion

In summary, human 3D-blood capillary models in a 48-microwell plate were successfully fabricated using fibrin gel as a tissue scaffold model. From the screening assay, we could not find any factor linking the chemical structure with their P' value (specific adsorption) and colocalization, but it was found that the possible interaction might be driven by hydrophobic interaction and high dispersion of the probe at a single molecular level in the culture medium. One possible pathway is the ability of the probe to quickly bind to the cell membrane within 8 minutes (Figure 2C) and then to be taken up by the cell, the time-scale fitting with the general cellular uptake of nanoparticles.[21] BV-NIR was also found to provide high adsorption on the surface of the endothelium in blood vessels when applied to mice for both *ex vivo* and *in vivo* assays. This *in vitro* model screening method also has potential for use in the construction of other types of vascularized tissues (lymphatic model [22], etc.) and the subsequent screening of various probes using the DOFL approach.

2.5 References

[1] K. A. Kelly, S. Y. Shaw, M. Nahrendorf, K. Kristoff, E. Aikawa, S. L. Schreiber, P. A. Clemons, R. Weissleder, *Integr. Biol.* **2009**, *1*, 311.

[2] K. Suzuki, K. Takahashi, Y. Matsuki, M. Kawakami, Y. Kawaguchi, T. Hidaka, Y. Sekiyama, Y. Mizukami, M. Kawagoe, H. Nakamura, *Jpn. J. Pharmacol.* **1992**, *60*, 349.

[3] W. J. M. Mulder, R. Koole, R. J. Brandwijk, G. Storm, P. T. K. Chin, G. J. Strijkers, C. De Mello Donegá, K. Nicolay, A. W. Griffioen, *Nano Lett.* **2006**, *6*, 1.

[4] W. Chen, P. A. Jarzyna, G. A. F. Van Tilborg, A. Van Nguyen, D. P. Cormode, A. Klink, A. W. Griffioen, G. J. Randolph, E. A. Fisher, W. J. M. Mulder, Z. A. Fayad, *FASEB J.* **2010**, *24*, 1689.

[5] J. M. Fontana, H. Yin, Y. Chen, R. Florez, H. Brismar, Y. Fu, *Int. J. Nanomedicine* **2017**, *12*, 8615.

[6] H. Kimura, Y. Sakai, T. Fujii, Drug Metab. *Pharmacokinet.* **2018**, *33*, 43.

[7] H. Sekine, T. Shimizu, K. Sakaguchi, I. Dobashi, M. Wada, M. Yamato, E. Kobayashi, M. Umezu, T. Okano, *Nat. Commun.* **2013**, *4*, 1399.

[8] J. S. Jeon, S. Bersini, M. Gilardi, G. Dubini, J. L. Charest, M. Moretti, R. D. Kamm, *Proc. Natl. Acad. Sci. U. S. A.* **2015**, *112*, 214.

[9] N. Jusoh, S. Oh, S. Kim, J. Kim, N. L. Jeon, *Lab Chip* **2015**, *15*, 3984.

[10] Y. Nashimoto, T. Hayashi, I. Kunita, A. Nakamasu, Y. S. Torisawa, M. Nakayama, H. Takigawa-Imamura, H. Kotera, K. Nishiyama, T. Miura, R. Yokokawa, *Integr. Biol. (United Kingdom)* **2017**, *9*, 506.

[11] M. A. Abdul Sisak, F. Louis, M. Matsusaki, *Polym. J.* **2020**, *52*, 871.

[12] M. A. Abdul Sisak, F. Louis, S. Hyeok Lee, Y. Chang, M. Matsusaki, *Micromachines* **2020**, *11*, 727.

[13] A. Samanta, M. Vendrell, R. Das, Y.-T. Chang, *Chem. Commun.* **2010**, *46*, 7406.

[14] L. Zhang, J. C. Er, X. Li, J. J. Heng, A. Samanta, Y. T. Chang, C. L. K. Lee, *Chem. Commun.* **2015**, *51*, 7386.

[15] J. Ang, Y. A. Lee, D. Raghothaman, P. Jayaraman, K. L. Teo, F. J. Khan, S. Reuveny, Y. T. Chang, N. Y. Kang, S. Oh, *Biotechnol. J.* **2019**, *14*, 1.

[16] N. Y. Kang, H. H. Ha, S. W. Yun, Y. H. Yu, Y. T. Chang, *Chem. Soc. Rev.* **2011**, *40*, 3613.

[17] S. W. Yun, N. Y. Kang, S. J. Park, H. H. Ha, Y. K. Kim, J. S. Lee, Y. T. Chang, *Acc. Chem. Res.* **2014**, *47*, 1277.

[18] W. Chi, Q. Qiao, R. Lee, W. Liu, Y. S. Teo, D. Gu, M. J. Lang, Y. T. Chang, Z. Xu, X. Liu, *Angew. Chemie - Int. Ed.* **2019**, *58*, 7073.

[19] A. Samanta, M. Vendrell, R. Das, Y.-T. Chang, *Chem. Commun.* **2010**, *46*, 7406.

[20] M. Matsusaki, R. Amekawa, M. Matsumoto, Y. Tanaka, A. Kubota, K. Nishida, M. Akashi, *Adv. Mater.* **2011**, *23*, 2957.

[21] A. Lin, A. Sabnis, S. Kona, S. Nattama, H. Patel, J.-F. Dong, K. T. Nguyen, *J. Biomed. Mater. Res. Part A* **2010**, *93*, 833.

[22] A. Nishiguchi, M. Matsusaki, M. R. Kano, H. Nishihara, D. Okano, Y. Asano, H. Shimoda, S. Kishimoto, S. Iwai, M. Akashi, *Biomaterials* **2018**, *179*, 144.

Chapter 3

Mechanism Assay of Interaction between Blood Vessels-Near Infrared Probe and Cell Surface Marker Proteins of Endothelial Cells

3.1. Introduction

As widely known the function of blood vessels is to deliver oxygen and nutrients for tissues and organs as well as transporting blood throughout our body. There are many diseases which are related to blood vessels such as atherosclerosis and ischemia.[1] Since organs in our body are not directly visible, *in vivo* blood vessels imaging is required to investigate their structure and perform real-time detection. Using fluorescence may help to visualize specific area or cells in real-time. As one of the widely used fluorescent labelling compounds, fluorescent probes have many advantages, such as fast detection speed, good repetitiveness, low dosage, and non-radiation.[2–4] Many studies have been done to perform live-cell imaging whether *in vitro* or *in vivo* applications, targeting specific cells or response to different environment by using organic fluorescent probes.[3,5–7]

Conventional method to design fluorescent probe is based on the specific target molecule. However, the fluorescent probe sometimes does not guarantee to work very well when applied in the real application or clinical trial due to several problems such as biological complexity in living systems and off-target effect due to low stability in the blood stream.[8,9] An alternative method is to generate multiple probes, without knowing the target in advance, by using a fluorescent probe library consisting of diverse structures, and then screen their potential targets.[10,11] Screening of fluorescent libraries can produce interesting fluorescent ligands that lead to the discovery of novel mechanisms and reveal new biological processes.[12,13] Using this method, in the previous chapter, we screened chemical probes containing diversity structures in a library format to find a new

fluorescent probe for live-blood capillary imaging at near-infrared (NIR) wavelength range.[14]

For this step, it is very important to select the most accurate screening system to achieve reliable result when applied in *in vivo* systems. Several studies for screening chemical probes have been done in 2D cell culture. However, 2D culture is different from 3D systems which in turn leads to misleading results when applied in *in vivo* tissues. To improve the applicability of probes to tissue staining, it may be the most straightforward to directly use tissues for the screening. However, it usually means using tissues coming from animal and so the interaction of chemical probe might be different from human native tissues and the screening assay subjected to a low throughput. Therefore, setting up the screening system similar to the final application is of utmost important consideration in the design of screening systems. Hence, in chapter 1 we have developed a new high-throughput screening method using *in vitro* human tissue models for screening the chemical probe library. We fabricated blood capillary models using hydrogel to serve as a 3D system to imitate the complexity of *in vivo* tissues.

In this chapter, we further investigate the mechanisms of the selected probe (CyA-B2) binding on endothelial cells membrane by cheminformatics approaches, competition binding assay, and photophysical properties of probes by density functional theory (DFT) calculation. Endothelial cells express many proteins surface marker [15,16] which might be the potential targets for CyA-B2 binding. Herein, we reported and confirmed the discovery of a novel molecular target for CyA-B2 that is CD133 expressed on endothelial cells.[17,18]

3.2. Experiment

3.2.1. Materials

Fibrinogen (F8630), thrombin (T4648), Triton X-100 (T8787), and phosphate-buffered saline (PBS, D5652) were purchased from Sigma-Aldrich (MO, USA). Collagen was purchased from Nippon Ham. Foods Ltd. (Osaka, Japan). Normal human dermal fibroblast (NHDF) was purchased from Lonza (Basel, Switzerland). Green fluorescent protein (GFP) labeled HUVECs was purchased from Angio-Proteomie (Massachusetts,

USA). Dulbecco's Modified Eagle Medium (DMEM, 08458-45) and 4 % paraformaldehyde (09154–85) were purchased from Nacalai Tesque (Kyoto, Japan). KBM VEC-1 basal medium (16030110) was purchased from Kohjin Bio Co. Ltd. (Saitama, Japan). Anti-CD14 antibody (ab181470), mouse IgG (ab37355), recombinant anti-multidrug resistance-associated protein (MRP1, also known as ABCC1) antibody (ab233383), and CD133 protein (ab160218) were purchased from abcam (Cambridge, United Kingdom). Anti-CD31 antibody (M0823) was purchased from Dako (Glostrup, Denmark). Anti-CD133 antibody (MA1-219), alpha-synuclein (SNCA, MA5-12272), solute carrier organic anion transporter family member 2B1 (SLCO2B1) polyclonal antibody (PA5-42453), and Hoechst 33342 (H3570) were purchased from Thermo Fisher Scientific (Waltham, USA). VEGF-A (226-01781) was purchased from Wako (Osaka, Japan). Tomato lectin (L-1170-2) was purchased from Vector Laboratories (Burlingame, CA, USA). Alexa Fluor 546 (anti-mouse, A-11003) and Alexa Fluor 647 (anti-mouse, A21235) were purchased from Invitrogen (MA, USA).

3.2.2. Dynamic light scattering (DLS) measurement

CyA-B2 probe was prepared as previously reported.[14] Briefly, CyA-B2 (1 µM) was mixed with urea and sodium chloride (NaCl) at various concentration in assay buffer (DMEM containing 10 % FBS and 1 % antibiotics). The mixture was pre-incubated at 37 ºC for 20 min prior measurement. Similar concentration of urea and NaCl as in previous report were used (urea: 0, 0.01, 0.1, 0.5, and 1.0 M; NaCl: 0, 1, 10, 50, and 100 mM). DLS (Malvern Zetasizer, Nano ZS Instruments, UK) analysis was measured at 37 ºC and the experiments were conducted in triplicate.

3.2.3. Density Functional Theory (DFT) calculation

From the screening results of chemical probes that has been done in our previous report [14] and which were then classified as high P' probes (>1.0E09 a.u.) and low P' probes (<1.0E09 a.u.). The investigation of the ground and excited state energy of a high P' and low P' probes and model system was carried out through density functional theory (DFT). The B3LYP/6-31G(d,p) SCRF=(Solvent=Water) and B3LYP/6-31G(d,p) levels were adopted to locate the highest occupied molecular orbital (HOMO) and lowest

unoccupied molecular orbital (LUMO) energy level of probes in water and gas phase. All calculations were performed with the Gaussian 16 software (Gaussian, Inc., Wallingford, CT, USA).

3.2.4. Target prediction by database screening

Target protein identification was tried by systematic database searching based on the chemical structure of probe molecule CyA-B2. The ChEMBL database (ver. 24); a manually curated bioactive molecule database of more than 1.5 million compounds with biological assay outcome [19] was employed for this purpose. Molecular representation was the extended connectivity fingerprint of bond diameter 4 (ECFP4) [20], folded into a 4096 bit-vector by modulo operation, and the Tanimoto similarity was used as a metric. From standardized molecular structures in the database, molecules similar to CyA-B2 were identified using a similarity threshold of 0.40 based on retrospective similarity searching analyses.[21] For the identified similar compounds, target information was extracted with the following criteria: *target_type*='SINGLE PROTEIN', *assay_relationship*='D' (direct compound-target interaction) with the highest confidence score of 9, *activity_comment* not 'Not Active' or 'Non-toxic' for avoiding not-active compounds or targets related to ADMET assays, and *standard_relation* not '>'. From these potential candidate proteins, proteins found in endothelial cells were manually selected as predicted target proteins (Figure 2a). The first three target proteins (SNCA, SLCO2B1 and ABCC1) were used for further experiment since they show high expression on endothelial cells based on the Human Protein Atlas [www.proteinatlas.org].

3.2.5. Competition binding assays

The 3D-blood capillary models were fabricated as described in our previous work.[14,22] In brief, the 10 μL of fibrin gels which consist of fibrinogen and thrombin was mixed with 0.15 mg of collagen microfiber, 1.5×10^4 of normal human dermal fibroblast (NHDF), and 7.5×10^3 of green fluorescent protein (GFP) labeled HUVECs (GFP-HUVEC) and were seeded in a 48-well plate, subsequently. Then, the seeded tissues were incubated at 37 °C for 30 min to allow the process of forming a gel. The tissues were cultured for 5 days in a mixed cell culture medium which are of Dulbecco's Modified

Eagle Medium (DMEM) for NHDF and endothelial cell's media KBM VEC-1 basal medium (details on https://kohjin-bio.jp/wp-content/uploads/KBMVEC1_0616.pdf) at ratio of 1:1. The mixed culture medium was changed every 2 days. The competition binding assays were done using variety of competitors consisting of a specific surface marker for endothelial cells such as anti-CD14 antibody, anti-CD31 antibody, anti-CD133 antibody, and mouse IgG (was used as a control antibody). VEGF-A and tomato lectin, which are molecules binding to VEGF receptors and glycoprotein, respectively, were also expressed on endothelial cells membrane. Alpha-synuclein (SNCA), which was obtained from ChEMBL database, was also used in this competition assay as it shows highest expression on endothelial cells either from the Human Protein Atlas and also in the 3D-tissues (Fig. S6a, b). All the competitors at various concentration (0, 0.01, 0.1, 0.5, and 1.0 µM) were incubated on the 3D-blood capillary models in presence of CyA-B2 (1 µM) for 20 min at 37 °C with 5 % CO_2. The tissues were then washed once with phosphate-buffered saline (PBS) prior to live imaging by a confocal laser scanning microscopy (CLSM, Yokogawa Corp. CQ1). The experiments were conducted in triplicate.

3.2.6. Immunostaining of antibodies

3D-tissues: After 5 days culture, the tissues were fixed with 4 % paraformaldehyde (PFA) for 20 min at room temperature. The tissues were then washed for 3× with PBS before being permeabilized by 0.2 % Triton X-100 in PBS for 15 min at room temperature. Next, the tissues were washed 3× with PBS and then incubated with 1 % BSA-PBS for 1 h at room temperature. The tissues were then ready for being stained with antibody where in our study we used alpha synuclein monoclonal (SNCA) antibody, recombinant anti-multidrug resistance-associated protein (MRP1, also known as ABCC1) antibody, and solute carrier organic anion transporter family member 2B1 (SLCO2B1) polyclonal antibody to investigate the expression of SNCA, MRP1, and SLCO2B1, respectively, on the blood capillaries. Anti-CD31 antibody was used as the positive control for expression of endothelial cells on the blood capillaries. All antibodies were diluted at 1:100 in 1 % BSA-PBS and were then incubated on the 3D-tissues for overnight at 4 °C. To observe the expression of each antibody, secondary antibody with the

fluorescence tag was used. Alexa Fluor 647, anti-mouse (for SNCA) and Alexa Fluor 546, anti-rabbit (for ABCC1 and SLCO2B1) and co-staining with Alexa Fluor 546 or Alexa Fluor 647 for CD31 were diluted in 1 % BSA-PBS (1:200) and incubated for 1 h at room temperature. Finally, the tissues were washed 3× with PBS prior to observation with confocal microscopy (CQ1).

2D monolayer cells: HUVECs and GFP-HUVECs (1.0×10^5) were seeded on the glass bottom dish (35 mm) and cultured for 24 h. After 1 day culture, the cells were washed several times with PBS before fixation process using 4 % PFA. The next step is similar to the method on 3D-tissue above. However, the purpose of this experiment is to confirm the expression of CD133 on both types of cells. So, we used anti-CD133 antibody (1:100 dilution in 1 % BSA in PBS) to stain the cells and incubated for overnight at 4 °C. After that, Alexa Fluor 546 (1:200 dilution in 1 % BSA in PBS) and Hoechst 33342 (1:1000 dilution in 1 % BSA in PBS) were stained and incubated at room temperature for 2 h. Finally, the cells were washed with PBS before observing the fluorescence using confocal microscope (CQ1).

3.2.7. IC_{50} values calculation

IC_{50} values (half maximal inhibitory concentration) for each competitor were calculated from the graph of competition binding assays using GraphPad Prism (version 8.0, GraphPad Software, San Diego, CA, USA). All calculations were done using the log (inhibitor) vs response curve-variable slope, three parameters and IC_{50} values were calculated according to the following equation (H. J. Motulsky, "Dose-response-Inhibition", GraphPad Curve Fitting Guide. https://www.graphpad.com/guides/prism/latest/curve-fitting/reg_dr_inhibit_variable.htm):

$$Y = \text{Bottom} + \frac{\text{Top} - \text{Bottom}}{1 + 10\text{^}((\text{LogIC}_{50} - X) \times \text{Hill Slope}}$$

3.2.8. Binding curve of CyA-B2 and CD133 protein

Various concentration of recombinant human CD133 protein (0.05 to 50 nM) was incubated with CyA-B2 (1 μM) in 0.1 % DMSO PBS for 5 min at 37 °C. The emission of CyA-B2 was measured by a spectrofluorometer with excitation at 640 nm. The experiment was also done to obtain the binding curve for low P' probe (CyA-D8) and CD133 protein and CyA-B2 or CyA-D8 and VEGFR1 as control samples. The binding constant (K_d) value was obtained by applying the Hill equation to the binding curve.[23,24]

3.2.9. Job plot assay

The binding ratio of probe-protein complex was determined by the method of continuous variation (job plot).[25–27] To the 0.2, 0.4, 0.5, 0.67, 1, 1.33, 1.5, 1.6, and 1.8 μM solution of CD133 protein, 1.8, 1.6, 1.5, 1.33, 1, 0.67, 0.5, 0.4, and 0.2 μM CyA-B2 were added, respectively. The overall concentration of probe and protein added remained constant: [Probe] + [Protein] = 2 μM. Every test solution had a total volume of 10 μL. After incubation for 5 min, the fluorescence intensities of the samples at 665 nm were measured by a NanoDrop™ 3300 Fluorospectrometer (Thermo Scientific™).

Statistical analysis: Results are presented as means ± s.d. The sample numbers (*n*) indicate the number of replicates in the experiments and are provided in the figure legends. Statistical analyses were performed using Excel (Microsoft). The unpaired two-tailed Student's *t*-test was used to determine the significances of differences between groups. **p*<0.05, ***p*<0.01, ****p*<0.001, *N.S.* = no significant.

3.3. Results and discussion

3.3.1. Electrostatic and Hydrogen Bonding Interaction Effects on CyA-B2 Distribution

To investigate the type of bonding interaction, first the effect of sodium chloride and urea addition was assessed since they act as inhibitors of probe interaction to its target through electrostatic interaction and hydrogen bonding, respectively. The experiment has been done on the 3D-blood capillary models by staining CyA-B2 in the presence of urea or NaCl in our previous study.[14] In the current report, to further understand the probe interaction, we investigated the distribution of the CyA-B2 probe in presence of

increasing concentrations of urea or sodium chloride in order to assess the possible probe-probe interaction (aggregation). Although, in *in vivo* staining we could not analyze the aggregation of CyA-B2 probe due to the presence of many blood proteins (albumin, glycoprotein, lipoproteins, etc.) which might be affecting the distribution of probe, however, the binding ability of the probe to the endothelium layer seemed to be possible anyway due to the visibility of the probe after *in vivo* imaging.[14] From **Figure 3.1a**, the distribution of CyA-B2 in the presence of urea (0-1.0 M) does not change its size indicating that the probe did not aggregate even at higher concentration of urea. Whereas additional of sodium chloride in the buffer (buffer used: DMEM containing 110 mM NaCl) could affect the size of CyA-B2 at 10-fold compared to the size with 0 mM NaCl (110 mM NaCl in DMEM). However, the size of aggregated CyA-B2 are still relatively small (<100 nm) which would not enough to inhibit the probe from reaching the target site.[28] This result might be due to the concentration used in this assay that are not enough to suppress the binding of probe and target via electrostatic interaction. The polydispersity

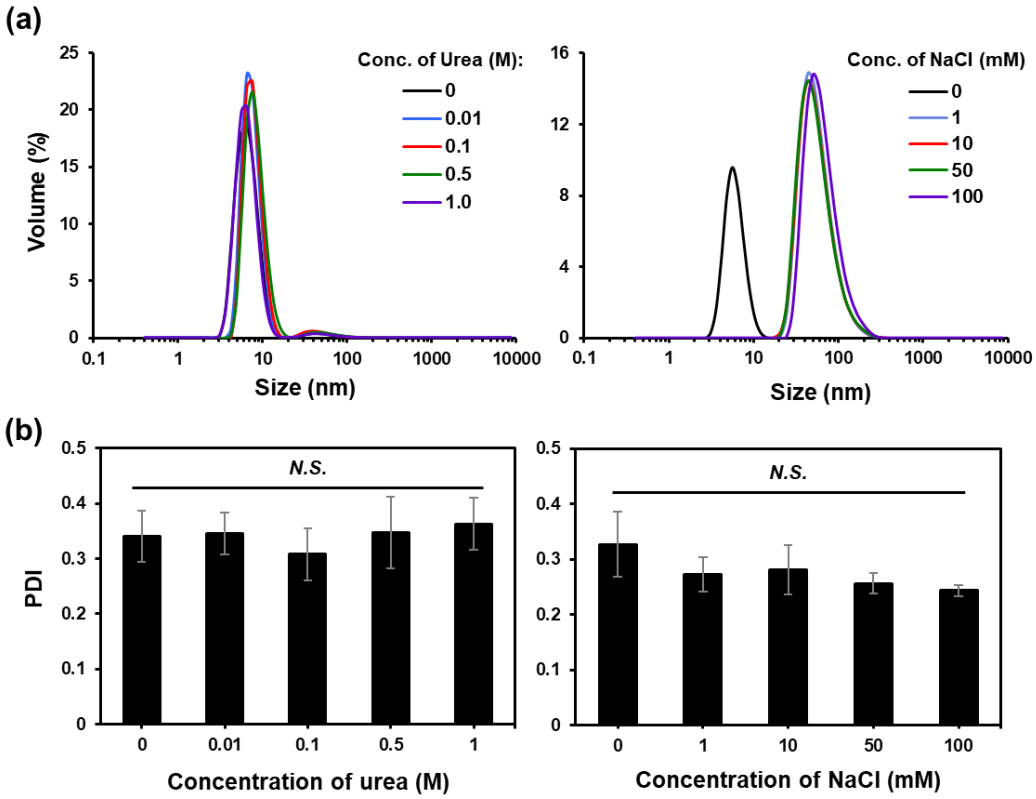

Figure 3.1. The effect of CyA-B2 distribution by dynamic light scattering (DLS) for their size distribution (intensity) (**a**) and PDI values (**b**) in the presence of various concentrations of urea and NaCl, respectively.

index (PDI) (**Figure 3.1b**) for both experiments show no difference from the control sample (without urea and NaCl) suggesting their homogenous distribution at given concentration of urea or NaCl. Thus, this experiment confirmed the results of no significant difference in the specific binding of CyA-B2 (P 'value) on blood capillaries as in the previous chapter. The distribution of CyA-B2 probes did not change remarkably following addition of urea or NaCl, suggesting the stability of CyA-B2 in both conditions with no binding inhibitions via hydrogen bonding and electrostatic interactions.

3.3.2. HOMO-LUMO of High and Low P' Probes

To get better insight on the differences between classified high P' probes and low P' probes, we investigate their photophysical properties by DFT calculation using Gaussian software. **Figure 3.2** displays the HOMO and LUMO contour plots computed for the CyA-B2 (high P' value) and CyA-D8 (low P' value) molecule in water as a solvent. The distribution of HOMO and LUMO are similar on both CyA-B2 and CyA-D8

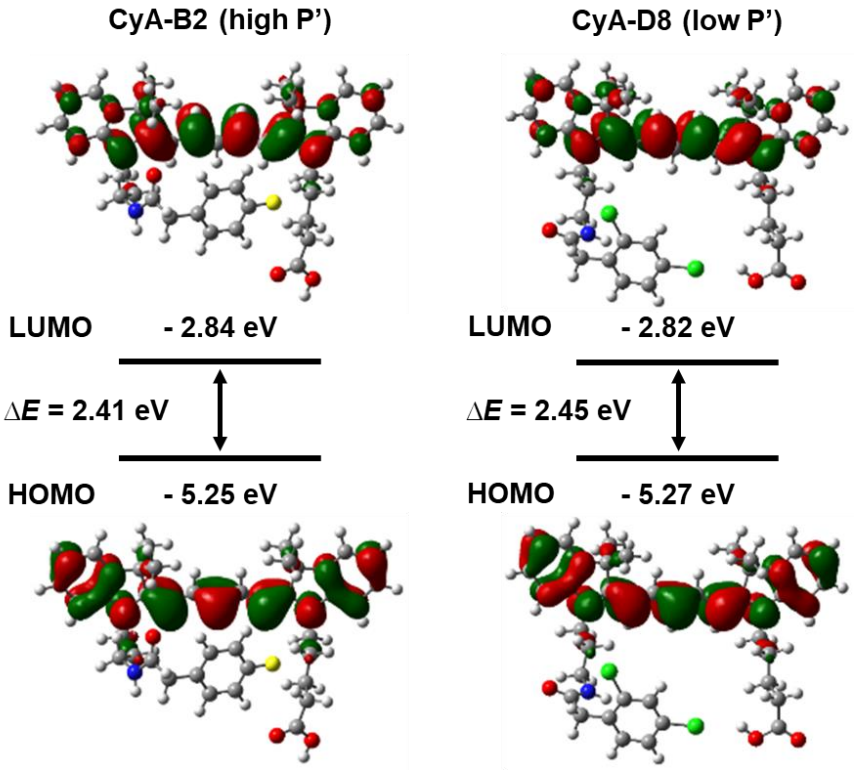

Figure 3.2. Depictions of the HOMO and LUMO of CyA-B2 (high P' probe) and CyA-D8 (low P' probe), respectively.

molecules, although they are from different class of probes. Similar results were observed with other high and low P' probes (including control molecule, Cy5).

In order to identify the difference in term of energy level between high P' probes and low P' probes, we measured the energy gap of each probe. The HOMO-LUMO gaps (energy level in eV) of high and low P' probes were calculated and plotted in **Figure 3.3**, and they showed no clear correlation between high and low P' probes. Only CyA-C2 (high P') showed a relatively lower HOMO-LUMO gap compared to other probes which might be due to its nature of substituent (NMe_2) that influence the energy level of HOMO.[29] Nevertheless, the screening result of chemical probes in the previous report [14] showed that the P' value of adsorbed CyA-C2 on the blood capillaries was actually found to be lower compared to CyA-B2 (the highest one). Overall, these results indicate that the fluorescence properties (HOMO-LUMO gaps) of the probes do not contribute so much to the results of high and low P 'values and remain unaffected even though each probe consists of different substitutes on the cyanine core structure. To find out detailed information from other fluorescent properties such as fluorescence quantum yield and lifetime, further studies need to be investigated.

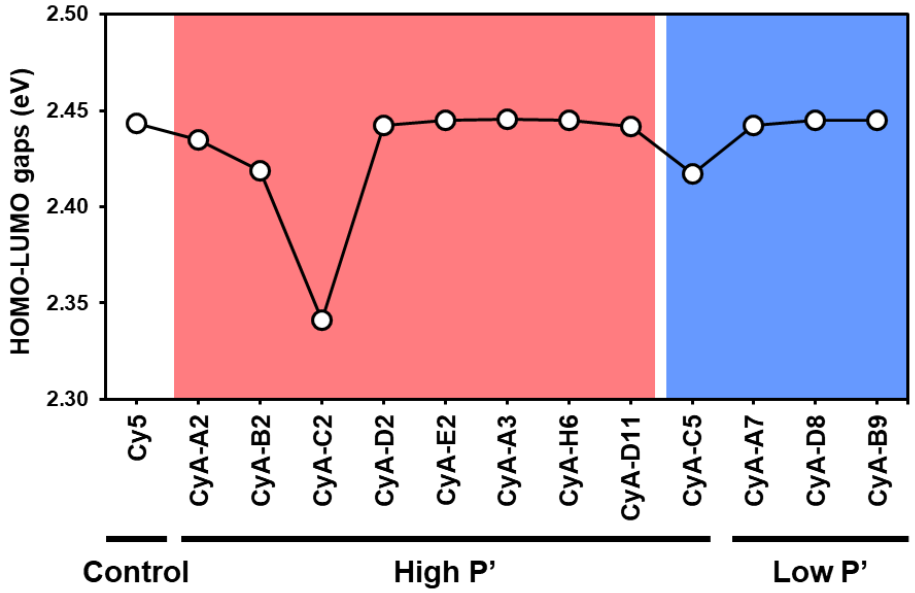

Figure 3.3. Summary of HOMO-LUMO gaps for all high P' probes (red region) and some of low P' probes (blue region). Relative energies of the HOMOs and LUMOs are provided in eV.

3.3.3. Prediction of Target by Similarity Searching on the ChEMBL Database

With the plethora of data from studies that have been already conducted, prediction of target proteins can be done by searching small molecules similar to CyA-B2 in the ChEMBL database (**Figure 3.4**). From standardized 1,721,776 unique compounds in the database, 32 similar compounds were identified with Tanimoto similarity values to CyA-B2 between 0.40 and 0.55. For any of the 32 compounds, 43 potential target macromolecules were associated with high confidence of assays. From these potential targets, six endothelial cell-related proteins were manually identified, as shown in **Table 3.1**. The corresponding six compounds with Tanimoto similarity values to CyA-B2 and CHEMBL IDs are reported in Figure S4. From these six targets, SNCA was selected for further *in vitro* testing due to its high expression rate on endothelial cells compared to other proteins based on the Human Protein Atlas data [www.proteinatlas.org] and confirmed in our 3D-blood capillary models (Figure S5).

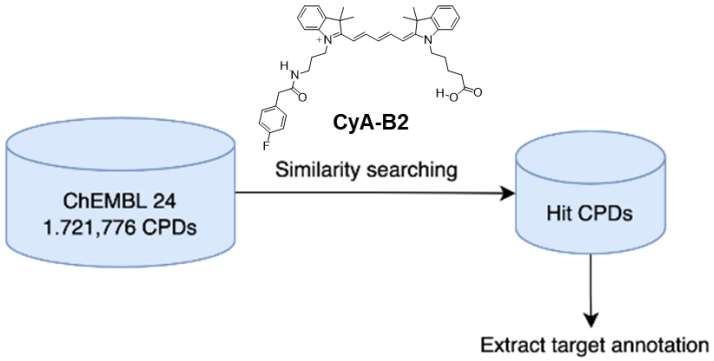

Figure 3.4. Analysis of screened chemical probes by chemoinformatics approaches. The procedure for target prediction of CyA-B2 using ChEMBL database.

Table 3.1: The results of biological targets (related to ECs) which have >~0.4 similarity of structure with CyA-B2.

Biological targets (related to endothelial cells)	**Similarity**
Alpha-synuclein (SNCA)	0.44
Solute carrier organic anion transporter family member 2B1 (SLCO2B1)	0.40
Multidrug resistance-associated protein 1 (ABCC1)	0.40
Sphingosine 1-phosphate receptor 2 (S1PR2)	0.44

Histamine H_2 receptor (HRH2)	0.48
Glutamate carboxypeptidase 2 (FOLH1)	0.49

3.3.4. Competition Binding Assays

To investigate the binding target protein for CyA-B2 on the vascular endothelial cells, several known endothelial cell surface markers such as CD14, CD31, CD133, alpha-synuclein (SNCA, discovered from ChEMBL database), vascular endothelial growth factor receptor, and glycoprotein were chosen as competition sites. The competition assay was performed on the 3D-blood capillary models and the live imaging of the probe was observed by confocal microscopy (CQ1). Live imaging of CyA-B2 was observed for each concentration of anti-CD133 antibody (**Figure 3.5a**). The fluorescence intensity of the specific adsorption of CyA-B2 (P') on the blood capillaries was monitored using Imaris software and plotted with various concentration of anti-CD133 antibody (**Figure 3.5b**, left). The P' value of CyA-B2 decreases when increasing the concentration of anti-CD133 antibody, while control IgG (isotype control which does not have specificity to the target but matches the class and type of the primary antibodies used) does not gave a significant difference in the P' value. Then, the IC_{50} value of anti-CD133

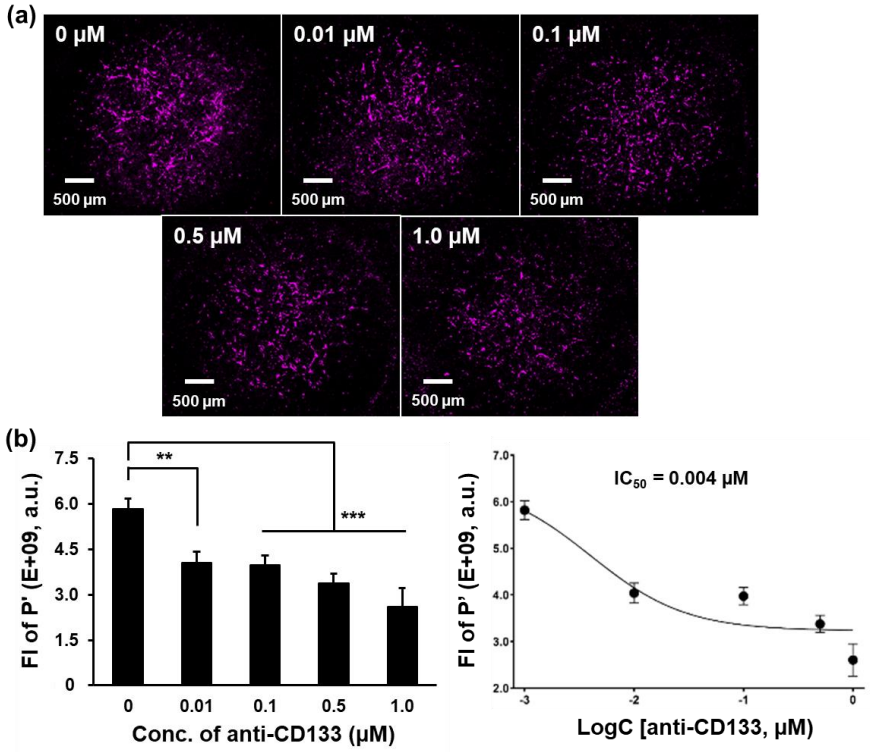

Figure 3.5. Competition binding assays of CyA-B2 with proteins or molecules having the same possible target. (**a**) Confocal images show the effect of CyA-B2 binding without (0 µM) and with (1.0 µM) presence of CD133 during incubation on 3D-blood capillary models. Scale bar is 500 µm. (**b**) Left graph shows the fluorescence intensity (FI) of specific adsorption (P') with various concentration of CD133. Data presented as mean ± s.d., (n=3), $**p < 0.01$, $***p < 0.001$. Right graph shows IC_{50} values from competition assay for CyA-B2 probe with antibodies (IgG, CD14, CD31, CD133, SNCA) and molecules (VEGF-A and tomato lectin).

antibody competition was calculated by the curve fitting to the fluorescence intensity of P' against logarithmic concentration of CD133 (**Figure 3.5b**, right). IC_{50} values for the other competitors were also calculated and were summarized in the **Table 3.2**. These IC_{50} values of the competition for the CyA-B2 adsorption on the CD133 marker of endothelial cells showed the highest suppression potential on the blood capillaries and was then followed by VEGFR > CD31 > CD14 > SNCA.

Table 3.2. Summary of IC_{50} values for potential competitors using high P' probes (in red) and low P' probes (in blue). All IC_{50} values were determined from the graph of P' value.

Probes	**CyA-B2**	**CyA-H6**	**CyA-D8**	**CyA-C5**
Competitors		**IC_{50} (µM)**		
Anti-CD133	0.004	566.2	N.D.	N.D.
VEGF-A	0.047	1209.0	N.D.	N.D.
Anti-CD31	0.064	–	–	–
Anti-CD14	0.166	–	–	–
*SNCA	0.305	–	–	–
Tomato lectin	N.D.	–	–	–
#IgG	N.D.	–	–	–

*SNCA: alpha-synuclein (protein discovered from ChEMBL database); #IgG: Immunoglobulin G (as negative control); N.D: data can't be detected from fluorescent titration; "-" means no data is obtained.

The competition binding assays were also done for several other probes used in our previous chemical probes screening results where we classified high P' probe (CyA-H6) and low P' probes (CyA-D8 and CyA-C5). These competition assays were done

using antibodies against CD133 and VEGF-A which had the lowest IC_{50} value from CyA-B2 probe assays. Then, IC_{50} value for each competitor was calculated and summarized in the **Table 3.2**. The results show that CyA-B2 has a lower IC_{50} value compared to CyA-H6 (which also had a high adsorption on the blood capillaries) indicating that CyA-B2 has a higher specificity towards CD133 compared to CyA-H6. In contrast, low P' probes (CyA-D8 and CyA-C5) showed no significant difference in competition binding suggesting no binding site with CD133. Based on this result, we postulated that CyA-B2 binding site was most likely to CD133 on the endothelial cell membrane and thus further investigated their binding strength.

3.3.5. Binding Affinity of CyA-B2 Probe and CD133 Protein

To confirm the specific interaction between CyA-B2 and CD133, the fluorescence spectra of CyA-B2 (1 µM) in the presence of increasing concentrations of CD133 protein (0-50 nM) were measured (**Figure 3.6a**, left). From these results, a remarkable fluorescence enhancement of CyA-B2 with increasing concentration of CD133 protein was found, whereas no fluorescence enhancement was observed when CyA-D8 (low P') was used instead of CyA-B2 with the same concentration of CD133 (**Figure. 3.6b**, left).

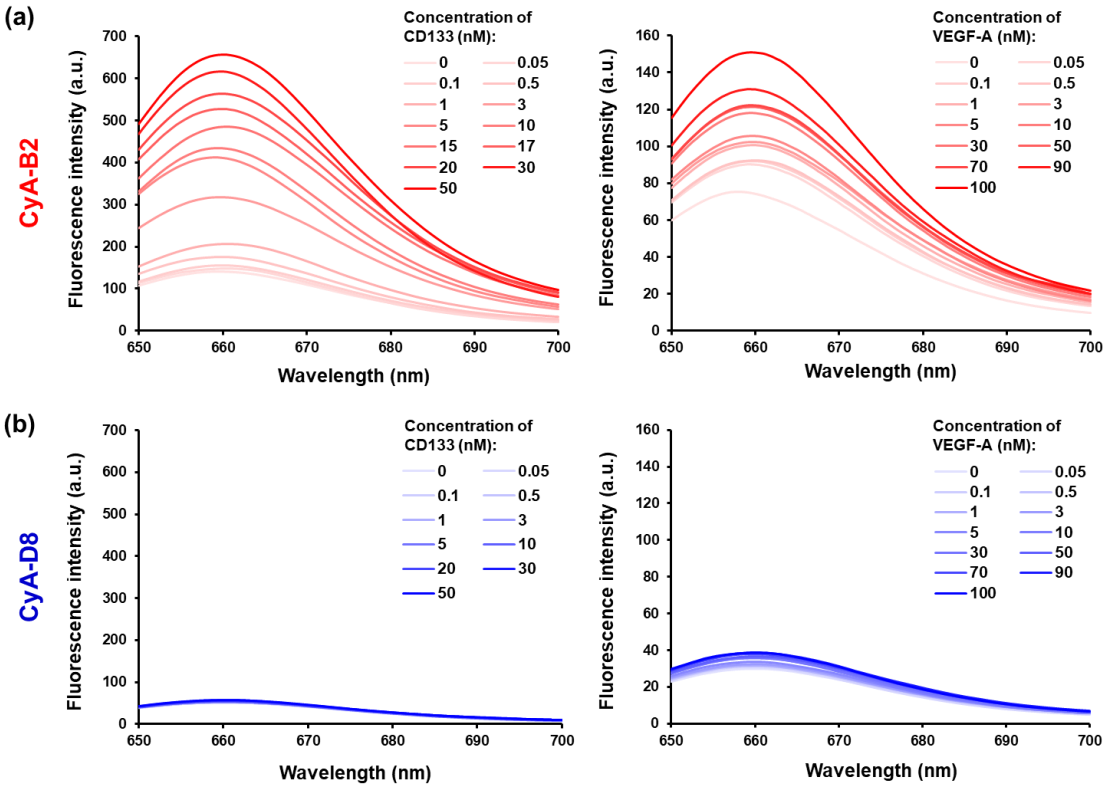

Figure 3.6. (**a**) Fluorescence spectra of CyA-B2 (high P' probe, 1 μM) in the presence of CD133 protein and VEGF-A. Concentrations of CD133 protein are used from 0.05-50 mM while VEGF-A are used from 0.05-100 mM. (**b**) Fluorescence spectra of CyA-D8 (low P' probe, 1 μM) in the presence of CD133 protein and VEGF-A. Concentrations of CD133 protein are 0.05-50 mM while VEGF-A are 0.05-100 mM.

The results suggested that there is a binding event between CD133 protein and CyA-B2 but not for CyA-D8 which proved the specificity of CyA-B2 towards CD133 protein. To further confirm this specificity with CD133, the same assay was performed in the presence of VEGF-A (0-100 nM) instead with CyA-B2 (**Figure 3.6a**, right) and CyA-D8 (**Figure 3.6b**, right). Only a slight fluorescence enhancement was observed for both CyA-B2 (high P') and CyA-D8 (low P') with increasing concentrations of VEGF-A. These results suggested that there is no specific binding event between VEGF-A with both CyA-B2 and CyA-D8. This is in accordance with the IC_{50} values measured in Table 3.2 showing a limited competitive binding inhibition with VEGF-A. Furthermore, the binding constant (K_d) between CD133 protein and CyA-B2 was calculated using Hill equation to be K_d = 2.40 nM (**Figure 3.7a**). In addition, the job plot assay as shown in **Figure 3.7b** indicated that the binding ratio of CyA-B2 and CD133 protein was 2:1.

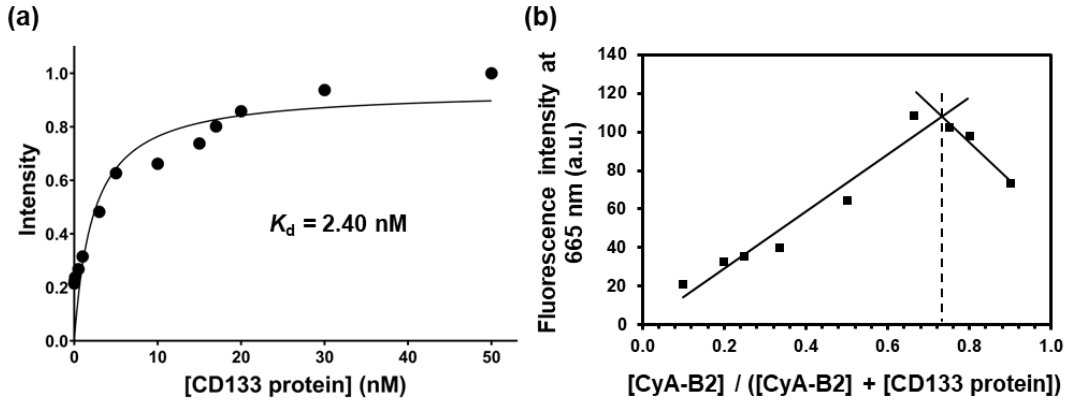

Figure 3.7. (**a**) The binding curve illustrates the binding constant (K_d = 2.40 nM) from the curve fitting. (**b**) Job plot assay for fluorescence intensity at 665 nm of the probe (CyA-B2)-protein (CD133) complex at different molar ratio.

3.4. Conclusion

In conclusion, we have discussed the mechanisms for the CyA-B2 fluorescent probe which were previously selected from library screening binding on the endothelial cells. The fluorescence properties (HOMO-LUMO) assessment first did not allow to understand any possible correlation. Nevertheless, using the chemical database (ChEMBL) we successfully determined possible target proteins for CyA-B2 and manually selected the one appearing surface marker of endothelial cells. In this report, we found CD133 expressed on cell surface of endothelial cells as a novel target molecule for the probe CyA-B2 binding. Although, CD133 is not only expressed in HUVEC cells but also in other types of endothelial cells such as endothelial colony-forming cells (ECFCs) and human aortic endothelial cells (HAECs) [18], yet for future applications CyA-B2 could be used as a bioprobe for detecting cells expressing CD133 like stem cells [30] and associated with several types of cancer, including some leukemias and brain tumors.[31]

3.5. References

[1] P. M. Vanhoutte, H. Shimokawa, M. Feletou, E. H. C. Tang, *Acta Physiologica* **2017**, *219*, 22.

[2] X. Fei, Y. Gu, *Progress in Natural Science* **2009**, *19*, 1.

[3] X. Liu, Y. T. Chang, *Chem Soc Rev* **2022**, *51*, 1573.

[4] J. Zhang, R. E. Campbell, A. Y. Ting, R. Y. Tsien, *Nature Reviews Molecular Cell Biology* **2002**, *3*, 906.

[5] M. Schäferling, *Angewandte Chemie - International Edition* **2012**, *51*, 3532.

[6] Q. Miao, D. C. Yeo, C. Wiraja, J. Zhang, X. Ning, C. Xu, K. Pu, *Angewandte Chemie* **2018**, *57*, 1256.

[7] H. S. Lv, J. Liu, J. Zhao, B. X. Zhao, J. Y. Miao, *Sensors and Actuators, B: Chemical* **2013**, *177*, 956.

[8] P. Workman, I. Collins, *Chemistry and Biology* **2010**, *17*, 561.

[9] J. Blagg, P. Workman, *Cancer Cell* **2017**, *32*, 9.

[10] N. Y. Kang, H. H. Ha, S. W. Yun, Y. H. Yu, Y. T. Chang, *Chemical Society Reviews* **2011**, *40*, 3613.

[11] S. W. Yun, N. Y. Kang, S. J. Park, H. H. Ha, Y. K. Kim, J. S. Lee, Y. T. Chang, *Accounts of Chemical Research* **2014**, *47*, 1277.

[12] L. Zhang, J. C. Er, K. K. Ghosh, W. J. Chung, J. Yoo, W. Xu, W. Zhao, A. T. Phan, Y. T. Chang, *Scientific Reports* **2014**, *4*, 3776.

[13] L. Zhang, J. C. Er, X. Li, J. J. Heng, A. Samanta, Y. T. Chang, C. L. K. Lee, *Chemical Communications* **2015**, *51*, 7386.

[14] M. A. Abdul Sisak, F. Louis, I. Aoki, S. H. Lee, Y. T. Chang, M. Matsusaki, *Small Methods* **2021**, *5*, DOI 10.1002/smtd.202100338.

[15] D. Ribatti, R. Tamma, S. Ruggieri, T. Annese, E. Crivellato, *Microcirculation* **2020**, *27*, e12587.

[16] M. C. Munisso, T. Yamaoka, *Journal of Artificial Organs* **2020**, *23*, 6.

[17] U. M. Gehling, S. Leyman Ergü, U. Schumacher, C. Wagener, K. Pantel, M. Otte, G. Schuch, P. Schafhausen, T. Mende, N. Kilic, K. Kluge, B. Schä, D. K. Hossfeld, W. Fiedler, *Blood* **2000**, *95*, 3106.

[18] E. Rossi, S. Poirault-Chassac, I. Bieche, R. Chocron, A. Schnitzler, A. Lokajczyk, P. Bourdoncle, B. Dizier, N. C. Bacha, N. Gendron, A. Blandinieres, C. L. Guerin, P. Gaussem, D. M. Smadja, *Stem Cell Reviews and Reports* **2019**, *15*, 590.

[19] A. Gaulton, A. Hersey, M. L. Nowotka, A. Patricia Bento, J. Chambers, D. Mendez, P. Mutowo, F. Atkinson, L. J. Bellis, E. Cibrian-Uhalte, M. Davies, N. Dedman, A. Karlsson, M. P. Magarinos, J. P. Overington, G. Papadatos, I. Smit, A. R. Leach, *Nucleic Acids Research* **2017**, *45*, D945.

[20] D. Rogers, M. Hahn, *Journal of Chemical Information and Modeling* **2010**, *50*, 742.

[21] M. Vogt, D. Stumpfe, H. Geppert, J. Bajorath, *Journal of Medicinal Chemistry* **2010**, *53*, 5707.

[22] M. A. Abdul Sisak, F. Louis, S. Hyeok Lee, Y. Chang, M. Matsusaki, *Micromachines (Basel)* **2020**, *11*, 727.

[23] A. v. Hill, *The Journal of Physiology* **1910**, *40*, iv.

[24] M. Möller, A. Denicola, *Biochemistry and Molecular Biology Education* **2002**, *30*, 309.

[25] P. Job, *Annali di Chimica* **1928**, *9*, 113.

[26] Charles. Y. Huang, *Methods in Enzymology* **1982**, *87*, 509.

[27] S. Lee, D. B. Sung, S. Kang, S. Parameswaran, J. H. Choi, J. S. Lee, M. S. Han, *Sensors (Switzerland)* **2019**, *19*, 5298.

[28] E. Blanco, H. Shen, M. Ferrari, *Nature Biotechnology* **2015**, *33*, 941.

[29] M. Chemek, S. ben Amor, W. Taouali, E. Faulques, M. Bourass, D. Khlaifia, A. Haj Said, K. Alimi, *Journal of Molecular Structure* **2021**, *1241*, 130599.

[30] Z. Li, *Experimental Hematology and Oncology* **2013**, *2*, 1.

[31] X. Cai, J. Li, X. Yuan, J. Xiao, S. Dooley, X. Wan, H. Weng, L. Lu, *Journal of Translational Medicine* **2018**, *16*, 1.

Chapter 4

Near-Infrared Chemical Probes on the 3D-lymphatic Capillary Models (3D-LCM) and its Possible Target Protein

4.1. Introduction

The circulatory network of the human body consists of the cardiovascular system and the lymphatic system that carries blood and lymph, respectively. Lymphatic vessels and blood vessels generally form a complex system of extensive and highly branched networks responsible for the circulation and transport of fluids, molecules, and cells in the body. A significant difference between blood capillaries and lymphatic capillaries is the composition of the fluid circulating blood vessels and lymph, and it provides important information about physiological processes. The importance of understanding the pivotal role of vasculatures in disease has led to great efforts in developing relevant *in vitro* 3D tissue models. To date, several researchers have reported the construction of 3D tissue models using hydrogel, [1-3] porous scaffold, [4] and cell sheet [5] as well as perfusable networks constructed in microchannels [6-9] have also been studied. Furthermore, a few studies have reported live imaging on lymphatic vessel using chemical probe.[10]

The successful fabrication of 3D-blood capillary models for the screening systems in the previous chapter had further inspired us to fabricate other vascular 3D tissue models especially lymphatic capillary models. Herein, in this chapter, 3D-lymphatic capillary model (3D-LCM) was fabricated and applied to microarray analysis for screen chemical probe libraries.

4.2. Experiment

4.2.1. Materials

Green fluorescent protein expressing human dermal lymphatic microvascular endothelial cells (GFP-LEC, cAP-0003GFP) was purchased from Angio-Proteomie (Massachusetts, USA). Normal human dermal fibroblast (NHDF) was purchased from Lonza (Basel, Switzerland). Dulbecco's Modified Eagle Medium (DMEM, 08458-45) was purchased from Nacalai Tesque (Kyoto, Japan). Thrombin (T4648), fibrinogen (F8630), and phosphate-buffered saline (PBS, D5652) were purchased from Sigma-Aldrich (St. Louis, MO, USA). KBM VEC-1 basal medium (16030110) was purchased from Kohjin Bio Co. Ltd. (Saitama, Japan). Anti-CD31 antibody (M0823) was purchased from Dako (Glostrup, Denmark). Lymphatic vessel endothelial hyaluronan receptor 1 (Lyve-1, 102-PA50AG) was purchased from Reliatech GmbH (Wolfenbüttel, Germany).

4.2.2. Fabrication of 3D-lympatic Capillary Models (3D-LCM)

In this chapter, a 3D-lymphatic capillary model (3D-LCM) was fabricated using fibrin gel similar to 3D-BCM. Basically, the components of 3D-LCM are similar to 3D-LCM, the only difference is the use of lymphatic endothelial cells (LECs) instead of HUVEC cells. Briefly, normal human dermal fibroblast (NHDF) and green fluorescent protein labeled LEC (GFP-LEC) were trypsinized (5 min, 37 °C) and then centrifuged at 1000 rpm for 5 min at room temperature for collecting the cells by removing the supernatant. 5 U/mL of thrombin was mixed with cells (NHDF and GFP-LEC) in Dulbecco modified Eagles's medium (DMEM High-Glucose) and regarded as solution 1. Then, solution 2 comprising 15 mg/mL of CMF-50 was mixed with 5 mg/mL of fibrinogen in DMEM (FBS free). Thus, the 10 μL of fibrin gels containing 0.15 mg of CMF-50, 3.0×10^4 of NHDF, and 7.5×10^3 of GFP-LECs were seeded in each well of a 48-well plate. After that, the tissue drops were incubated at 37 °C for 30 min to allow the gelation process upon the reaction of fibrinogen and thrombin. Finally, the tissues were cultured for 5 days at 37 °C with 5 % CO_2 using mixed cell culture medium which is a mixture of DMEM and KBM VEC-1 basal medium at ratio of 1:1. The mix culture medium was changed every 2 days.

4.2.3. Screening of High and Low P' probes on 3D-LCM

For the screening of chemical probe libraries, we decided to use previous screened probe on the 3D-BCM (classified as high and low P' probes). Four probes from high P' group (CyA-A2, CyA-B2, CyA-D2, and CyA-H6) and four probes from low P' group (CyA-C5, CyA-A7, CyA-D8, and CyA-B9) were chosen for further screening on the 3D-LCM. Briefly, the 0.65 µg/mL probes (1 µM in DMEM with 0.1 % DMSO) were used for staining of 3D-LCM (tissues) and incubated for 20 min at 37 °C in an incubator. The tissues were then washed with PBS to remove the unbound probes. Live imaging of probes adsorption was acquired by a confocal laser scanning microscopy (CLSM, Yokogawa Corp. CQ1) at 37 °C. Maximum intensity projection of the full sample, 40 % excitation power for each fluorescence channel (GFP channel: excitation wavelength = 488 nm; probe channel: probe excitation wavelength = 640 nm), 300 ms exposure time, keeping same brightness and contrast for all samples to enable the comparison. The exported images were finally used to analyze the colocalization of the probes to the lymph capillaries using Imaris software.

4.2.4. Optimization of Concentration and Incubation Time of CyA-B2 on 3D-LCM

The concentration of CyA-B2 (also hit compound for 3D-LCM) was optimized by using various concentration (0.1, 1.0, 3.0, 5.0, and 10.0 µM) as well as their incubation time (0, 1, 5, 10, 15, and 20 min) for staining of the tissues. All tissues were incubated at 37 °C and washed by PBS prior to live imaging observation by CLSM. The quantification of the specific probes binding (P') values and colocalization (%) were measured by Imaris software as described in the previous chapter. Each condition was examined in triplicates.

4.2.5. Competition Binding Assay of CyA-B2 on 3D-LCM

The competition binding assays were done using competitors of specific surface marker for lymphatic endothelial cells which are anti-CD31 antibody and lymphatic vessel endothelial hyaluronan receptor 1 (Lyve-1). The competitors at various concentration (0, 0.01, 0.1, 0.5, and 1.0 µM) were incubated on the 3D-LCM in presence of CyA-B2 (1 µM) for 20 min at 37 °C with 5 % CO_2. The tissues were then washed once with phosphate-buffered saline (PBS) prior to live imaging observed by CLSM. The experiments were conducted in triplicate.

4.3. Results and discussion

4.3.1. Fabrication of 3D-lympatic Capillary Models (3D-LCM)

As shown from confocal microscopy observations in **Figure 4.1**, highly dense and homogenous lymph capillary networks on the tissue were successfully fabricated after 5 days culture. For this 3D-LCM, the number of NHDF was actually 2-fold higher than that of 3D-BCM resulting higher dense network compared to 3D-BCM. This phenomenon is believed due to the angiogenic factor secreted by NHDF to induce migration, proliferation, and differentiation thus leading to the activation of endothelial cells.[11] Hence, the total amount of angiogenic factors is an essential factor for vascularization.

Therefore, this is a simple, easy, and relatively rapid technique which is also capable of preparation of the other type of vascular 3D tissue (lymphatic capillary models). Furthermore, the application of this 3D tissue could be a microarray analysis, and thus would be a powerful tool for screening assay not only for chemical probe libraries but also for therapeutic assay, generally.

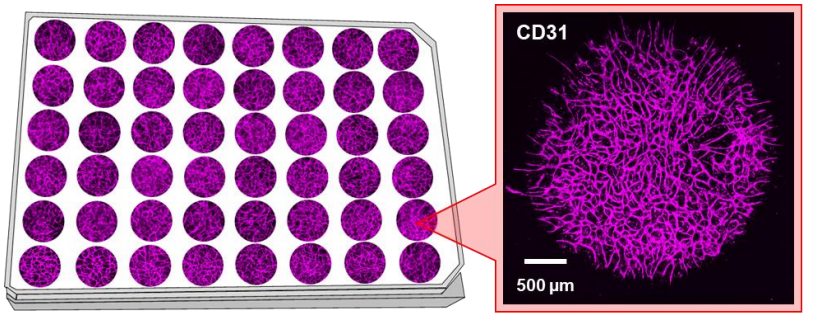

Figure 4.1. Application of screening systems for 3D-lymphatic capillary models (3D-LCM). Representative anti-CD31 immunostaining (endothelial marker) of the 48 different 3D-LCM constructed in the 48-well plate illustration.

4.3.2. High and Low P' Probes Staining on 3D-LCM

In order to apply chemical probe libraries on the 3D-LCM, we decided to use only CyA probe libraries (excluding CyB and CyC probe libraries) since they showed reliable result on the previous 3D-BCM. Furthermore, since 3D-LCM and 3D-BCM consist of

nearly identical components except for endothelial cell type, we therefore assumed that previously categorized probes as high and low P 'probes might have similar staining results on 3D- LCM. Thus, several high and low P' probes were screened through 3D-LCM.

As shown in **Figure 4.2**, most of the high P' probes are still classified as high P' probes as they show higher adsorption on the lymph capillaries (except CyA-D2). Interestingly, CyA-B2 also gave the highest P' value which can be further studied to identify its target for lymphatic endothelial cells and subsequently compared its similarity with CD133 which was discovered as the binding site for CyA-B2 probe on the 3D-BCM in the previous chapter.

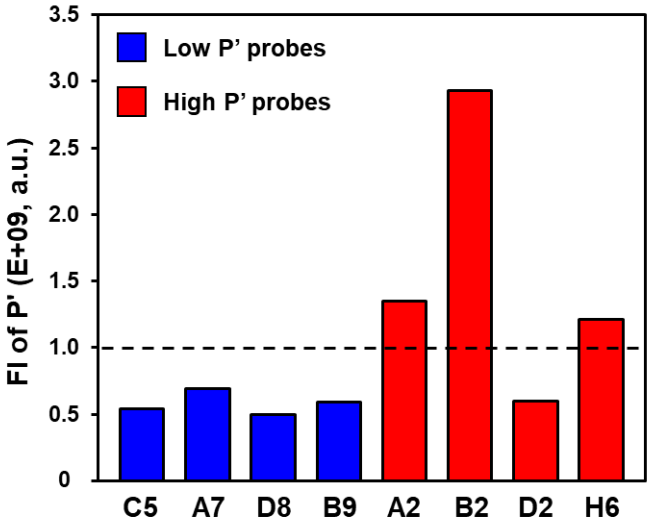

Figure 4.2. Application of screening systems for 3D-lymphatic capillary models (3D-LCM). Screening result of high P' probes (CyA-A2, CyA-B2, CyA-D3, and CyA-H6) and low P' probes (CyA-C5, CyA-A7, CyA-D8, and CyA-B9) on the 3D-LCM.

4.3.3. Optimized Concentration and Incubation Time of CyA-B2 on 3D-LCM

The concentration and incubation time of the hit compound (CyA-B2) were optimized and P' value and colocalization were calculated by Imaris software. In **Figure 4.3a** the P' values were found to increase as the concentrations of CyA-B2 increased, whereas the colocalization values showed relatively no significant difference from low to high concentration, suggesting the higher specific adsorption but constant unspecific

adsorption of the probes on 3D tissue. However, both the P' value and colocalization gradually increased with increasing incubation time and finally reached saturation after 30 minutes of incubation (**Figure 4.3b**).

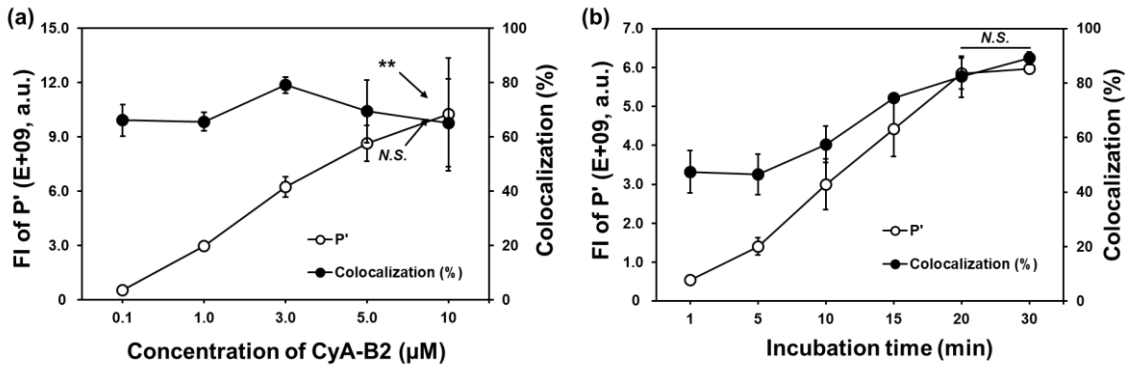

Figure 4.3. The P' intensity and colocalization of CyA-B2 probe against concentration (**a**) and incubation time (**b**), respectively. Data presented as mean ± s.d., (n=3), $^{**}p < 0.01$, *N.S.* not significant.

4.3.4. Identification of Target Protein of CyA-B2 on Lymphatic Endothelial Cells

To investigate the binding target protein for CyA-B2 on the lymphatic endothelial cells, surface markers CD31 and Lyve1, were chosen as a competition site. The competition assay was performed on the 3D-lymphatic capillary models and the live imaging of the probe was observed by CLSM. Live imaging of CyA-B2 was observed for each concentration of anti-CD31 antibody (as an example, **Figure 4.4**).

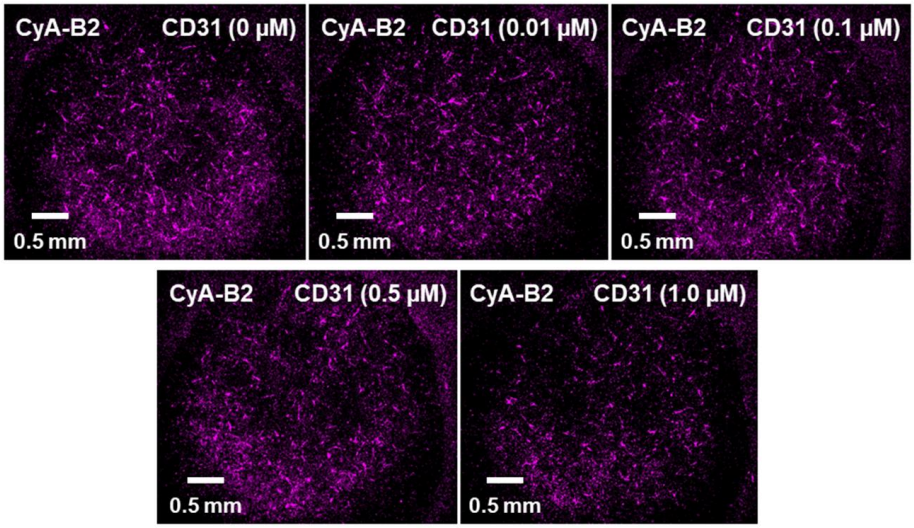

Figure 4.4. Competition binding assays of CyA-B2 with proteins having the same possible target. Representative confocal images show the effect of CyA-B2 binding in the absence (0 µM) and presence of anti-CD31 antibody (0.01-1.0 µM) during incubation on 3D-lymphatic capillary models.

For the quantitative analysis, the fluorescence intensity of the specific adsorption of CyA-B2 (P') on the lymph capillaries was monitored using Imaris software and plotted with various concentration of anti-CD31 antibody (**Figure 4.5a**). It showed that the P' value of CyA-B2 decreases with increasing the concentration of anti-CD31 antibody. Then, the IC_{50} value of anti-CD31 antibody competition was calculated from the curve fitting to the fluorescence intensity of P' against logarithmic concentration of anti-CD31 (**Figure 4.5b**). These IC_{50} values of the competition for the CyA-B2 adsorption on the CD31 marker showed lower suppression on 3D-LCM compared to the 3D-BCM, suggesting lower expression of CD31 marker on lymphatic endothelial cells (LEC) compared to HUVEC.[12] IC_{50} values for the Lyve-1 antibody were also calculated and were summarized in the **Table 4.1**.

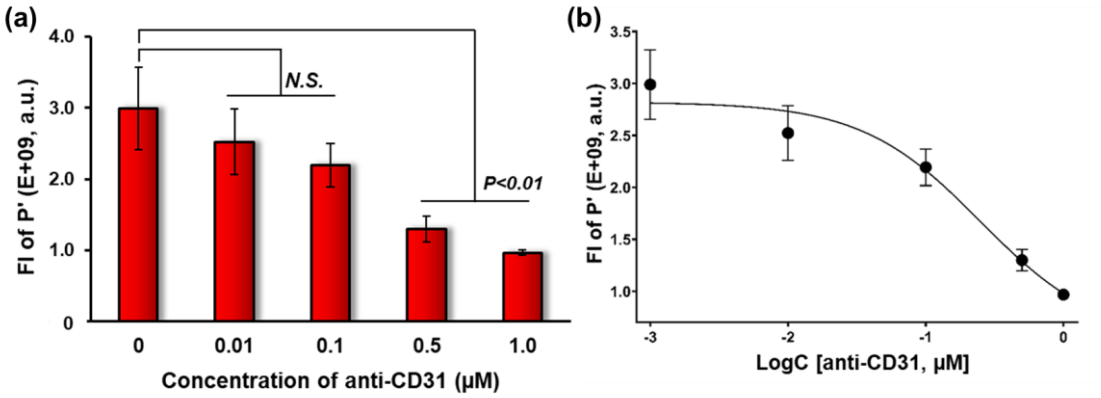

Figure 4.5. (**a**) Fluorescence intensity (FI) of specific adsorption (P') with various concentration of anti-CD31 antibody. Data presented as mean ± s.d., (*n*=3). (**b**) IC_{50} values from competition assay for CyA-B2 probe with anti-CD31 antibody on 3D-LCM.

Table 4.1. Summary of IC_{50} values for potential competitors using CyA-B2 probes. The IC_{50} values were determined from the curve fitting of graph for P' values against various concentration of antibody. "-" means no data is available.

Competitors	**IC_{50} (µM)**	
	3D-BCM	**3D-LCM**

Anti-CD31 antibody	0.064	0.25
Anti-LYVE-1 antibody	−	0.012

4.4. Conclusion

In conclusion, 3D-lymphatic capillary model (3D-LCM) was successfully fabricated as inspired from the previous 3D-blood capillary model (3D-BCM). This 3D-LCM was also high-throughput systems and subsequently used as screening the chemical probe libraries. It was found that CyA-B2 probe (classified as highest P' probe for the 3D-BCM) showed the highest specificity on the lymph capillaries compared to the other probes (high and low P' probes). Interestingly, CyA-B2 gave an increase in specific adsorption on lymph capillaries as its concentration increases without an increase in nonspecific adsorption which is different from the results for 3D-BCM even though the components for both 3D tissues are basically similar (except for vascular cells source). Furthermore, the competition binding assay showed that Lyve-1 (lymphatic endothelial marker) gives a relatively low IC_{50} value suggesting that CyA-B2 could also bind to Lyve-1 receptors on lymph capillaries. Thus, it is interesting to study the similarities between CD133 (binding site for CyA-B2 on blood capillaries) and Lyve-1 in terms of their sequence, structure, charge, etc. in order to understand how CyA-B2 probe binds to these protein/markers.

4.5. References

[1] J. C. Culver, J. C. Hoffmann, R. A. Poché, J. H. Slater, J. L. West, M. E. Dickinson, *Advanced Materials* **2012**, *24*, 2344.

[2] M. P. Cuchiara, D. J. Gould, M. K. McHale, M. E. Dickinson, J. L. West, *Advanced Functional Materials* **2012**, *22*, 4511.

[3] H. Onoe, T. Okitsu, A. Itou, M. Kato-Negishi, R. Gojo, D. Kiriya, K. Sato, S. Miura, S. Iwanaga, K. Kuribayashi-Shigetomi, Y. T. Matsunaga, Y. Shimoyama, S. Takeuchi, *Nature Materials* **2013**, *12*, 584.

[4] S. Levenberg, J. Rouwkema, M. Macdonald, E. S. Garfein, D. S. Kohane, D. C. Darland, R. Marini, C. A. van Blitterswijk, R. C. Mulligan, P. A. D'Amore, R. Langer, *Nature Biotechnology* **2005**, *23*, 879.

[5] T. Sasagawa, T. Shimizu, S. Sekiya, Y. Haraguchi, M. Yamato, Y. Sawa, T. Okano, *Biomaterials* **2010**, *31*, 1646.

[6] J. S. Miller, K. R. Stevens, M. T. Yang, B. M. Baker, D. H. T. Nguyen, D. M. Cohen, E. Toro, A. A. Chen, P. A. Galie, X. Yu, R. Chaturvedi, S. N. Bhatia, C. S. Chen, *Nature Materials* **2012**, *11*, 768.

[7] Y. Zheng, J. Chen, M. Craven, N. W. Choi, S. Totorica, A. Diaz-Santana, P. Kermani, B. Hempstead, C. Fischbach-Teschl, J. A. López, A. D. Stroock, *Proc Natl Acad Sci USA* **2012**, *109*, 9342.

[8] S. Kim, H. Lee, M. Chung, N. L. Jeon, *Lab on a Chip* **2013**, *13*, 1489.

[9] K. Sakaguchi, T. Shimizu, S. Horaguchi, H. Sekine, M. Yamato, M. Umezu, T. Okano, *Scientific Reports* **2013**, *3*, 1316.

[10] J. S. Yoo, S. C. Lee, Z. Y. Jow, P. Y. X. Koh, Y. T. Chang, *Cancer Research* **2014**, *74*, 44.

[11] A. Nishiguchi, M. Matsusaki, Y. Asano, H. Shimoda, M. Akashi, *Biomaterials* **2014**, *35*, 4739.

[12] F. Spinella, E. Garrafa, V. di Castro, L. Rosanò, M. R. Nicotra, A. Caruso, P. G. Natali, A. Bagnato, *Cancer Research* **2009**, *69*, 2669.

Concluding Remarks

The micro-droplet of 3D-blood capillary models using collagen microfiber-based fibrin gels were successfully fabricated and cultured in a 48-wells plate to serve as a medium or relatively high-throughput assay. The blood capillary tissues were validated, and their reproducibility was proven by the quantification of their mean CD31 fluorescence intensity and their total branching points measured based on their confocal images. This method can be a powerful microarray assay for screening application, providing useful data due to their more physiologically relevance as compared to 2D assay.

The author then reported the discovery of a blood vessel organic probe in near-infrared (NIR) wavelength range (BV-NIR) through an engineered blood capillary-based screening system, which is a more physiological than a conventional monolayer cell culture condition. The selected Cy5 based probe showed the highest specific adsorption property out of 240 candidates on the endothelium and was equivalent to an anti-CD31 antibody in terms of intensity. The BV-NIR (CyA-B2) probe was found with a strong and stable intensity in *in vitro*, *ex vivo*, and *in vivo* live imaging of the endothelium even after histological immunostaining processes as well, showing a great potential as a convenient tool for live imaging.

Then, by studying the competition assays of CyA-B2 using several potential surface markers of endothelial cells, the author found potential marker/protein which is CD133 that has the lowest IC_{50} value compared to other specific markers or molecules for endothelial cells. Hence, CD133 protein which is expressed on the endothelial cell membrane was proposed to be the binding site (**Scheme 1**) due to the suppression of CyA-B2 binding on the blood capillaries by applying CD133 antibodies in the competition assays. Since, CD133 is also expressed on many types of cancer cells, CyA-B2 will be useful as a bioprobe to monitor or diagnostic tumor growth. In addition, in future application the CyA-B2 could be used as a bioprobe for detecting cells expressing CD133 like stem cells and associated with several types of cancer, including some leukemias and

brain tumors. Furthermore, CyA-B2 showed a high binding constant (K_d = 2.4 nM) to CD133, therefore it has potential to be used as a theranostic agent on vascular diseases.

Finally in chapter 4, 3D-lymphatic capillary models were successfully fabricated and used as screening systems for chemical probe libraries to find a specific Lymphatic Capillary-Near Infrared probe (LC-NIR). Interestingly, based on the screening results of high and low P' probe on the 3D-LCM, CyA-B2 still showed the highest adsorption on lymph capillaries which is the same results obtained on 3D-BCM. Results from competition binding assay demonstrate that Lyve-1 is a potential binding site for CyA-B2 probe on the lymphatic endothelial cells. In order to know in detail the interaction between CyA-B2 probe on both blood and lymph capillaries, the similarity between CD133 protein and Lyve-1 receptor can be further studied in terms of their structure, gene sequence, charge and so on.

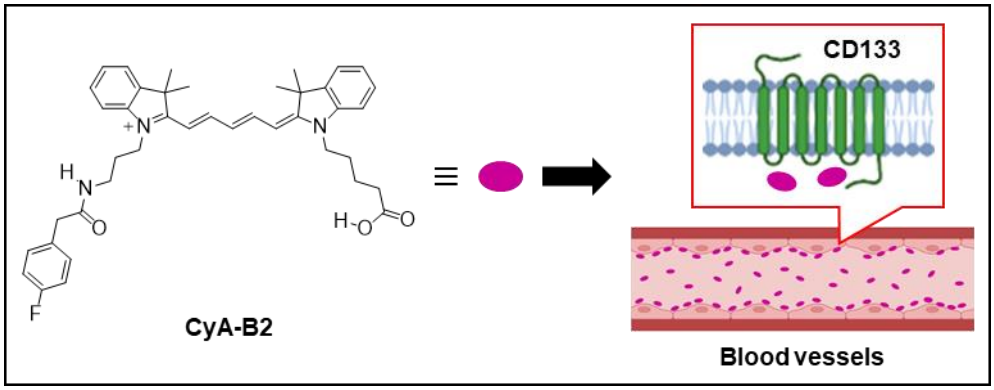

Scheme 1. Schematic illustration of biodistribution of CyA-B2 in blood vessels and their binding site on CD133 protein surface marker of endothelial cells.

Supporting Information

A

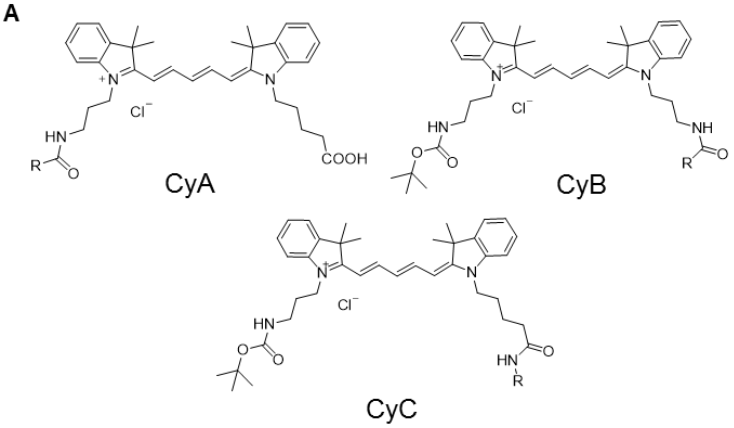

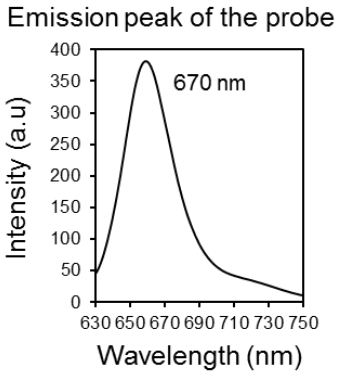

B

CyA-A2	CyA-C3	CyA-E4	CyA-G5	CyA-A7	CyA-C8	CyA-E9	CyA-G10
							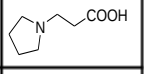
CyA-B2	CyA-D3	CyA-F4	CyA-H5	CyA-B7	CyA-D8	CyA-F9	CyA-H10
							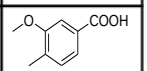
CyA-C2	CyA-E3	CyA-G4	CyA-A6	CyA-C7	CyA-E8	CyA-G9	CyA-A11
				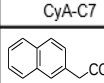			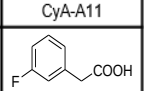
CyA-D2	CyA-F3	CyA-H4	CyA-B6	CyA-D7	CyA-F8	CyA-H9	CyA-B11
							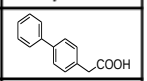
CyA-E2	CyA-G3	CyA-A5	CyA-C6	CyA-E7	CyA-G8	CyA-A10	CyA-C11
							
CyA-F2	CyA-H3	CyA-B5	CyA-D6	CyA-F7	CyA-H8	CyA-B10	CyA-D11
CyA-G2	CyA-A4	CyA-C5	CyA-E6	CyA-G7	CyA-A9	CyA-C10	CyA-E11
CyA-H2	CyA-B4	CyA-D5	CyA-F6	CyA-H7	CyA-B9	CyA-D10	CyA-F11
CyA-A3	CyA-C4	CyA-E5	CyA-G6	CyA-A8	CyA-C9	CyA-E10	CyA-G11
CyA-B3	CyA-D4	CyA-F5	CyA-H6	CyA-B8	CyA-D9	CyA-F10	CyA-H11

CyB-A2	CyB-C3	CyB-E4	CyB-G5	CyB-A7	CyB-C8	CyB-E9	CyB-G10
	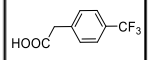			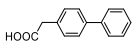	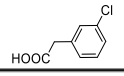		
CyB-B2	CyB-D3	CyB-F4	CyB-H5	CyB-B7	CyB-D8	CyB-F9	CyB-H10
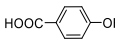						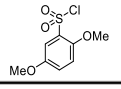	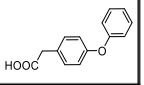
CyB-C2	CyB-E3	CyB-G4	CyB-A6	CyB-C7	CyB-E8	CyB-G9	CyB-A11
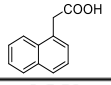			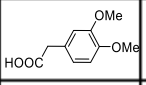				
CyB-D2	CyB-F3	CyB-H4	CyB-B6	CyB-D7	CyB-F8	CyB-H9	CyB-B11
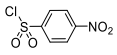						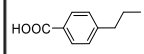	
CyB-E2	CyB-G3	CyB-A5	CyB-C6	CyB-E7	CyB-G8	CyB-A10	CyB-C11
		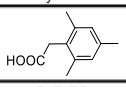	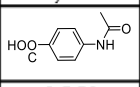				
CyB-F2	CyB-H3	CyB-B5	CyB-D6	CyB-F7	CyB-H8	CyB-B10	CyB-D11
CyB-G2	CyB-A4	CyB-C5	CyB-E6	CyB-G7	CyB-A9	CyB-C10	CyB-E11
CyB-H2	CyB-B4	CyB-D5	CyB-F6	CyB-H7	CyB-B9	CyB-D10	CyB-F11
CyB-A3	CyB-C4	CyB-E5	CyB-G6	CyB-A8	CyB-C9	CyB-E10	CyB-G11
CyB-B3	CyB-D4	CyB-F5	CyB-H6	CyB-B8	CyB-D9	CyB-F10	CyB-H11

CyC-A2	CyC-C3	CyC-E4	CyC-G5	CyC-A7	CyC-C8	CyC-E9	CyC-G10
		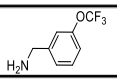				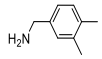	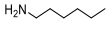
CyC-B2	CyC-D3	CyC-F4	CyC-H5	CyC-B7	CyC-D8	CyC-F9	CyC-H10
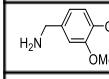					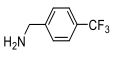	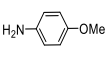	
CyC-C2	CyC-E3	CyC-G4	CyC-A6	CyC-C7	CyC-E8	CyC-G9	CyC-A11
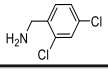	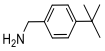	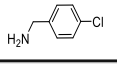					
CyC-D2	CyC-F3	CyC-H4	CyC-B6	CyC-D7	CyC-F8	CyC-H9	CyC-B11
			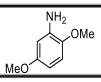				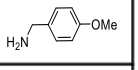
CyC-E2	CyC-G3	CyC-A5	CyC-C6	CyC-E7	CyC-G8	CyC-A10	CyC-C11
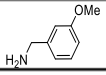							
CyC-F2	CyC-H3	CyC-B5	CyC-D6	CyC-F7	CyC-H8	CyC-B10	CyC-D11
CyC-G2	CyC-A4	CyC-C5	CyC-E6	CyC-G7	CyC-A9	CyC-C10	CyC-E11
CyC-H2	CyC-B4	CyC-D5	CyC-F6	CyC-H7	CyC-B9	CyC-D10	CyC-F11
CyC-A3	CyC-C4	CyC-E5	CyC-G6	CyC-A8	CyC-C9	CyC-E10	CyC-G11
CyC-B3	CyC-D4	CyC-F5	CyC-H6	CyC-B8	CyC-D9	CyC-F10	CyC-H11

Figure S1. (a) Core structures of CyA, CyB, and CyC, and their emission wavelength. (b) The substituent (R-group) structures for each core structure of CyA, CyB and CyC, respectively.

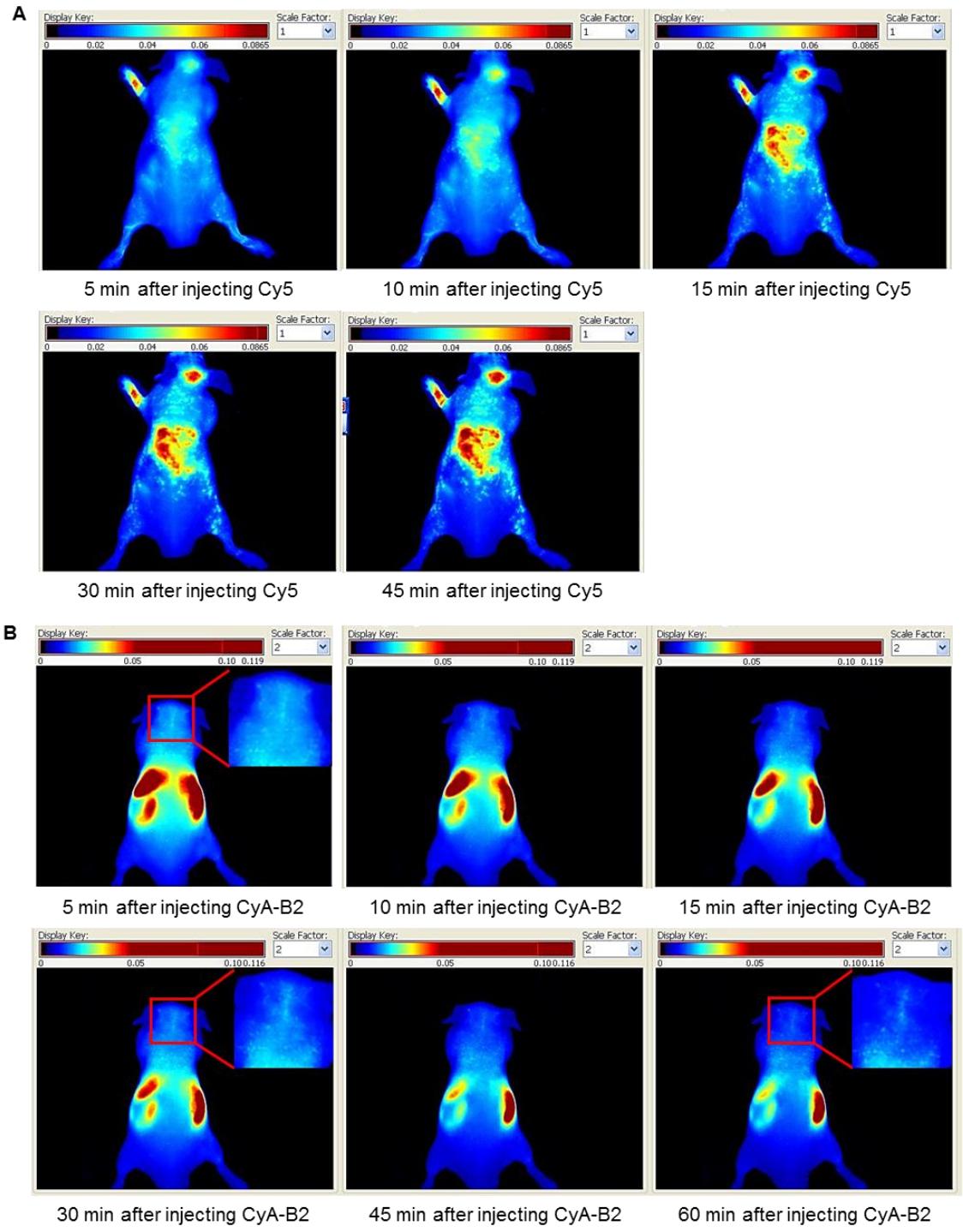

Figure S2. *In vivo* fluorescence images for (a) Cy5 and (b) CyA-B2 at 5, 10, 15, 30, 45, and 60 minutes after injection (No data for 60 minutes in Cy5). FITC-dextran was injected to the mouse 30 minutes after injection of the probes. FITC-dextran (2000k Da) was used as a reference for the intravascular space of the blood vessels. The red box indicates the potential blood vessels imaging on the mouse using *in vivo* fluorescence imaging system.

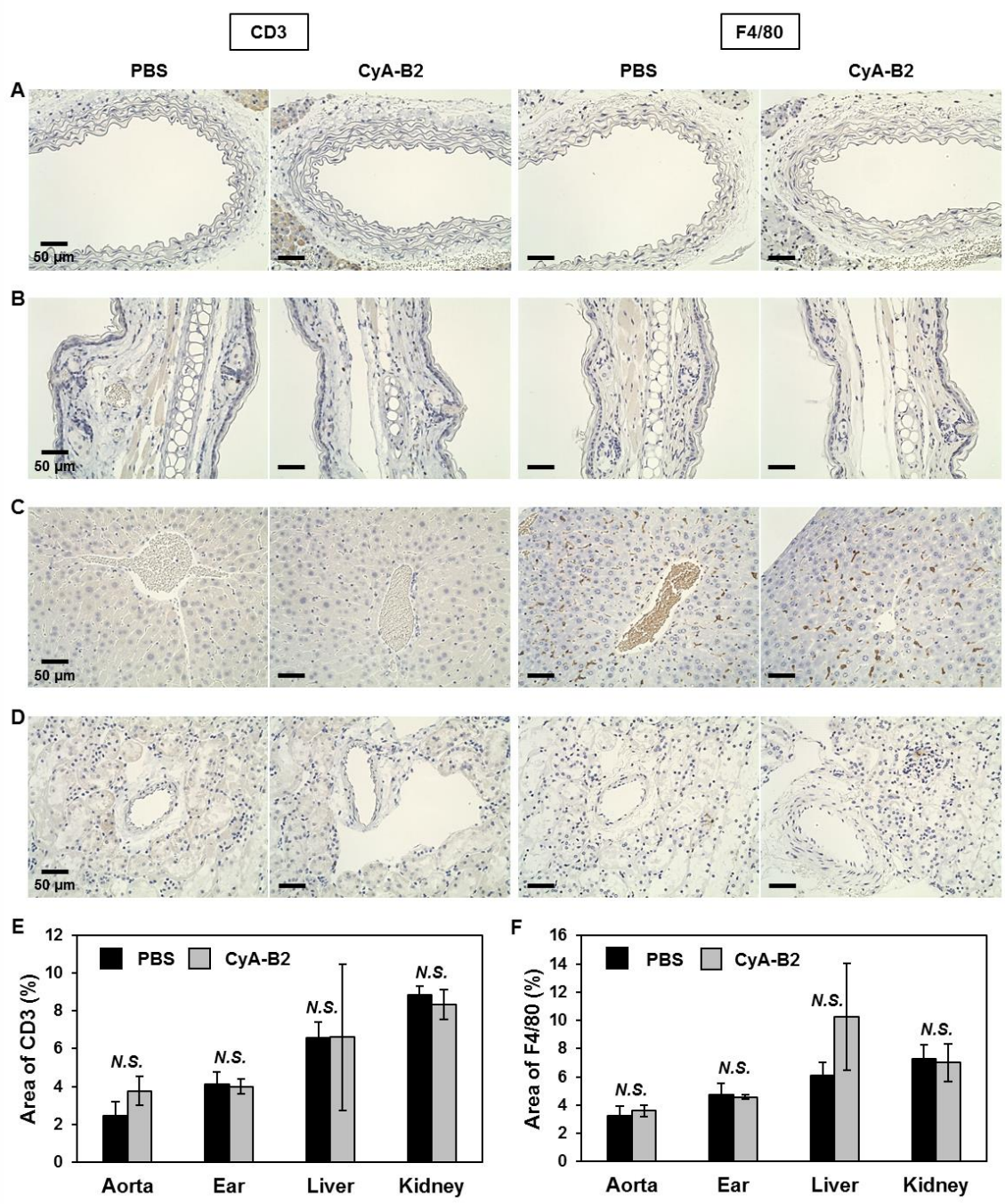

Figure S3. Immune response of T cells of CD3 and microphages of F4/80 on the mouse (a) aorta, (b) ear, (c) liver, and (d) kidney which injected with PBS (0.1% DMSO) and CyA-B2, respectively. Quantification data of (e) CD3 and (f) F4/80 area (%) were measured using ImageJ software. Data presented as mean ± s.d., (*n*=3), *N.S.*, no significant.

Compounds	Protein targets
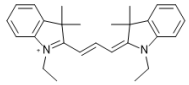 ID: CHEMBL1186511 Similarity: 0.44	• Alpha-synuclein (SNCA) • Sphingosine 1-phosphate receptor 2 (S1PR2)
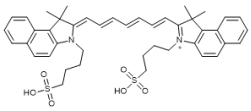 CHEMBL1615807 Similarity: 0.40	• Solute carrier organic anion transporter family member 2B1 (SLCO2B1) • Multidrug resistance-associated protein 1 (ABCC1)
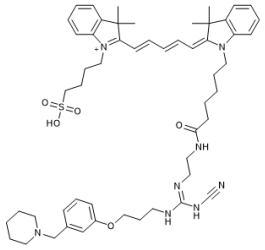 CHEMBL213357 Similarity: 0.48	Histamine H_2 receptor (HRH2)
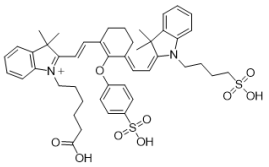 CHEMBL2079720 Similarity: 0.49	Glutamate carboxypeptidase 2 (FOLH1)

Figure S4. Chemical structures of compounds similar to CyA-B2 and their protein targets obtained from ChEMBL database.

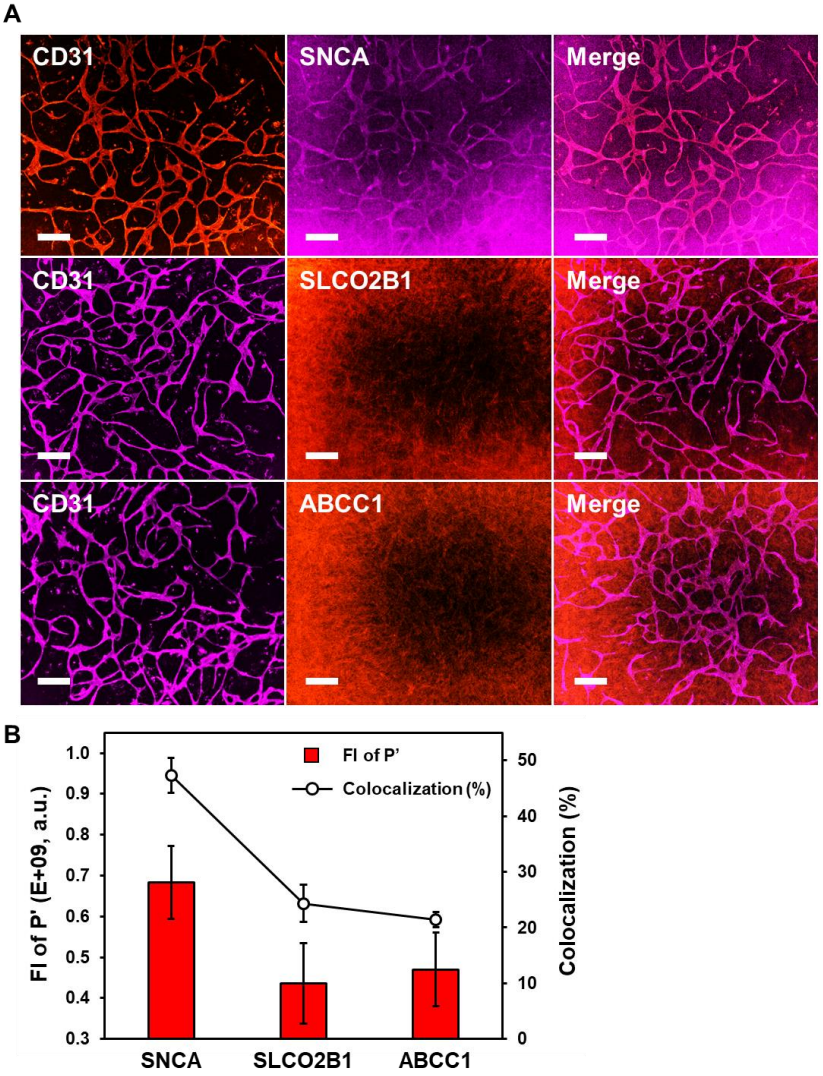

Figure S5. (a) Confocal images of immunostaining of alpha-synuclein (SNCA), solute carrier organic anion transporter family member 2B1 (SLCO2B1) and multidrug resistance-associated protein 1 (ABCC1). Scale bar is 200 μm. (b) Quantification of fluorescence intensity of specific proteins on CD31 (P') and its colocalization (%) counted by Imaris.

List of publications

Chapter 1

1. Fabrication of Blood Capillary Models for Live Imaging Microarray Analysis.
   Muhammad Asri Abdul Sisak, Fiona Louis, Sun Hyeok Lee, Young-Tae Chang, and Michiya Matsusaki.
   Micromachines **2020**, *11*, 727-738.

Chapter 2

2. A Near-Infrared Organic Fluorescent Probe for Broad Applications for Blood Vessels Imaging by High-Throughput Screening via 3D-Blood Vessel Models.
   Muhammad Asri Abdul Sisak, Fiona Louis, Ichio Aoki, Sun Hyeok Lee, Young-Tae Chang, and Michiya Matsusaki.
   Small methods **2021**, *5*, 2100338.

Chapter 3

3. Mechanism Assay of Interaction between Blood Vessels-Near Infrared Probe and Cell Surface Marker Proteins of Endothelial Cells.
   Muhammad Asri Abdul Sisak, Fiona Louis, Tomoyuki Miyao, Sun Hyeok Lee, Young-Tae Chang, and Michiya Matsusaki.
   Materials Today Bio **2022**, accepted.

Chapter 4

4. Chemical Probes on the 3D-lymphatic Capillary Models and its Possible Target Protein.
   Muhammad Asri Abdul Sisak, Fiona Louis, and Michiya Matsusaki.
   In preparation.

Supplementary publications

1. *In vitro* fabrication and application of engineered vascular hydrogels.
   Muhammad Asri Abdul Sisak, Fiona Louis, and Michiya Matsusaki.
   Polymer Journal **2020**, *52*, 871–881.

Acknowledgements

This research was carried out from 2019 to 2022 at the Department of Applied Chemistry, Graduate School of Engineering, Osaka University. This work was supported by Precursory Research for Embryonic Science and Technology (PRESTO) from Japan Science Technology Agency (JST) and the Japan Agency for Medical Research and Development (AMED)

I would like to express my sincere gratitude to my advisor Professor Michiya Matsusaki for his continuous support, helpful suggestions, and encouragement throughout my doctoral study. I would like also to express my sincere thanks to Dr. Fiona Louis, who provided encouragement, guidance and support from an early stage until allowed me to develop my understanding in my research, particularly in the field of cellular biology.

I am deeply grateful to the thesis committee: Prof. Kazuya Kikuchi and Prof. Mamoru Fujistuka, for their insightful comments and their contributions of time. I would also like to express my deep appreciation to the collaborative research. Firstly, Professor Young-Tae Chang and his student Mr. Sun Hyeok Lee from Pohang University of Science and Technology (POSTECH), Korea for kindly providing chemical probe libraries as well as their helpful comments and suggestions. Secondly, Professor Ichio Aoki and Mrs. Sayaka Shibata from National Institutes for Quantum and Radiological Science and Technology (QST), Chiba, Japan for animal study and *in vivo* imaging. Next, Associate Professor Tomoyuki Miyao from Nara Institute of Science and Technology (NAIST) for the analysis of screened probe by machine learning and identification of target protein by chemoinformatics.

Next, I would like to express my gratitude to the Assistant Professor in Matsusaki Lab Dr. Masahiko Nakamoto and Dr. Kenta Homma for their valuable advice and comments for my research. Then, to the post-doctoral in Matsusaki Lab Dr. Xie Zhengtian, Dr. Zeng Jinfeng and Dr. Naoko Sasaki and former post-doctoral Dr. Kang Dong-Hee, Dr. Hirotaka Nakatsuji and Dr. Agathe Figarol for their helpful advice, comments, suggestion to my research.

I would also like to thank both administrative assistants Ms. Eri Enomoto and Ms. Chika Sugiki for their kind help and assistance in laboratory affairs and daily life.

I would also like to thank the previous and current colleagues in the Matsusaki Lab. Thanks to Guest Associate Prof. Shiro Kitano, Guest Associate Prof. Shinji Irie, Visiting researcher Asuka Kato, Yasuyuki Naito, Yuka Yoshinouchi, and Dr. Keisuke Sumiyoshi. Thanks to Ms. Yukiko Sorayama, Ms. Nanbu Saori, Ms. Misaki Komeda, Mr. Kousuke Yanagisawa, Mr. Yudai Shioji, Ms. Natsuko Kato, Mr. Kouki Nishi, Mr. Yuta Okada, Mr. Yasuhiro Naka, Mr. Yuichi Yukawa, Mr. Liu Hao, Mr. Kazuma Ishiguro, Mr. Noboru Hiraoka, Ms. Li Jinyu, Ms. Nozomi Kasahara, Mr. Daisuke Tomioka, Mr. Tomoyuki Suezawa, Mr. Shogo Shimada, Mr. Ryo Mitsuyasu, Mr. Rei Miyata, Ms. Zhang Yuning, Ms. Pei Lingyu, Ms. Marie Piantino, Mr. Yucheng Shang, Ms. Asli Sena Karanfil, Ms. Zhang Zhuying, Ms. Sukulya Bunuasunthon, Mr. Yuki Koba , Mr. Tomoya Matsuo, Mr. Kazuki Moroishi, Mr. Kazuki Yoshida, Mr. Tamaki Kumauchi, Mr. Ryosuke Isobe, Mr. Yusuke Kajiura, Mr. Rentaro Sakamoto, Ms. Kaori Hayazaki, Ms. Misa Miyamoto, Ms. Wu Chun-Yi (Jenny), Mr. Ryoto Itani, Mr. Kanta Iwamoto, Ms. Aya Nagura, Ms. Itsuki Miyaguni and Ms. Hong Young Kyoung for their hearty supports and kind assistance for both research and daily life.

I would like to thank the Japanese Ministry of Education, Culture, Sports, Science and Technology (MEXT) for awarding the Monbukagakusho Scholarship for my studies at Osaka University, Japan.

Lastly, I would like to express my heartfelt appreciation to my father Mr. Abdul Sisak and my siblings for their thoughtful attention and continuous encouragements.

Finally, I sincerely wish for the further development of Matsusaki Lab in the future.

June 2022

MUHAMMAD ASRI BIN ABDUL SISAK